

All-optical wavelength conversion of higher-order modulation format data signals

Sepideh T. Naimi

B.Sc., M.Sc.

**A Dissertation submitted in fulfillment of the requirements
for the award of Doctor of Philosophy (Ph.D.) to the**



Dublin City University

Faculty of Engineering and Computing

School of Electronic Engineering

Supervisor: Prof. Liam P. Barry

November, 2015

Declaration

I hereby certify that this material, which I now submit for assessment on the programme of study leading to the award of Doctor of Philosophy (Ph.D.) is entirely my own work, and that I have exercised reasonable care to ensure that the work is original, and does not to the best of my knowledge breach any law of copyright, and has not been taken from the work of others save and to the extent that such work has been cited and acknowledged within the text of my work.

Signed:

Student ID.:11212007

Date:

Dedication

To my late father Shams Naimi.

His words of inspiration and encouragement

in pursuit of excellence, still linger

Acknowledgements

I would like first to thank my supervisor Prof. Liam P. Barry who believed, from the beginning, in my ability to do research in his group and who encouraged and supported me during this project. At many stages in the course of this research project, I benefited from his advice, particularly so when exploring new ideas. I have been extremely lucky to have a supervisor who cared so much about my work, and who responded to my questions so promptly.

I would like to address a special thanks to Dr. Seán P. Ó Duill, who has a great part in shaping my research work and helped me tremendously at every step forward.

I would like to thank all my colleagues past and present in radio and optical communication lab, thank you so much for your help but most importantly for your friendship.

Finally, many thanks and lots of appreciation must go to my parents and Sajad for all the support and encouragement. My family has been a constant source of love, concern, support and strength all these years. I would like to express my heart-felt gratitude to them. All the support they have provided me is the greatest gift any one has given me.

Table of Contents

Declaration.....	i
Acknowledgements.....	ii
Table of Contents.....	iii
List of Figures.....	vi
List of Tables.....	xi
List of Acronyms.....	xii
Abstract.....	xiv
Introduction.....	xv
Chapter 1- Review of Advanced Optical Network.....	1
1.1 Introduction.....	1
1.2 Optical Switching Networks.....	2
1.3 Review of Advanced Modulation Formats.....	4
1.3.1 Differential Quadrature phase shift keying (DQPSK).....	4
1.3.2 Optical 16- quadrature amplitude modulation (16-QAM).....	7
1.4 Wavelength Conversion Technologies.....	14
1.4.1 Optoelectronic (O/E-E/O) Wavelength Conversion.....	14
1.4.2 All optical wavelength conversion.....	15
1.5 Summary and conclusion.....	19
Bibliography.....	20
Chapter 2- All- Optical wavelength conversion based on Four Wave Mixing in Semiconductor optical Amplifier.....	22
2.1 Introduction.....	22
2.2 Principle of Semiconductor optical amplifier.....	22
2.3 Four Wave Mixing in Semiconductor Optical Amplifier.....	25
2.4 SOA model.....	25

2.4.1	Basic SOA model based on interband parameters	25
2.4.2	Modified SOA model based on interband and intraband parameters	27
2.4.3	Improved SOA model including internal loss.....	29
2.5	Theory of Phase noise due to FWM in SOA	30
2.6	Summary and conclusion.....	32
	Bibliography	33
Chapter 3- Simulations of OSNR and Laser Linewidth Limits for Wavelength Conversion of DQPSK Signals Using FWM		36
3.1	Introduction.....	36
3.2	Background and simulator	37
3.3	Single pump scheme	42
3.4	Dual pump scheme.....	46
3.5	Summary and conclusion.....	51
	Bibliography	53
Chapter 4- Pump Phase Noise Tolerance of All Optical Wavelength Conversion of M-QAM Signals Using Four-Wave Mixing		55
4.1	Introduction.....	55
4.2	Background and simulator	56
4.3	Linewidth Limits for Wavelength Converting 16-QAM Signals Using FWM.....	65
4.3.1	Single Pump All- optical Wavelength Conversion of 16-QAM	65
4.3.2	Dual Pump all- Optical Wavelength Conversion of 16-QAM.....	71
4.4	Wavelength Converting 64-QAM Signals.....	73
4.5	Summary and conclusion.....	75
	Bibliography	77
Chapter 5- All Optical Wavelength of Conversion of Nyquist-WDM Superchannels Based on Advanced Modulation Format Using FWM in SOAs		79
5.1	Introduction.....	79
5.2	Background and simulator	83

5.3	Results.....	91
5.3.1	DQPSK.....	91
5.3.2	16-QAM	98
5.4	Summary and conclusion.....	105
	Bibliography	108
Chapter 6- Phase Noise Tolerant Wavelength Conversion of Nyquist-WDM Superchannels Using FWM in SOAs		111
6.1	Introduction.....	111
6.2	Results.....	113
6.2.1	16-QAM	113
6.2.2	64-QAM	115
6.3	Summary and conclusion.....	118
	Bibliography	119
Chapter 7: Conclusion		121
7.1	Conclusion	121
7.2	Suggestions for future Work.....	125
APPENDIX A- Data Sheet.....		127
APPENDIX B- List of Publications arising from this work		128

List of Figures

Fig.1-1 Typical packet switched network based on wavelength routing	3
Fig.1-2 The DQPSK encoder with two parallel.....	5
Fig.1-3 DQPSK optical demodulator based on differential detection	5
Fig.1-4 Square-16-QAM constellation diagram	8
Fig.1-5 Schematic of a multi-format coherent optical transmission system for high-order modulation. (a) Transmitter (TX), (b) Receiver (RX) [11],[14].....	9
Fig.1-6 Optical multi-level modulation transmitters (a) Serial configuration, (b) IQ-configuration with MZM and PM [13]	11
Fig.1-7 O/E- E/O Wavelength conversion method.....	15
Fig.1-8 Different types of optoelectronic wavelength converters (a) Cross gain modulation (XGM) (b) Cross phase modulation (XPM)	16
Fig.1-9 All-optical wavelength conversion using four-wave mixing in a semiconductor optical mmplifier.....	18
Fig.2-1 Schematic of a SOA with the amplification process.....	23
Fig.2-2 SOA gain vs. output power	24
Fig.2-3 Spectral placement of the pumps, input signal and converted idlers for the single pump and dual pump wavelength converter	27
Fig.3-1 Schematic of simulation platform to calculate the BER due to OSNR and linewidth for the dual pump scheme. The input and detected constellations for 100 symbols of 10 Gbaud DQPSK when the pump P_1 has a linewidth of 3 MHz are shown to highlight the impact of the phase noise transfer from pump to converted idler.....	39
Fig.3-2 Calculated (a) input spectrum and (b) output spectrum of the dual pump scheme showing the spectral location of the DQPSK signal, pumps P_1 and P_2 along with the converted idlers.....	41
Fig.3-3 (a) Calculated BER versus OSNR of converted 10 Gbaud DQPSK signal using the single pump scheme with pump linewidth as parameter. [*] denotes theoretical BER calculation for zero pump linewidth. (b) The required OSNR to achieve a BER of 10^{-4} and 10^{-3} for any given pump linewidth. BER values below 10^{-5} are not trustworthy due to the limited number of bits simulated.	43
Fig.3-4 (a) Calculated BER versus OSNR of converted 25 Gbaud DQPSK signal using the single pump scheme with pump linewidth as parameter. [*] denotes theoretical BER	

calculation for zero pump linewidth. (b) The required OSNR to achieve a BER of 10^{-4} and 10^{-3} for any given pump linewidth. BER values below 10^{-5} are not trustworthy due to the limited number of bits employed in the simulation.	45
Fig.3-5 (a) Calculated BER versus OSNR of the converted 10 Gbaud DQPSK signal using the dual pump scheme with pump linewidth as parameter. [*] denotes theoretical BER calculation for zero pump linewidth. (b) The required OSNR to achieve a BER of 10^{-4} and 10^{-3} for any given pump linewidth. BER values below 10^{-5} are not trustworthy due to the limited number of bits employed in the simulation.	49
Fig.3-6 Calculated BER versus OSNR of converted 25 Gbaud DQPSK signal using the dual pump scheme with pump linewidth as parameter. The linewidths of both pumps are equal. [*] denotes theoretical BER calculation for zero pump linewidth (b) The required OSNR to achieve a BER of 10^{-4} and 10^{-3} for average pump linewidth for the two cases when the pumps have equal linewidths and when the linewidth of P_2 is kept constant at 8 MHz. BER values below 10^{-5} are not trustworthy due to the limited number of bits employed in the simulation	50
Fig.4-1 Schematic of simulation platform to calculate the BER due to OSNR and linewidth for the dual pump scheme. The input and detected constellations for 100 symbols of 10 Gbaud 16-QAM when the pump P_1 has a linewidth of 1 MHz are shown to highlight the impact of the phase noise transfer from pump to converted idler.....	60
Fig.4-2 Calculated (a) input spectra and (b) output spectra of the dual pump scheme showing the spectral location of the 16-QAM signal, pumps P_1 and P_2 , and the converted idlers.	63
Fig.4-3(a) Structure of homodyne coherent detection (b) Decision-directed phase-locked loop carrier phase recovery (DD-PLL), (c) Amplitude normalized decision-directed phase-locked loop carrier phase recovery.	64
Fig.4-4 Calculated μ versus OSNR of pump linewidth of 16-QAM signal using the single pump scheme with for both DD-PLL and ANDD-PLL. The receiver using the DD-PLL was unable to detect the 16-QAM signal for pump linewidths greater than 1 MHz.	65
Fig.4-5 Calculated BER versus OSNR of degenerate wavelength conversion of 16-QAM signals at 10 Gbaud using DD-PLL and ANDD-PLL.	66
Fig.4-6 the required OSNR of degenerate FWM to achieve a BER of 10^{-3} and 10^{-4} using DD-PLL and AND-PLL.	68
Fig.4-7 Investigation of ASE noise effect on the single pump wavelength conversion of 16-QAM signal at 10 Gbaud using FWM in SOA and DD-PLL.	70

Fig.4-8 Investigation of ASE noise effect on the single pump wavelength conversion of 16-QAM signal at 10 Gbaud using FWM in SOA and ANDD-PLL.....	70
Fig.4-9 (a) Comparison of relevant linewidth of degenerate and non-degenerate FWM based wavelength conversion of 16-QAM signal at 10 Gbaud using two separate pumps and DD-PLL. (b) The required OSNR of non-degenerate FWM to achieve a BER of 10^{-3} and 10^{-4} using DD-PLL and AND-PLL.....	72
Fig.4-10 AOWC of 64-QAM schematic using FWM in SOA with the optical spectra at the SOA input and output. Constellation diagram of the 64-QAM signal and detected idler with pump linewidth is set to 50 kHz.	73
Fig.4-11 BER versus OSNR of degenerate wavelength conversion of 64-QAM signals at 10 Gbaud using ANDD-PLL.	75
Fig.5-1 Comparison of wavelength conversion of N-WDM superchannel based on Optical-Electrical- Optical (O-E-O) conversion and all-optical wavelength conversion of N-WDM superchannel based on FWM in SOA.	81
Fig.5-2 (a) Generation of N-WDM superchannel with 1 th Subcarrier eye diagram and superchannel spectra (b) Simulation schematic of AOWC of Nyquist-WDM superchannel. (c) Superchannel receiver.	86
Fig.5-3 Calculated (a) input spectra and (b) output spectra of the dual pump scheme showing the spectral location of the N-WDM superchannel, pumps P_1 and P_2 , and the converted idlers. Root Raised Cosine (RRC) pulse shaping is employed. N.B. the resolution bandwidth is 100 kHz.....	90
Fig.5-4 Calculated (a) input spectra of single pump WC of N-WDM superchannel based on 150 GHz detuning between central frequency of superchannel and pump (b) output spectra of the single pump WC of superchannel using 150 GHz superchannel–pump detuning. (c) Output spectra of the single pump WC of superchannel using 200 GHz superchannel–pump detuning. (d) BER vs. OSNR for degenerate WC of 448 Gb/s N-WDM superchannel using 8×28 DQPSK and different detunings. Pump linewidth=5 MHz and all the results are based on root raised cosine (RRC) pulse shaping.....	93
Fig.5-5 BER vs. OSNR calculations of back to back and single pump (degenerate FWM) AOWC of Nyquist-WDM superchannel based on DQPSK modulation format (a) RRC pulse shaping and different pump power (b) RC pulse shaping and optimised pump power of 20mW. For more clarity, results are based on 1 st , 4 th and 8 th subcarriers only.	95
Fig.5-6 BER vs. OSNR calculations of back to back and single pump (degenerate FWM) AOWC of Nyquist-WDM superchannel based on DQPSK modulation format and different	

level of ASE noise figures from SOA. For more clarity, results are based on 1 st , 4 th and 8 th subcarriers.	97
Fig.5-7 Comparison of degenerate and non-degenerate FWM based wavelength conversion of N-WDM superchannel based on DQPSK employing RRC. The pump linewidth (s) is 5/10 MHz for degenerate and nondegenerate WC. For clarity, Results are considered for 1 th , 4 th , 8 th subcarriers.	98
Fig.5-8 (a) BER vs. OSNR calculations of back to back and single pump AOWC of Nyquist-WDM superchannel based on 16-QAM modulation format, different level of pump power. (b) Constellations of degenerate WC of N-WDM superchannel based on 5mW pump power for 1 th and 4 th subcarrier. (c) Constellations of degenerate WC of N-WDM superchannel based on 20 mW for 1 th and 4 th subcarriers. The results are based on RRC pulse shaping. ...	100
Fig.5-9 BER vs.OSNR calculations of back to back and single pump AOWC of Nyquist-WDM superchannel based on 16-QAM modulation format based on RC Pulse shaping and optimised pump power of 20mW.	101
Fig.5-10 (a) Constellations of degenerate WC of N-WDM superchannel based on (a) RRC pulse shaping (b) RC pulse shaping. All the results are for 1 st and 4 th subcarrier and based on optimised pump power of 20 mW	102
Fig.5-11 BER vs. OSNR calculations of back to back and single pump (degenerate FWM) AOWC of Nyquist-WDM superchannel based on 16-QAM modulation format and different level of ASE noise figures from SOA. Results are based on 1 st , 4 th and 8 th subcarriers RRC pulse shaping and optimised pump power of 20 mW.....	103
Fig.5-12 Comparison of degenerate and non-degenerate FWM based wavelength conversion of N-WDM superchannel based on 16-QAM. The pump linewidth (s) is 100/200 kHz for degenerate and nondegenerate Results are considered for 1 th , 4 th , 8 th subcarriers, RRC pulse shaping and optimised pump power of 20 mW.	104
Fig. 6-1 Schematic of phase noise tolerant all optical wavelength conversion of N-WDM superchannel based on OCG and using FWM in SOA.....	114
Fig. 6-2 Calculated BER vs. OSNR results for the subcarriers of the superchannel for the cases of back to back, correlated and uncorrelated phase noise. For more clarity, results are only shown for 1 st , 4 th and 8 th subcarrier.....	115
Fig. 6-3 Schematic of phase noise tolerant all optical wavelength conversion of N-WDM superchannel based on optical comb generator and using FWM in SOA..	116
Fig. 6-4 Calculated BER vs. OSNR results for the subcarriers of the superchannel after the wavelength conversion scheme. Identical BER results of the phase noise tolerant idler are	

obtained for the correlated pump phase noise as for the case when the pump linewidth equals zero. When the phase noise on the pumps is uncorrelated, and each pump having a 5 MHz linewidth, then the scheme completely fails. For more clarity, the results are based on 1st, 3th, and 6th subcarriers.117

List of Tables

Table 1-1 Receiver mapping of phase change to bits [11].....	7
Table 4-1 SOA parameters.....	58
Table 5-1 SOA parameters.....	85
Table 7-1 Implementation of all- optical wavelength conversion of advanced modulation format using FWM in SOA (a) DQPSK (b) M-QA.....	123
Table 7-2 Implementation of degenerate FWM- based wavelength conversion of N-WDM superchannel using FWM in SOA.....	124

List of Acronyms

ANDD-PLL	Amplified Normalised Decision Directed Phase Locked Loop
AOWC	All Optical Wavelength Conversion
ASE	Amplified Spontaneous Emission
BD	Balance Detector
BER	Bit Error Rate
CW	Continuous Wave
DD-PLL	Decision Directed Phase Locked Loop
DQPSK	Differential Quadrature Phase Shift Keying
DSP	Digital Signal Processing
FEC	Forward Error Correction
FWM	Four Wave Mixing
I-Q Modulator	In phase-Quadrature Modulator
LO	Local Oscillator
MZM	Mach-Zehnder Modulator
OBS	Optical Burst Switching
OCS	Optical Circuit Switching
OPS	Optical Packet Switching
OSNR	Optical Signal to Noise Ratio

PAPR	Peak to Average Power Ratio
PD	Photo Diode
PLL	Phase Locked Loop
PM	Phase Modulation
PMD	Polarization Mode Dispersion
QAM	Quadrature Amplitude Modulation
SOA	Semiconductor Optical Amplifier
SVEA	Slowly Varying Envelope Approximation
WDM	Wavelength Division Multiplexing
XGM	Cross Gain Modulation
XPM	Cross Phase modulation

Abstract

The future optical switched wavelength division multiplexed (WDM) networks will require all optical wavelength conversion to avoid contention in a node when two signals on the same wavelength are being switched to the same output fiber. These future networks will also employ advanced modulation formats in order to increase the capacity of optical networks. In order to perform wavelength conversion operations on advanced modulation formats, a coherent nonlinear process, such as four-wave mixing (FWM), is required to preserve the amplitude and phase information. The phase noise transfer problem has crucial significance for the exploitation of FWM-based wavelength converters for advanced modulation formats because the phase noise transfer degrades the overall system performance. In this work, the required optical signal to noise ratio (OSNR) and laser phase noise (linewidth) limits are calculated via Monte Carlo simulations for the wavelength conversion of advanced modulation formats including DQPSK and M-QAM. Due to the sensitivity of M-QAM signals with respect to phase noise, the conversion performance is investigated using two different decision-directed phase-locked loop carrier phase recovery algorithms. In order to develop a validated numerical model for all-optical wavelength conversion of advanced modulation formats, the required OSNR versus pump linewidth at two values of bit error rate (BER) of 10^{-3} and 10^{-4} for DQPSK, 16-QAM and 64-QAM are reported for degenerate and non-degenerate FWM. With these calculations, the performance of wavelength conversion of advanced modulation formats will be guaranteed by selecting lasers with linewidths below these linewidth limits. As a next step of this work, All-optical wavelength conversion of Nyquist-WDM Superchannel using FWM in an SOA based on advanced modulation formats such as DQPSK, 16 and 64- QAM are demonstrated.

Introduction

All optical wavelength conversion of advanced modulation formats has a significant role in the next generation optical communication systems. All optical wavelength conversion (AOWC) would be required to improve the flexibility of conventional wavelength division multiplexing (WDM) networks. In addition, the data carrying capacity of lightwave communication systems can be increased using advanced modulation formats such as DQPSK, 16- and 64-QAM. Four-wave mixing (FWM) in semiconductor optical amplifiers (SOA) is the best candidate to perform wavelength conversion of signals with advanced modulation formats due to: transparency to modulation format and transparency to baud rate. The aim of this thesis is to study all-optical wavelength conversion of higher-order modulation format data signals. For this purpose, the required OSNR and laser phase noise (linewidth) limits for the WC of DQPSK, 16 and 64-quadrature amplitude modulation (16-QAM and 64-QAM) using degenerate and nondegenerate FWM in a semiconductor optical amplifier are calculated via Monte Carlo simulations. Particular attention is paid to the phase noise transfer from the pump(s) to the converted signals. The classes of laser that can be used as the pump source to implement the schemes are highlighted by the calculations of the required pump laser linewidths to achieve specific system bit error rate performance at the forward error correction threshold. In order to improve the system performance, different techniques are applied for the wavelength conversion of advanced modulation formats, i.e. different phase lock loops to track the phase noise. The results are consistent with theories of phase noise transfer between the pump and converted signals. The effect of amplified spontaneous emission generated within the semiconductor optical amplifier is also considered on these schemes. Even though, the analysis carried out in this work is specifically focused on using an SOA for FWM, the results apply equally to the use of highly nonlinear fiber

(HNLF). As a next step, all-optical wavelength conversion of Nyquist-WDM superchannel using FWM in an SOA based on advanced modulation format such as DQPSK, 16 and 64-QAM is demonstrated. The performance of the converted superchannel is impaired by crosstalk due to cross-gain modulation (XGM) of the pump. It is shown that optimum performance of the converted superchannel is achieved by optimising the detuning between the continuous-wave pump and the central wavelength of the superchannel as well as pump power. Finally, the phase noise tolerant wavelength conversion of Nyquist-WDM superchannel is investigated through simulation using FWM in an SOA.

The structure of this thesis is as follows:

Chapter 1 reviews advanced optical networks. Firstly, advanced modulation formats employed to achieve greater spectral efficiency and maximize the overall network capacity are reviewed. Secondly, different wavelength conversion techniques are explained. Finally, it is discussed how wavelength conversion and advanced modulation formats can contribute to increase the capacity and flexibility of next generation optical networks, and which of the current techniques are the most promising candidate to meet these requirements.

Chapter 2 aims to study Four-wave mixing in semiconductor optical amplifiers (SOAs) as an important tool for all-optical wavelength conversion. The effect of phase noise transfer from the pump(s) to generated idlers based on single pump (i.e. degenerate FWM) and dual pumps (nondegenerate FWM) are also discussed in this chapter.

Chapter 3 describes the pump laser linewidths required to achieve specific system performance when undertaking wavelength conversion of DQPSK data signals at 10 and 25 Gbaud using four-wave mixing in a semiconductor optical amplifier. The results highlight the class of laser that can be used to implement this scheme. It is shown that the limits are

consistent with expected theories and indicate guidelines for implementing multiple wavelength conversions using this scheme in an optical network.

Chapter 4 demonstrates all optical wavelength conversion of quadrature amplitude modulation (QAM) including 16-QAM and 64-QAM using degenerate and nondegenerate FWM in a semiconductor optical amplifier. Particular attention is paid to the phase noise transfer from the pump(s) to the converted signal. The class of laser that can be used as the pump source to implement the scheme is highlighted by the calculations of the required pump laser linewidths to achieve specific system bit error rate performance with FEC implemented.

Chapter 5 investigates the performance of all-optical wavelength conversion (AOWC) of Nyquist-WDM superchannels for future implementation in optical networks. Advanced modulation formats of DQPSK and 16-QAM are considered for the subchannel modulation format achieving raw bit rates of 448 and 896 Gbit/s respectively. The performance of AOWC of Nyquist-WDM superchannel using degenerate and nondegenerate four-wave mixing (FWM) in a semiconductor optical amplifier (SOA) is demonstrated through simulations. Effects of raised cosine (RC) and root raised cosine (RRC) signal pulse shaping are considered within the wavelength conversion process. It is found that the performance of the converted superchannel is severely impaired by crosstalk due to cross-gain modulation (XGM) of the pump by the superchannel. Optimum performance of the converted superchannel is achieved by setting the detuning between the continuous-wave pump and the central wavelength of the superchannel to be around 200 GHz and using pumps of double the gain saturation power of the SOA with 23 dB pump to signal power ratio.

Chapter 6 proposes and demonstrates the phase noise tolerant wavelength conversion of Nyquist-WDM superchannel comprising of a 8×28 Gbaud 16-QAM (total bit rate of 896Gb/s) and 6×28 Gbaud 64-QAM signals (raw bit rate of around 1.008Tbit/s) through

simulation using FWM in an SOA. The results are shown for both scenarios when the phase noise of the pumps is correlated and uncorrelated (separate free running lasers). It is shown that by the use of a dual correlated pumping technique the performance of wavelength conversion process is guaranteed and it is not limited by phase noise on the optical pumps.

Chapter 7 highlights the main conclusions of this study. The future research directions will also be discussed at the end of this chapter.

Chapter 1- Review of Advanced Optical Network

1.1 Introduction

The development of lasers in the 1960s and low loss fibres in the early 1970s made the first fiber optic communication system possible in 1978. The concept of optical communication starts from the idea that the large volume of data is transmitted over optical fiber by using of the laser transmitter. At that time, the passing of optical signals through an optical fiber and their transmission over several hundred kilometers was very challenging. However, over the years, great improvements in optical fiber and a significant decrease in optical loss within the fiber have made optical communications technology applicable over long distances. Despite these great advances in optical communications, the capacity of optical networks needs to grow by 29% per annum in order to meet the ever-increasing network end-user demands [1]. To meet these demands new approaches are sought to avoid the so-called ‘capacity crunch’. High capacity next generation networks will require advanced modulation formats with more than one bit per symbol to achieve greater spectral efficiency and maximize the overall network capacity [2]. In addition to the move toward advanced modulation formats for increased spectral efficiency, there is also a drive to develop WDM networks that are more flexible and can reconfigure quickly to make the most efficient use of the available capacity

of WDM channels [3],[4]. In this chapter, it is discussed how wavelength conversion and advanced modulation formats can contribute to increase the capacity and flexibility of next generation optical networks and which of the current technologies are the most promising to meet these requirements.

1.2 Optical Switching Networks

Switching technologies based on wavelength division multiplexing (WDM) have been increasingly deployed over the last decades in order to meet ever-increasing bandwidth requirements. Information is sent from an origin to destination through WDM channels via intermediate network nodes. At these nodes, the switching takes place to route the bits from the origin to the destination along a determined pathway. The switching can be implemented in either the electrical or the optical domain. However, from the above-mentioned ever-increasing transmission capacity, the switching in the electrical domain experiences more and more difficulties because there are many wavelength channels in today's WDM networks. Therefore, large number of optical receivers, modulators and lasers will be required at each network nodes resulting in increased expense and energy consumption. The main purpose of the optical switches is to connect two optical transmission pathways. The switches are as such that the data remains in optical domain during its entire travel duration and is never converted from optical to electrical or vice versa. The migration of switching functions from electronics to optics will be gradual, and will take place in several stages. Already, the first stage has started and the initial form of wavelength routed networks is based on optical circuit switching (OCS) which is an optical networking technology. In OCS, the network is configured to establish a circuit, from an origin to destination node, by adjusting the optical cross connects circuits in the core routers in a manner that the optical data signal can travel in an all-optical manner from the entry to the exit node. This approach suffers from the

disadvantages of circuit switching such as time requirement to set up and to destroy, and while the circuit is established, the resources will not be efficiently used under dynamic internet traffic loads. The next phase in the switching evolution is optical burst /packet switching (OBS/ OPS) with the advantages of bandwidth-efficiency of high bit rate transport service under heavy traffic, flexibility and cost effectiveness. An example of a wavelength-labelled packet switched network is shown in Fig.1-1, where a data packet is routed through an optical network based on the underlying wavelength of the packet. The origin of a data packet is at the edge router 1 and this packet must pass through various core routers (CR) to reach a destination node edge router 2. Depending on network traffic conditions, it may be necessary to convert the packet to a new wavelength as it passes through the network to avoid contention. Therefore, future packet-switched wavelength division multiplexed (WDM) networks [5] will require all optical wavelength conversion to avoid contention in a node when two signals on the same wavelength are being switched to the same output fiber; thus improving the efficiency under heavy network loads by fully utilizing all the available WDM channels.

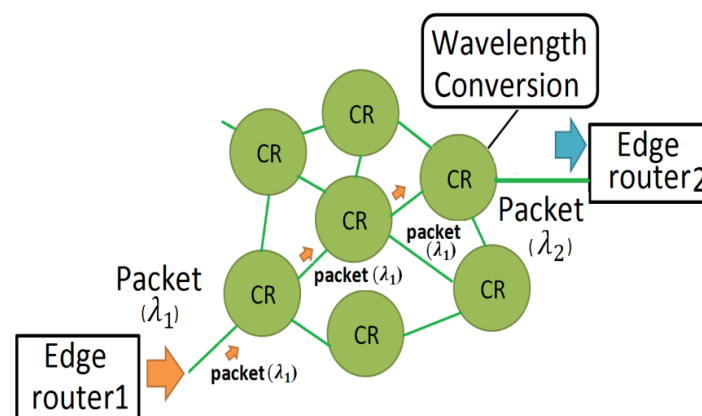


Fig.1-1 Typical packet switched network based on wavelength routing. A packet originating from edge router 1 is to be routed through to edge router 2

Detailed investigation of different wavelength conversion techniques are discussed in following sections of this chapter.

1.3 Review of Advanced Modulation Formats

Optical communication systems have been primarily adopting on-off-keying (OOK) signals, which convey the information on the intensity of the optical carrier. Recently, advanced optical modulation formats have attracted increased attention [6-8]. The clear trend in order to increase the bit rate in modern wavelength division multiplexed (WDM) fiber systems is the use of advanced modulation formats that exploit a mix of intensity and phase modulation [9]. Quadrature phase shift keying (DQPSK) and optical M-Quadrature amplitude modulation (M-QAM) are the most promising advanced modulation formats in the next generation of optical communication networks to achieve greater spectral efficiency and maximize the overall network capacity [10]. In this section, the theory behind differential quadrature phase shift keying (DQPSK) and M-quadrature amplitude modulation (M-QAM) modulation formats are discussed.

1.3.1 Differential Quadrature phase shift keying (DQPSK)

In differential quadrature phase shift keying, the symbol information is encoded as the phase change from one symbol period to the next rather than as an absolute phase. In this case, the receiver has to detect phase changes and not the absolute value of the phase [11]. The optical DQPSK encoder in this thesis is based on two parallel Mach-Zehnder modulators (MZMs) to generate four phase levels [11], [12], as shown in Fig.1-2. The proposed DQPSK encoder is composed of one 3 dB optical power splitter, two parallel Mach-Zehnder modulators (MZMs), one optical phase shift and one optical power combiner. The MZMs are biased for

minimum optical transmission and driven with NRZ data with amplitude $2V\pi$. Signals from the in-phase (I (k)) and quadrature (Q (k)) arms are recombined with a relative optical phase shift of $\pi/2$. The schematic representation of optical DQPSK decoder based on differential detection is shown in Fig.1-3. The decoder consists of a pair of Mach- Zehnder interferometers, each with an optical delay time τ equal to the symbol period $2/B$ (B is the bit rate) [11].

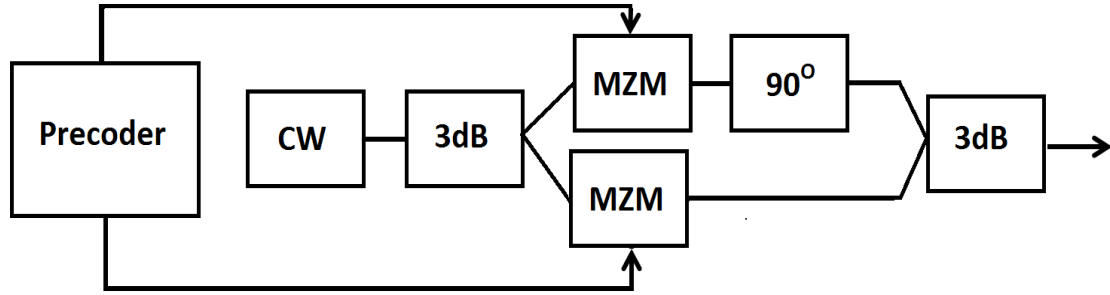


Fig.1-2 the DQPSK encoder with two parallel

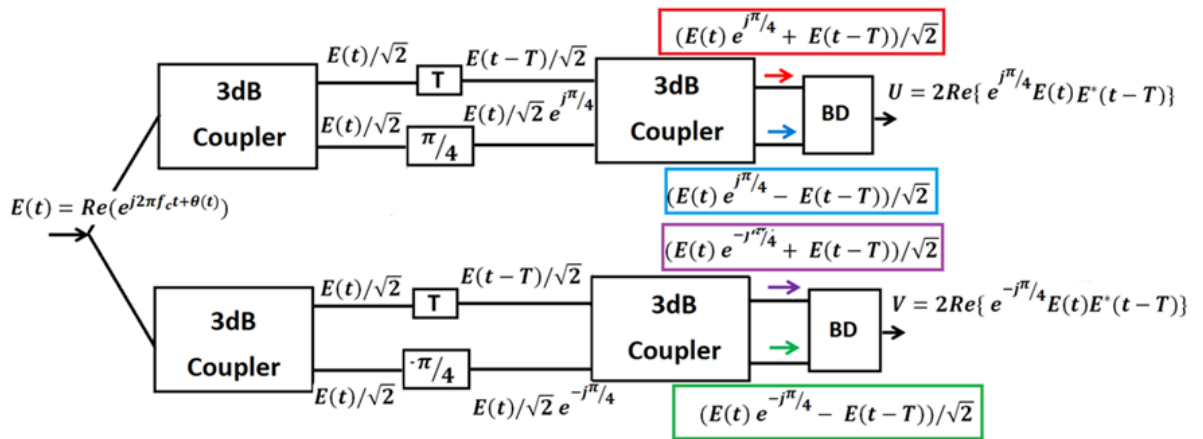


Fig.1-3 DQPSK optical demodulator based on differential detection

The differential optical phase between interferometer arms is set to $\pi/4$ and $-\pi/4$ for upper and lower branches, respectively. Balanced optical detectors are employed for each interferometer; each detector pair has a bandwidth commensurate with a symbol rate $B/2$. Provided that the receiver is polarization insensitive, adaptive polarization control is not needed for optical DQPSK decoding. As shown in Fig.1-3, E is the received electric field which is phase modulated. The optical coupler provides the sum and difference of the input signals at its two outputs.

The outputs U and V are a function of the phase difference of the input signal E as below [11]:

$$E(t) = e^{j\phi}, \quad (K-1)T < t < KT \quad (1-1)$$

$$\begin{aligned} U &= \text{Re} \{ e^{j\pi/4} E(t) E^*(t-T) \} = \text{Re} \{ e^{j\pi/4} e^{j\phi(k)} e^{-j\phi(k-1)} \} = e^{j\pi/4} e^{j\phi(k)-\phi(k-1)} \quad (1-2) \\ &= \cos(\pi/4 + \Delta\phi) \end{aligned}$$

$$\begin{aligned} V &= \text{Re} \{ e^{-j\pi/4} E(t) E^*(t-T) \} = \text{Re} \{ e^{-j\pi/4} e^{j\phi(k)} e^{-j\phi(k-1)} \} \quad (1-3) \\ &= e^{-j\pi/4} e^{j\phi(k)-\phi(k-1)} = \cos(-\pi/4 + \Delta\phi) \\ &= \cos(-\pi/2 + \pi/4 + \Delta\phi) = \sin(\pi/4 + \Delta\phi) \end{aligned}$$

The values of U and V can then be used to estimate the transmitted symbol as it is shown Table 1-1 [11].

Table 1-1 Receiver mapping of phase change to bits [11]

$\Delta\theta$	0	$\pi/2$	π	$3\pi/2$
U	$1/\sqrt{2}$	$-1/\sqrt{2}$	$-1/\sqrt{2}$	$1/\sqrt{2}$
V	$1/\sqrt{2}$	$1/\sqrt{2}$	$-1/\sqrt{2}$	$-1/\sqrt{2}$
Logic(U)=X	1	0	0	1
Logic(V)=Y	1	1	0	0

1.3.2 Optical 16- quadrature amplitude modulation (16-QAM)

In this section, we focus on square-16-QAM which is novel for optical transmission systems and one step ahead of recently investigated DQPSK [13]. Constellation diagram of 16 QAM is shown in Fig.1-4. The data carrying capacity of lightwave communication systems can be increased by a factor of 4 over traditional on-off keyed transmission by employing signals with 16- quadrature amplitude modulation (16-QAM) format. Therefore, 16-QAM offers a high spectral efficiency, which makes it a candidate for future high capacity and high spectrally efficient optical transmission systems. In the next section, the overview of 16-QAM concept is discussed. Following chapters concentrate on square-16-QAM and comparison of different transmitter configurations. Different possible optical transmitters for square-16-QAM are compared with respect to optical and electrical complexity. The homodyne IQ-receiver is also illustrated in Fig.1-5(b). In general, the proposed M-QAM transmitter (Fig.1-5(a)) consists of level generator, modulator driver and an optical

modulator. The conventional optical IQ-modulator is shown in Fig.1-5(a) [11]. The light of a continuous wave (CW) laser is split into two arms. The carrier has to be shifted by 90° in one arm. The orthogonal carriers are then intensity modulated in both arms by Mach-Zehnder-Modulators (MZM), which are biased at the minimum transmission point and driven by four RF driving signal for the case of 16-QAM. In such manner, the in-phase (I) and quadrature (Q) components of the optical multi-level modulation signal are created. After combining them with a 3dB-coupler, the optical M-QAM signals are generated. The role of the level generator is to create the electrical multi-level driving signals from the incoming data stream. The complexity of this component depends on the used modulation format. At receiver side, a homodyne IQ-receiver is used for signal detection. The received signal and the light of a local oscillator (LO) are combined in a 2×4 90° hybrid. The output signals of the 2×4 90° hybrids are detected by two balanced photo-detectors (BD). The resulting electrical in-phase and quadrature signals are then further processed by high-speed digital signal processing.

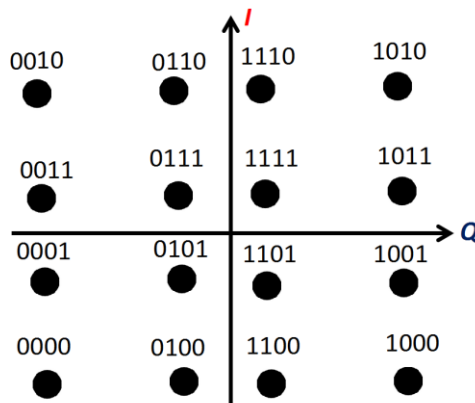
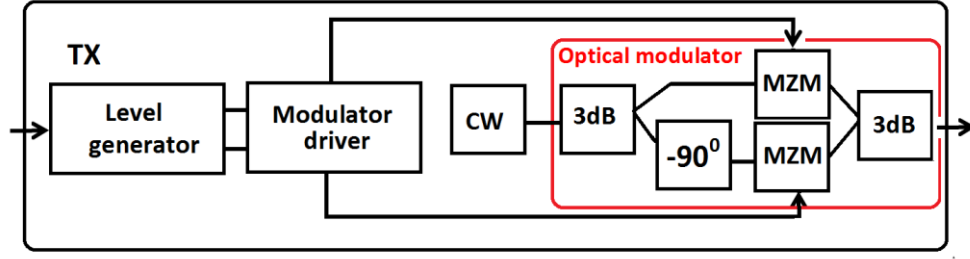
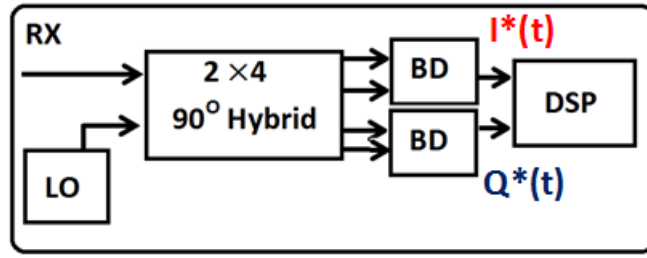


Fig.1-4 Square-16-QAM constellation diagram



(a)



(b)

Fig.1-5 Schematic of a multi-format coherent optical transmission system for high-order modulation.

(a) Transmitter (TX), (b) Receiver (RX), BD: Balanced photo Detector, LO: Local Oscillator [11], [14].

Digital signal processing also allows the implementation of electronic distortion equalization (EDE) to compensate the optical transmission impairments, such as chromatic dispersion, polarization mode dispersion or fiber nonlinearities [11].

1.3.2.1 Comparison of Different Transmitter for Optical Square-16-QAM Modulation

Different possible transmitter structures for optical M-QAM modulation were proposed in [11], [14]. The optical IQ-modulator shown in Fig.1-5(a) is the conventional, but not the only possible structure to generate multi-level optical modulation signals. Another two different

16-QAM transmitters are shown in Fig.1-6. Each structure has its own advantages and drawbacks.

The serial configuration, Fig.1-6(a), is a simple optical part, but the electrical driving signals is a complex part, and has a high number of states (i.e. 12-ary signals are required for phase modulation for square-16-QAM). In [15], it was shown that the optical part can be even more simplified using only one dual-drive MZM. However, this structure requires then 16-ary electrical driving signals at the two MZM electrodes for square-16-QAM. The IQ-transmitters, Fig.1-5(a) and Fig.1-6(b) have more optical complexities are composed of two arms, but the electrical driving signals have smaller number of states. In Fig.1-6(b), the optical part of this structure can be simplified by replacing the single-drive MZMs and phase modulators (PM) by dual-drive MZMs, which can be simultaneously driven in the push-pull mode for intensity modulation and in the push-push mode for phase modulation. However, the electrical driving signals have to be combined before feeding into the MZM inputs [14]. In [14], it was also shown that the choice of the transmitter does not depend only on optical and electrical complexity. In fact, differences in the transmitter setups lead to different properties of the multi-level modulation signals. It should be noted that the following chapters of this thesis only concentrate on conventional IQ-configuration in order to generate optical M-QAM modulation (Fig. 1-5(a)).

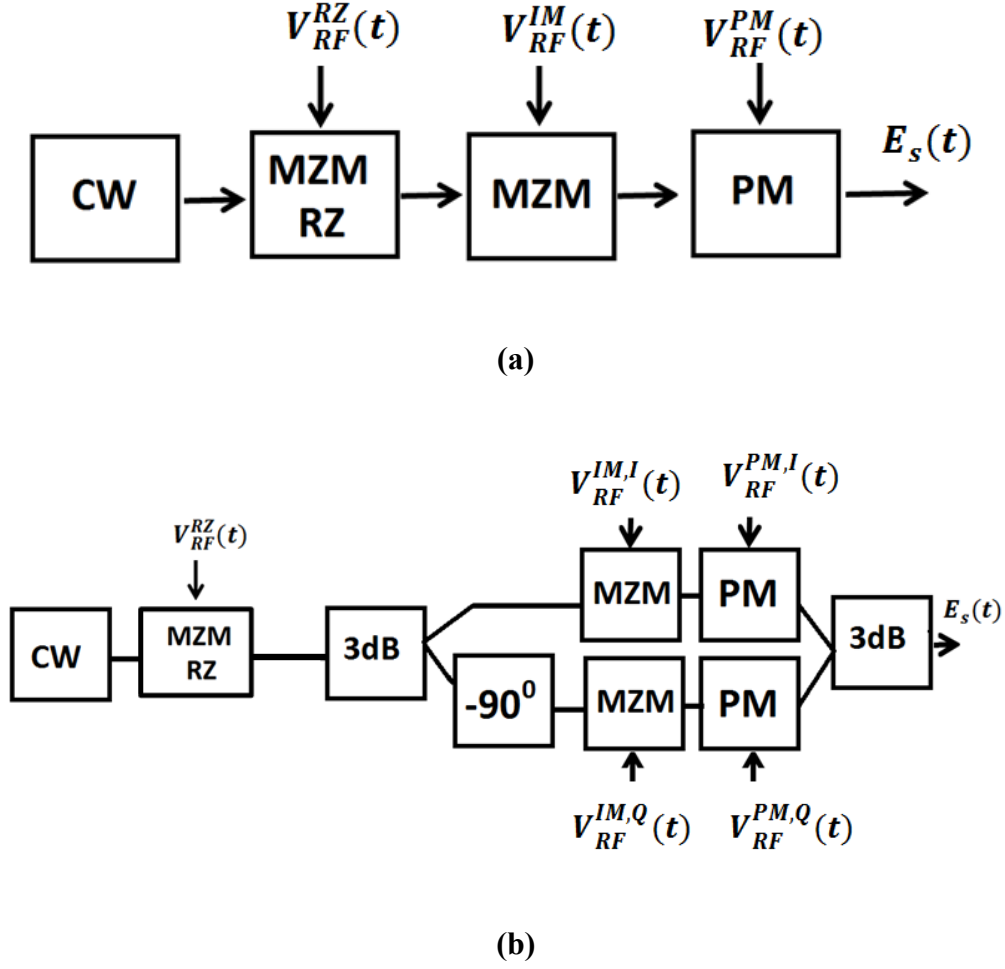


Fig.1-6 Optical multi-level modulation transmitters (a) Serial configuration, (b) IQ-configuration with MZM and PM [13]

1.3.2.2 Homodyne IQ-receiver for 16 QAM

An optical multi-level modulation signal can be detected by a homodyne IQ-receiver with general configuration is shown in Fig.1-5(b) and it is valid for any M-QAM modulation format when neglecting polarization issues. Polarisation issue can be managed by polarization adjustment. The normalized electrical field of the incoming optical multi-level modulation signal and from the local oscillator laser (LO) can be written in complex notation (neglecting transmission impairments) as [11], [14]:

$$E_s(t) = a(t)e^{j\phi(t)}\sqrt{P_s}e^{j(\omega_s t + \phi_s + \phi_{NS})} \quad (1-4)$$

$$= [I(t) + jQ(t)] \cdot \sqrt{\frac{P_s}{2}} \cdot e^{j(\omega_s t + \phi_s + \phi_{NS})} = E_I(t) + jE_Q(t)$$

$$E_{LO} = \sqrt{P_{LO}}e^{j(\omega_{LO} t + \phi_{LO} + \phi_{NLO})} \quad (1-5)$$

In (1-4) and (1-5) P_s and P_{LO} represent the CW power, ω_s and ω_{LO} angular frequencies, ϕ_s and ϕ_{LO} initial phases, and ϕ_{NS} and ϕ_{NLO} the phase noise of signal and LO laser, respectively. $a(t)$ and $\phi(t)$ are the amplitude and phase, and $I(t)$ and $Q(t)$ the in-phase and quadrature components of the transmitted complex envelope. $E_I(t)$ and $E_Q(t)$ are the optical in-phase and quadrature normalized electrical field components of the optical multi-level modulation signal. For homodyne detection, the frequencies of signal and LO are required to be the same. However, in practice this is not easily achieved, and there will always be a small frequency offset due to imperfections in manufacturing, temperature effects and other impairments of the optical hybrid in particular. Therefore, the phase difference between the in-phase (I) and quadrature (Q) components deviate from the ideal 90° separation. Such a deviation is referred to as a phase error. In many systems the phase error results in a significant transmission penalty characterized by a higher bit error rate (BER) and, in optical systems, higher required optical signal to noise ratio (OSNR) for a given BER. Phase error can be corrected with the digital error correction technique which estimates the phase error and applies a correction factor derived from the phase error to one or both of the in-phase and quadrature components of the input signal. Digital phase error correction is implemented in a digital signal processor (DSP).

The signal wave and the LO waves combine in an optical 2 × 4 90° hybrid and yield the output fields [11], [14]:

$$\begin{bmatrix} E1 \\ E2 \\ E3 \\ E4 \end{bmatrix} = \frac{1}{2} \cdot \begin{bmatrix} 1 & 1 \\ 1 & j \\ 1 & -1 \\ 1 & -j \end{bmatrix} \cdot \begin{bmatrix} Es(t) \\ E_{LO}(t) \end{bmatrix} = \begin{bmatrix} \frac{Es(t)}{2} + \frac{ELO}{2} \\ \frac{Es(t)}{2} + j \frac{ELO}{2} \\ \frac{Es(t)}{2} - \frac{ELO}{2} \\ \frac{Es(t)}{2} - j \frac{ELO}{2} \end{bmatrix} \quad (1-6)$$

Detecting E_1 and E_3 with the upper, and E_2 and E_4 with the lower balanced detector (BD), we get the photocurrents [11]:

$$I^*(t) = R \cdot \left\{ \sqrt{\frac{P_S}{2}} \cdot I(t) \cdot \sqrt{P_{LO}} \cdot \cos(\Delta\phi) + \sqrt{\frac{P_S}{2}} \cdot \phi(t) \cdot \sqrt{P_{LO}} \sin(\Delta\phi) \right\} + n_1(t) - n_3(t) \quad (1-7)$$

$$Q^*(t) = R \cdot \left\{ -\sqrt{\frac{P_S}{2}} \cdot I(t) \cdot \sqrt{P_{LO}} \cdot \cos(\Delta\phi) + \sqrt{\frac{P_S}{2}} \cdot \phi(t) \cdot \sqrt{P_{LO}} \sin(\Delta\phi) \right\} + n_2(t) - n_4(t) \quad (1-8)$$

In (1-7) and (1-8), $n_i(t)$, $i=1, \dots, 4$ represents the dark current noise of photodiodes. R is responsivity and $\Delta\phi$ is the phase error due to frequency offset. Phase offset and laser phase noise is given by [11]:

$$\Delta\phi = (\omega_{LO} - \omega_s)t + (\phi_{LO} - \phi_s) + (\phi_{NLO} - \phi_{NS}) \quad (1-9)$$

By assuming zero phase error and neglecting the shot noise, Eqs (1-7) and (1-8) reduce to [11]:

$$I^*(t) = R \cdot I(t) \cdot \sqrt{\frac{P_S}{2}} \cdot \sqrt{P_{LO}} \quad (1-10(a))$$

$$Q^*(t) = R \cdot Q(t) \cdot \sqrt{\frac{P_S}{2}} \cdot \sqrt{P_{LO}} \quad (1-10(b))$$

From (1-10 (a)) and (1-10(b)), we can see that the in-phase and quadrature components of the transmitted complex envelope, $I(t)$ and $Q(t)$ are obtained separately in the two arms for zero phase error. Therefore, homodyne IQ-receiver (coherent receiver) is very suited to detect optical multi-level modulation signals.

1.4 Wavelength Conversion Technologies

Wavelength conversion is an important function in Wavelength Division Multiplexing (WDM) network, as it enables better utilization of bandwidth and reduces blocking probabilities, which is caused by the factors of insufficient network resources such as wavelength. Different wavelength conversion techniques are discussed in detail in the following sections.

1.4.1 Optoelectronic (O/E-E/O) Wavelength Conversion

In this approach, the input signal at the wavelength of λ_1 is required to be converted into an electrical bit pattern, and then amplification and reshaping are performed in the electrical domain before the signal is converted to an optical signal at the desired wavelength λ_2 (shown in Fig.1-7) [16], [17]. This technique is relatively easy to implement as it uses standard components. It has other advantages including insensitivity to input polarization and the possibility of amplification. Among its disadvantages is limited transparency to bit rate and data format, limited by the electronics employed.

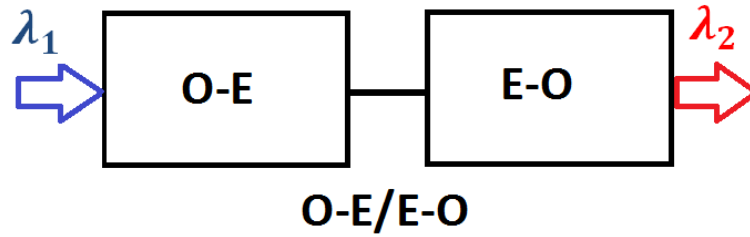


Fig.1-7 O/E- E/O wavelength conversion method

1.4.2 All optical wavelength conversion

Optical gating and Wave-mixing are two wavelength conversion techniques that can be considered to be all-optical. In these all-optical methods, the optical signal is allowed to remain in the optical domain throughout the conversion process. It should be noted that in these methods, all-optical, refers to the fact that there is no O/E conversion involved.

1.4.2.1 Optical Gating

The useful reference on the subject is [18]. Optical gating is a series of techniques using cross-modulation to achieve wavelength conversion (Fig.1-8). These techniques utilize active semiconductor optical devices such as SOA. Cross modulation methods can be separated into cross-gain modulation (XGM) and cross-phase modulation (XPM). The principle behind using an SOA in the cross-gain modulation (XGM) scheme is shown in Fig.1-8(a). The intensity-modulated input signal modulates the gain in the SOA due to gain saturation. A continuous-wave (CW) signal at the desired output wavelength (λ_c) is modulated by the gain variation so that it carries the same information as the original input signal.

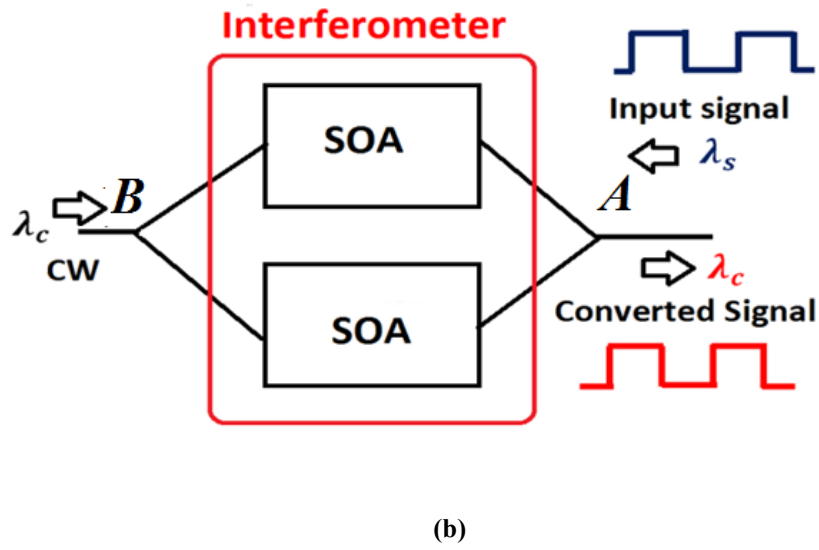
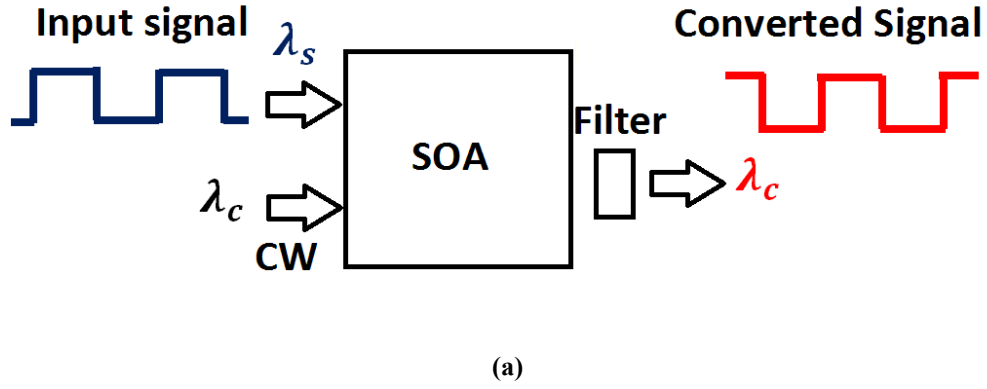


**Fig.1-8 Different types of optoelectronic wavelength converters (a) Cross gain modulation (XGM)
(b) Cross phase modulation (XPM)**

The signal and the CW beam can be either co- or counterpropagating. A counterpropagating approach has the advantage of not requiring the filter [18]. A typical XGM SOA- based converter is polarization independent but suffers from an inverted output signal. Fig.1-8(b) shows cross-phase modulation using an SOA for wavelength conversion which makes it possible to generate a non-inverted output signal with improved extinction ratio. The XPM relies on the fact that the refractive index in the active region of an SOA depends on the carrier density. Therefore, when an intensity-modulated signal propagates through the active region of an SOA it depletes the carrier density, thereby modulating the refractive index,

which results in phase modulation of a CW beam propagating through the SOA simultaneously. This phase modulation can be converted into intensity modulation by using an interferometer such as a Mach-Zehnder interferometer (MZI). Figure 1-8(b) shows one possible configuration of a wavelength converter using cross-phase modulation [18]. Both arms of the MZI have exactly the same length, with each arm incorporating an SOA. The signal is sent in at one end (A) and the probe at the other end (B). The couplers in the MZI are designed with an asymmetric coupling ratio $\gamma \neq 0.5$. When the signal is present, it induces a phase change in each amplifier. The phase change induced by each amplifier on the probe is different because different amounts of signal power are present in the two amplifiers. The MZI translates this relative phase difference between its two arms on the probe into an intensity-modulated signal at the output.

1.4.2.2 Wave Mixing

Wavelength conversion methods using coherent effects are typically based on wave-mixing properties (Fig.1-9) [19]. Wave-mixing arises from a nonlinear optical response of a medium when more than one wave is present and results in the generation of new waves with intensities proportional to the product of the interacting wave intensities. Wave-mixing is transparent to phase and amplitude information. It is also the only approach that offers strict transparency to baudrate. Four-wave mixing (FWM) is a third-order nonlinearity in silica fibers, which causes three optical waves of frequencies f_i and f_j and f_k ($k \neq i, j$) to combine to generate a new (fourth) wave with the frequency equal to $f_{ijk} = f_i \pm f_j \pm f_k$. FWM is also achievable in other passive waveguides such as semiconductor waveguides and in an active medium such as semiconductor optical amplifier (SOA). Four-wave mixing is a promising technique for wavelength conversion in optical networks owing to its ultrafast response and high transparency to bit rate and modulation format. In this thesis, FWM in SOA is

considered for the purpose of wavelength conversion. By using this technique, the four-wave mixing power is amplified by using an SOA and if we have a signal at frequency f_s and a pump at frequency of f_p , then four-wave mixing will generate new converted signals (idlers) at frequencies $2f_p - f_s$ and $2f_s - f_p$, as long as all these frequencies lie within the amplifier bandwidth (Fig.1-9).

The main advantage of four-wave mixing is that it is truly transparent because the effect does not depend on the modulation format and the bit rate. The disadvantages are that the other waves must be filtered out at the SOA output, and the conversion efficiency goes down significantly as the wavelength detuning between the signal and converted idler is increased. Regardless of the FWM conversion efficiency; there is also one major drawback using SOA-based FWM and that is the issue of the large phase-noise transfer between the pump(s) and the converted idlers. This issue is of crucial importance when converting advanced modulation formats such as DQPSK and M-QAM signals using FWM because the increased phase uncertainty at the receiver degrades the overall system performance. Detailed investigations of SOA-based all-optical wavelength convertors are discussed in the following chapter.

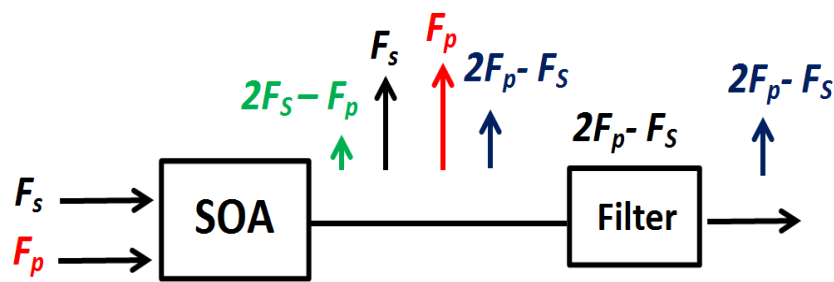


Fig.1-9 All- optical Wavelength Conversion using Four-Wave Mixing in a Semiconductor Optical Amplifier

1.5 Summary and conclusion

Future optically switched wavelength division multiplexed (WDM) networks will require all optical wavelength conversion to avoid contention in a node when two signals on the same wavelength are being switched to the same output fiber. Wavelength conversion can be used in WDM networks to improve efficiency. These future networks will also employ advanced modulation formats with data encoded in the amplitude as well as the phase of the optical carrier such as differential quadrature phase shift keying (DQPSK) and 16-quadrature modulation (QAM). In this chapter, DQPSK and M-QAM modulation formats were introduced and different transmitters for optical square M-QAM modulation were also presented, with homodyne IQ-receiver used for the detection of M-QAM. Different wavelength conversion techniques such as OEO, cross phase modulation, cross gain modulation and four wave mixing were also discussed. In order to perform wavelength conversion operations on DQPSK and M-QAM signals, a coherent nonlinear process, such as four-wave mixing (FWM), is required. Four-Wave Mixing (FWM) is a promising technique for wavelength conversion in optical networks owing to its ultrafast response and high transparency to bit rate and modulation format. Irrespective of the FWM conversion efficiency; the issue of phase noise transfer between pump(s) and idlers is of crucial importance when converting advanced modulation formats such as DQPSK and M-QAM signals using FWM. This issue will be discussed in more detail in the next chapter.

Bibliography

- [1] Cisco Visual Networking Index: Forecast and Methodology, 2013–2018. Available from <http://www.cisco.com>.
- [2] J.G. Proakis, M. Salehi, 'Digital Communications (5th edition), ISBN-10: 0072957166, McGraw-Hill, 2008
- [3] E. Simsarian, J. Gripp, A.H. Gnauck, G. Raybon, P.J. Winzer, "Fast-tuning 224-Gb/s Intradyne receiver for optical packet networks," presented at the Optical Fiber Communication Conf., *OFC*, San Diego, CA, USA, 2010 , paper PDPB5.
- [4] S. Shinada, H. Furukawa, N. Wada, "Huge capacity optical packet switching and buffering," *Optics Express*, vol. 19, no. 26, pp.B406–B414, 2011.
- [5] G. Chang, J. Yun, Y.K.K. Yeo, A. Chowdhury, Z. Jia, "Enabling technologies for next-generation optical packet-switching networks'', *Proceedings of the IEEE*, vol. 94, no.5, pp. 892 - 910, 2006.
- [6] P. J. Winzer and R. -J. Essiambre, "Advanced optical modulation formats," presented at European Conference on Optical Communication, ECOC, Rimini, Italy, 2003, paper Th2.6.1.
- [7] G. Charlet, "Progress in optical modulation formats for high-bit rate WDM transmissions," *IEEE J. Sel. Top. Quantum Electron*, vol.12, no. 4, pp.469–483, 2006.
- [8]. A. H. Gnauck and P. J. Winzer, "Optical phase-shift-keyed transmission," *J. Lightwave Technol.* vol. 23, no.1,pp.115– 130, 2005.
- [9] A. H. Gnauck, R. W. Tkach, A. R. Chraplyvy, and T. Li, "High capacity transmission systems," *J Lightwave Technol.*, vol. 26, no. 9, pp. 1032–1045, 2008.
- [10] A. H. Gnauck, P. J. Winzer, S. Chandrasekhar, X. Liu, B. Zhu, and D. W. Peckham, "Spectrally efficient long-haul WDM transmission using 224-Gb/s polarization-multiplexed 16-QAM," *J. Lightwave Technol.*, vol. 29, no. 4, pp. 373–377, 2011.
- [11] M.Seimetz, ' High-Order Modulation for Optical Fiber Transmission', ISBN:978-3-540-93770-8, Springer, 2009.
- [12] R.A. Griffin and A.C. Carter, "Optical differential quadrature phaseshift key (ODQPSK) for optical transmission", presented at the Optical Fiber Communication Conf, *OFC*, CA, USA, paperWX6

- [13] C. Wree, J. Leibrich, W. Rosenkranz, "RZ-DQPSK format with high spectral efficiency and high robustness towards fiber nonlinearities", presented at European Conference on Optical Communication, *ECOC*, Copenhagen, Denmark, 2002, paper 9.6.6.
- [14] M. Seimetz, 'Multi-format Transmitters for Coherent Optical M-PSK and M-QAM Transmission', presented at International Conference on Transparent Optical Networks, *ICTON*, Barcelona, 2005, Paper Th.B1.5.
- [15] K.P. Ho, H.-W. Cui, "Generation of Arbitrary Quadrature Signals Using One Dual-Drive Modulator", *J. of Lightwave Technol.*, Vol. 23, no. 2, pp. 764-770, 2005.
- [16] J. C. Simon, L. Billess, A. Dupas and L. Bramerie , "All optical regeneration techniques", presented at European Conference on Optical Communication , *ECOC*, Nice, France, 1999, paper 256.
- [17] D. Campi, C. Coriasso, "Wavelength Conversion Technologies", *Photonic Network Communications* ,vol. 2, no.1,pp. 85-95, 2000
- [18] M.J. Connelly, 'Semiconductor Optical Amplifiers', ISBN 0-7923-7657-9, Kluwer Academic Press, 2002.
- [19] B. Mukharjee, 'Optical WDM Networks', ISBN 978-0-387-29188-8, Springer, 2006.

Chapter 2- All- Optical wavelength conversion based on Four Wave Mixing in Semiconductor optical Amplifier

2.1 Introduction

Four wave mixing (FWM) in semiconductor optical amplifiers is an important tool for all-optical wavelength conversion. In this chapter, the main applications of SOA as a nonlinear optical component concentrating on FWM are explained. Then, the effect of phase noise transfer from the pump(s) to generated idlers based on single pump (i.e. degenerate FWM) and dual pumps (nondegenerate FWM) are discussed. It should be noted that in this thesis, the SOA is an important device to implement wavelength conversion and the detailed derivation of the semiconductor equations as well as a deep description of the microscopic theory behind the optoelectronic processes involved is out of the scope of this work. Many references are available about those topics and will be introduced when necessary in this and subsequent chapters.

2.2 Principle of Semiconductor optical amplifier

The schematic of a Semiconductor Optical Amplifier (SOA) is shown in Fig.2-1 [1], [2]. A semiconductor optical amplifier (SOA) is an optical amplifier based on a semiconductor gain medium. A SOA is very similar to a laser diode where the end mirrors have been replaced

with anti-reflection coatings (with no feedback). SOAs amplify incident light based on stimulated emission. An external electric pump current injects electrons (carriers) into the semiconductor active region which can recombine in radiative or non-radiative forms. In the case of radiative recombination of an electron-hole pair a photon is emitted. There are three main radiative recombination mechanisms in semiconductors: spontaneous emission, stimulated emission and stimulated absorption [1]. When the semiconductor is injected electrically by a current source, the number of carriers in the conduction band exceeds that in the valence band, which creates a population inversion and an incident photon can stimulate the transition of an electron from the conduction band to the valence band. In this case, semiconductor exhibits optical gain. The stimulated emission is presented by the emission of a photon that has the same properties (frequency, phase and direction) of the incident photon. There is also a non-zero probability that an electron in the conduction band recombines spontaneously with a hole in the valence band. This recombination occurs with the emission of a photon with random phase and direction. Those random generated photons can be further amplified through stimulated emission and are the main noise source in semiconductor optical amplifiers. This process is known as amplified spontaneous emission (ASE) noise.

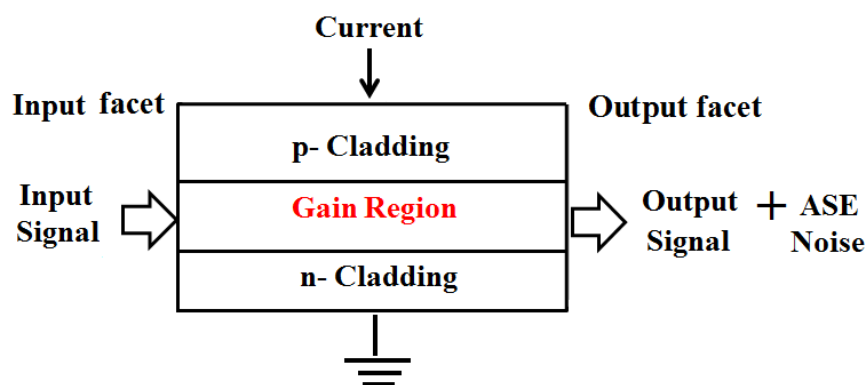


Fig.2-1 Schematic of a SOA with the amplification process

In the case of stimulated absorption, an incoming photon with energy higher than the bandgap energy can be absorbed, resulting in the creation of an electron in the conduction band by raising one electron from the valence band.

The important parameters used to characterize a SOA are gain, gain bandwidth, saturation output power and ASE noise. The optical gain of the unit is controlled by the SOA current and it is the factor which the input signal is amplified. It is measured as the ratio of output power to input power (in dB). The gain bandwidth defines the range of bandwidth where the amplification operates. A wide gain bandwidth is desirable to amplify a wide range of signal wavelengths. The saturation output power is the maximum output power achievable after amplification beyond which no amplification is reached. As the input power to the SOA is increased, the gain decreases due to depletion in the carrier density of the active region of the SOA. As it is shown in Fig.2-2, the saturation output power is defined as the optical power at which the gain drops by 3 dB from the small signal value. The typical value of saturation output power is in the range of 5-20dBm [1].

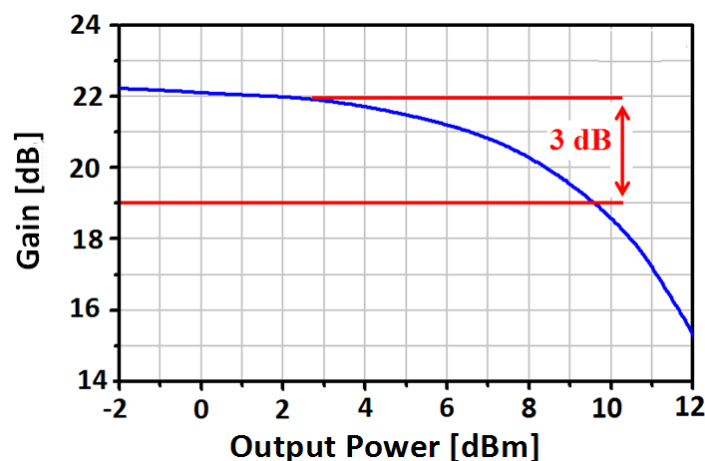


Fig.2-2 SOA gain vs. output power

2.3 Four Wave Mixing in Semiconductor Optical Amplifier

SOAs have been used in optical communication systems operating at signal wavelengths near 1.5 μm , and offering a gain of up to $\approx 30\text{dB}$ with the polarisation sensitivity less than 2 dB [3-6]. Today, the most attractive applications of SOA are associated with their nonlinear optical properties. As was discussed in section 1.4, the injection of light into an SOA changes the carrier density and carrier distribution within the energy bands which causes modulation of the gain and refractive index in the active region of the amplifier, and results in cross gain modulation and cross phase modulation. Another approach, and probably the most extensively studied, to apply all optical wavelength conversion is the four-wave mixing process within semiconductor optical amplifiers.

FWM in SOAs [7] offers numerous advantages to the system designer. Firstly, unlike cross-phase modulation [8] and cross-gain modulation wavelength conversion techniques [9], [10], FWM preserves both the phase and amplitude information; also FWM is transparent to the signal baud rate. In the next section, the mechanisms behind FWM are discussed. The details of modeling of wavelength conversion using SOAs based on inter-band process include carrier density pulsations (CDP) and intraband processes of carrier heating (CH), and spectral hole burning (SHB) and internal scattering loss are investigated.

2.4 SOA model

2.4.1 Basic SOA model based on interband parameters

For a detailed description of the fundamental aspects of FWM in SOA the reader might refer for example to [7], [11-14]. FWM in SOAs is created due to the creation of complex gain and refractive index gratings [7], [12], [13] primarily caused by the beating between the signal and the nearest co-propagating pump. The scenario is shown in Fig.2-3 where three input

waves co-propagate in an SOA, pump 1 (P_1), pump 2 (P_2) and input DQPSK or M- QAM signal (S). A gain grating is caused by the beating between the signal and pump 1 (There is also a gain grating created by the two pumps, though this is much weaker than gain grating between signal and P_1). The converted idlers are created by the scattering of the pumps due to the gain grating. When the detuning between signal and P_1 is in the order of tens of GHz, interband effect which involves the recombination of carrier and hole in the material conduction and valence bands are dominant. The characteristic time of interband process is carrier lifetime which is in the order of hundreds of picoseconds.

The SOA gain dynamics due to the interband process can be modelled according [15]:

$$\frac{dh}{dt} = \frac{h_0 - h(t)}{\tau_s} - \frac{[\exp\{h(t)\} - 1] |E_{in}(t)|^2}{P_{sat} \tau_s} \quad (2-1)$$

where the second term on the right hand side of (2-1) describes SOA gain depletion due to simulated emission and first term describes gain recovery back to unsaturated value determined by DC bias current. h is the net gain coefficient integrated over the entire length of the SOA, i.e. $h(t) = \int_0^L g(z, t) dz$, h_0 is the unsaturated device gain under constant current bias, τ_s is the carrier lifetime and P_{sat} is the saturation power and E_{in} is the input optical field, normalised such that $|E_{in}|^2$ is the optical power.

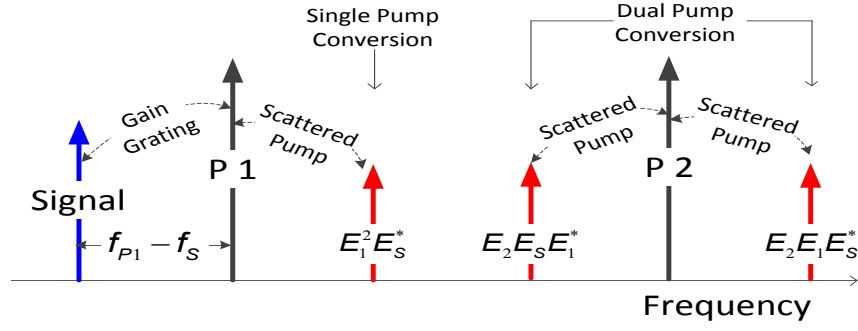


Fig.2-3 Spectral placement of the pumps, input signal and converted idlers for the single pump and dual pump wavelength converter.

2.4.2 Modified SOA model based on interband and intraband parameters

FWM in SOAs arises from different physical process. As was discussed in the previous subsection, the intraband process is dominant at the detuning of signal and pump in the order of tens of GHz. The intraband effects are associated with basically two phenomena. Spectral-hole burning (SHB) and carrier heating (CH). SHB refers to the burning of a spectral hole in the carrier distribution due to stimulated emission causing a deviation from the Fermi distribution. SHB is the formation of a dip in the gain spectrum [7, 12, 13, 16, 18]. The dip occurs by the recombination of electrons and holes at a specific energy and the subsequent redistribution of carrier energies due to carrier-carrier scattering. Carrier-carrier scattering is the average time taken by carrier population to reach a heated equilibrium from initial non-heated equilibrium. The scattering process takes place on a time scale of the order of 50-100 fs and leads to a dip width of about 20-40 meV [1]. It also ensures that the temperature equilibrium is established among the carriers within 50- 100 fs [1]. Additionally, free carriers at low-energy levels are removed by stimulated emission, causing the carrier distribution to be artificially heated, this phenomenon is called carrier heating (CH). The characteristic time is due to carrier-phonon scattering, and it is in the order of several hundred femtoseconds. In

this subsection, the process of FWM is based on inter- and intra-band contributions to the nonlinear gain dynamics in SOAs; thus the SOA model is modified to include CH and SHB effects in addition to the inter-band process (CDP) [7],[12-13]. By considering intraband parameters of SOA, the rate equations describing the spatially-integrated gain contributions from CDP, CH and SHB are given by [16-18]:

$$\frac{dh_{cdp}(t)}{dt} = \frac{h_0 - h_{cdp}(t)}{\tau_s} - \frac{[\exp\{h_{cdp}(t)\} - 1]|E_{in}(t)|^2}{\tau_s P_{sat}} \quad (2-2)$$

$$\frac{dh_{ch}(t)}{dt} = -\frac{h_{ch}}{\tau_{ch}} - \frac{\varepsilon_{ch}(\exp\{h_{cdp}\} - 1)|E_{in}|^2}{\tau_{ch}} \quad (2-3)$$

$$\frac{dh_{shb}(t)}{dt} = -\frac{h_{shb}}{\tau_1} - \frac{\varepsilon_{shb}(\exp\{h_{cdp}\} - 1)|E_{in}|^2}{\tau_1} - \frac{dh_{ch}}{dt} - \frac{dh_{cdp}}{dt} \quad (2-4)$$

The total overall optical power gain of the SOA is given by:

$$G(t)_{tot} = \exp[h_{cdp}(t) + h_{ch}(t) + h_{shb}(t)] \quad (2-5)$$

h_0 is the unsaturated integrated gain coefficient determined by the constant current; τ_1 , τ_{CH} and τ_s are carrier-carrier scattering time, carrier-phonon scattering time and carrier lifetime, respectively. E_{in} is the input optical field and is normalised such that $|E_{in}|^2$ represents the input optical power to the SOA, P_{sat} is the saturation power and the other parameters, ε_{ch} and ε_{shb} , are the nonlinear gain suppression factors due to CH and SHB with the units of w^{-1} . Under strong CW gain saturation conditions, the average device gain is smaller than h_0 , thus allowing the last term on the right hand side (RHS) of Eq (2-4) to be neglected. It will be discussed in chapter 4.2 in more detail that under certain circumstance, Eqs (2-3) and (2-4)

can be solved quite efficiently allowing the CH and SHB contributions to be written directly as:

$$h_{ch}(t) = -\varepsilon_{ch} \left(\exp\{h_{cdp}(t)\} - 1 \right) |E_{in}|^2 \quad (2-6)$$

$$h_{shb}(t) = -\varepsilon_{shb} \left(\exp\{h_{cdp}(t)\} - 1 \right) |E_{in}|^2 \quad (2-7)$$

2.4.3 Improved SOA model including internal loss

As a next step of this thesis, the SOA model is modified to accurately include for the internal scattering losses [19] which is necessary for the case of large pump powers. This revised, lumped SOA model in [19] was found to replicate the output powers of the pumps and idlers from FWM experiments using highly-nonlinear SOAs for optical signal processing functions [17].

SOA gain dynamics due to the inclusion of SOA internal loss as well as inter-band and intraband contributions can be modeled according to [13, 16-19, 21]:

$$\frac{dh_{cdp}(t)}{dt} = \frac{h_0 - h_{cdp}(t)}{\tau_s} - \frac{h_{cdp}}{h_{cdp} - \alpha_{loss}L} \cdot \frac{\left[\exp\{h_{cdp}(t) - \alpha_{loss}L\} - 1 \right] |E_{in}(t)|^2}{\tau_s P_{Sat}} \quad (2-8)$$

$$h_{ch}(t) = -\varepsilon_{ch} \frac{h_{cdp}(t)}{h_{cdp}(t) - \alpha_{loss}L} \left(\exp\{h_{cdp}(t) - \alpha_{loss}L\} - 1 \right) |E_{in}|^2 \quad (2-9)$$

$$h_{shb}(t) = -\varepsilon_{shb} \frac{h_{cdp}(t)}{h_{cdp}(t) - \alpha_{loss}L} \left(\exp\{h_{cdp}(t) - \alpha_{loss}L\} - 1 \right) |E_{in}|^2 \quad (2-10)$$

where E_{in} is the normalized total input optical field such that $|E_{in}(t)|^2$ represents the SOA input optical power. $\alpha_{loss}L$ is the internal scattering coefficient, L represents the SOA length. ε_{ch} and ε_{shb} are the nonlinear gain compression factors due to carrier heating and spectral hole burning, and P_{sat} is the gain saturation. It must be added that in this thesis, the SOA model is solved numerically using the modified Euler method.

2.5 Theory of Phase noise due to FWM in SOA

The output of semiconductor laser is not perfectly monochromatic but rather exhibits some phase noise [22-25]. This leads to a finite linewidth of the laser output. For simple cases, this fundamental limit for the linewidth was calculated by Schawlow and Townes [24]. It was then later found by Henry [24] that the increased linewidths result from a coupling between intensity and phase noise, caused by a dependence of the refractive index on the carrier density in the semiconductor. Henry introduced the linewidth enhancement factor (also called Henry factor or alpha factor) to quantify this amplitude–phase coupling mechanism; essentially, α is a proportionality factor relating phase changes to changes of the gain:

$$\Delta\phi = \frac{\alpha}{2}\Delta g \quad (2-11)$$

The factor 1/2 serves to convert the change of power gain Δg to the change of amplitude gain. It is also found by Henry that the linewidth of the laser is increased by the factor $(1+\alpha^2)$, which turned out to be in agreement with experimental result [24,25]. Phase noise can be quantified by the power spectral density $S_\phi(f)$ [25], having units of rad^2/Hz (or simply Hz^{-1} , as radians are dimensionless). Phase noise is directly related to frequency noise, as the instantaneous frequency is essentially the temporal derivative of the phase. For example, white (frequency-independent) frequency noise corresponds to phase noise with $S_\phi(f) \approx 1/f^2$.

When the four-wave mixing (FWM) process is used for all-optical wavelength conversion of advanced modulation formats where information is encoded on the phase and amplitude of the optical carrier, it is important to understand the phase noise transfer from the pump(s) to the generated idlers. The spectral broadening of the generated idlers in FWM was first reported in [26] and studied in more detail in [27] based on quantifying of the linewidth ($\Delta\omega$). However, direct measurement of the phase error variance ($\sigma_{\Delta\phi}^2$) has been possible using coherent detection in [28-30]. It should be considered that in this thesis, only the case of phase noise generated from white frequency modulation (FM) noise is considered and thus the increasing low frequency FM-noise (also termed $1/f$ noise) is neglected. In this case, $\Delta\omega$ and $\sigma_{\Delta\phi}^2$ have a linear relation [27]. Therefore, the relation between the linewidths of the signal and the generated idlers are similar to those between their phase error variances [30]. It was shown theoretically with confirmed experimental results using CW pumps and signal in that the linewidth of the converted idler for the case of degenerate (signal pump) FWM is [27],[30]:

$$\Delta\omega_{Idler}=4\Delta\omega_{Pump} + \Delta\omega_{Signal} \quad (2-12)$$

For the case of nondegenerate (dual pump) FWM, the linewidth of the converted idler equals:

$$\Delta\omega_{Idler} = \Delta\omega_{Pump-1} + \Delta\omega_{Pump-2} + \Delta\omega_{Signal} \quad (2-13)$$

This phase noise transfer is likely to cause a deleterious effect for signals with phase encoding because the phase noise transfer will induce an uncertainty in the phase of the converted signal; thus the issue of phase noise transfer cannot be neglected as it is likely to determine the choice of laser to be employed as the pump in such wavelength conversion schemes. In the following chapters, the required optical signal to noise ratio (OSNR) and laser phase noise (linewidth) limits are calculated that would allow for wavelength

conversion of advanced modulation formats including DQPSK, 16QAM and 64-QAM signals using FWM with acceptable bit error rates (BER) of 10^{-3} and 10^{-4} .

2.6 Summary and conclusion

In this chapter, the principle of semiconductor optical amplifier operation has been reviewed. The details of modelling wavelength conversion using SOAs based on inter-band carrier density pulsations (CDP), intraband carrier heating (CH), and spectral hole burning (SHB) effects are investigated. As a next step, the SOA model is modified to accurately include for the internal scattering losses [20] which is necessary for the case of large pump powers. In addition, the effect of phase noise transfer from the pump(s) to generated idlers base on single pump (i.e. degenerate FWM) and dual pumps (nondegerate FWM) are discussed.

Bibliography

- [1] M.J. Connelly, ‘Semiconductor Optical Amplifiers’, ISBN 0-7923-7657-9, Kluwer Academic Press, 2002.
- [2] N.K. Dutta, Q.Wang , ‘Semiconductor Optical Amplifiers’, ISBN 981-256-397-0, World scientific Press, 2013.
- [3] R. Schimpe, B. Bauer, C. Schanen, G. Franz, G. Kristen, and S. Prohl, “1.5 μm InGaAsP tilted buried-facet optical amplifier’, presented at Conf on Lasers and Electro-Optics/International Quantum Electronics ,*CLEO ’91*, 1991.
- [4] P. Doussiere, F. Pommerau, D. Leclerc, R. Ngo, M. Goix, T. Fillion, P. Bousselet, and G. Laube, “Polarization independent 1550 nm semiconductor optical amplifier packaged module with 29 dB fiber to fiber gain,” in *Optical Amplifiers and their Applications, OAA ’95*, Tech. Dig, pp. 119–122, .., 1995.
- [5] F. Girardin, J. Eckner, G. Guekos, R. Dall’ Ara, A. Mecozzi, A. D’Ottavi, F. Martelli, S. Scotti, and P. Spano, “Low noise and very high efficiency four-wave mixing in 1.5 mm long semiconductor optical amplifiers,” *IEEE Photon. Technol. Lett*, vol. 9, no.6, pp. 746–748, June 1997.
- [6] A. E. Kelly, I. F. Lealman, L. J. Rivers, S. D. Perrin, and M. Silver, “Low noise figure (7.2 dB) and high gain (29 dB) semiconductor optical amplifier with a single layer AR coating,” *Electron. Lett.*, vol. 33, no.6 , pp. 536–538, 1997.
- [7] G. P. Agrawal, “Population pulsations and nondegenerate four-wave mixing in semiconductor lasers and amplifiers,” *J. Opt. Soc. Amer. B*, vol. 5, no.1 , pp. 147–158, 1988.
- [8] J. Yu and P. Jeppesen, ‘80-Gb/s Wavelength Conversion Based on Cross-Phase Modulation in High-Nonlinearity Dispersion-Shifted Fiber and Optical Filtering’’, *IEEE Photon. Tech Lett*. vol. 13, no. 8, pp. 833 – 835, 2001.
- [9] E. Tangdionga, Y. Liu, H. de Waardt, G.D. Khoe and H.J.S. Dorren, “Demultiplexing 160/320 Gb/s to 40 Gb/s using a single SOA Assisted by an Optical Filter,” presented at the Optical Fiber Communication Conf., *OFC*, Anaheim CA., 2006, paper OTuB5,
- [10] J. Leuthold, D. M. Marom, S. Cabot, J. J. Jaques, R. Ryf, and C. R. Giles, “All-Optical Wavelength Conversion Using a Pulse Reformatting Optical Filter”, *IEEE Journ. of Lightw. Tech*, vol. 22, no. 1, pp. 186- 191, 2004.

- [11] J. Zhou, N. Park, J. W. Dawson, K. J. Vahala, M. A. Newkirk, and B. I. Miller, “Terahertz four-wave mixing spectroscopy for study of ultrafast dynamics in a semiconductor optical amplifier,” *Appl. Phys. Lett.*, vol. 63,no.9 , pp. 1179–1181, 1993.
- [12] A. Uskov, J. Mørk, and J. Mark, “Wave mixing in semiconductor laser amplifiers due to carrier heating and spectral-hole burning”, *IEEE J. Quantum Electron.*, vol. 30, no.8, pp. 1769–1781, 1994.
- [13] A. Mecozzi, S. Scotti, A. D’Ottavi, E. Iannone, and P. Spano, “Four wave mixing in traveling-wave semiconductor amplifiers,” *IEEE J. Quantum Electron.*, vol. 31, no.4, pp. 689–699, 1995.
- [14] I. Koltchanov, S. Kindt, K. Petermann, S. Diez, R. Ludwig, R. Schnabel, and H. G. Weber, “Gain dispersion and saturation effects in four-wave mixing in semiconductor laser amplifiers,” *IEEE J. Quantum Electron.*, vol. 32, no.4 , pp. 712–720, 1996.
- [15] G. P. Agrawal and N. A. Olsson, “Self phase modulation and spectral broadening of optical pulses in semiconductor laser amplifiers,” *IEEE J. Quantum Electron.*, vol. 25, no. 11, pp. 2297–2306, 1989.
- [16] A.Mecozzi and J.Mørk “Saturation Effects in Nondegenerate Four-Wave Mixing Between Short Optical Pulses in Semiconductor Laser Amplifiers”, *IEEE J. of Sel. Top. in Quant. Electron*, vol. 3, no.5, 1997.
- [17] D.Cassioli, S. Scotti, and A. Mecozzi “A Time-Domain Computer Simulator of the Nonlinear Response of Semiconductor Optical Amplifiers,” *IEEE J. of Quant. Electron*, *IEEE*, vol. 36, no. 9, 2000.
- [18] S. T Naimi, S. O Duill, and L.P. Barry, ‘Detailed Investigation of the Pump Phase Noise Tolerance for the Wavelength Conversion of 16-QAM Signals Using FWM,” *IEEE/OSA JOCN*, vol. 6, no. 9, pp. 793-800, 2014.
- [19] S. P. Ó Dúill, L.P. Barry “Improved reduced models for single-pass and reflective semiconductor optical amplifiers,” *J. Opt. Commun.*, vol. 334, no.1, pp. 170-173, 2015.
- [20] R. P. Webb, M. Power, and R. J. Manning, “Phase-sensitive frequency conversion of quadrature modulated signals,” *OSA Opt. Expr.* , vol. 21, no. 10, pp. 12713-12727, 2013.
- [21] D. Marcuse, “Computer simulation of FSK laser spectra and of FSK-to-ASK conversion,” *J. Lightwave Technol.*, vol. 8, no. 7, pp. 1110–1122, 1990.
- [22] A. L. Schawlow, C.H. Townes, ‘Infrared and optical maser’, *Physical Review*, vol. 112, pp. 1940-1949, 1958.

- [23] C.H. Henry, ‘Theory of the linewidth of semiconductor lasers’, *IEEE Journal of Quantum Electronic*, vol. QE-18, no.2 , pp. 259 - 264, 1982.
- [24] C.H. Henry, ‘Phase noise in semiconductor lasers’, *IEEE/OSA Journal of Lightwave Technology*, vol. LT-4 , no. 3, pp. 298 - 311, 1986
- [25] Tam N. Huynh, 2014, ‘Spectrally Efficient Modulation Formats for Fast Reconfigurable Optical Networks’.*Ph.D. thesis*, Dublin City University.
- [26] K. O. Hill, D. C. Johnson, B. S. Kawasaki, and R. I. MacDonald, “CW three wave mixing in single mode optical fibers,” *J. App. Phys.* vol. 49, pp.5098–5106 ,1978.
- [27] R. Hui and A. Mecozzi, “Phase noise of four-wave mixing in semiconductor lasers,” *Appl. Phys. Lett*, vol.60,pp. 2454– 2456 , 1992.
- [28] K. Kikuchi, “Characterization of semiconductor-laser phase noise and estimation of bit-error rate performance with low-speed offline digital coherent receivers,”, *Opt. Express*, vol. 20, no.5, pp. 5291–5302, 2012.
- [29] T. N. Huynh, L. Nguyen, and L. P. Barry, “Delayed self-heterodyne phase noise measurements with coherent phase modulation detection,” *IEEE Photon. Technol. Lett*, vol. 24, no. 4, pp. 249–251, 2012.
- [30] A. P. Anthur, R. T. Watts, K. Shi, J. O’ Carroll, D. Venkitesh, and Liam P. Barry, “Dual correlated pumping scheme for phase noise preservation in all-optical wavelength conversion,” *Opt. Express*, vol. 21, no. 13, pp.15568-15579, 2013.

Chapter 3- Simulations of OSNR and Laser Linewidth Limits for Wavelength Conversion of DQPSK Signals Using FWM

3.1 Introduction

All optical wavelength conversion (AOWC) would be required to improve the flexibility of conventional wavelength division multiplexing (WDM) networks. In addition, the data carrying capacity of lightwave communication systems can be increased by a factor of two over traditional on-off keyed transmission by employing signals with DQPSK format. As was discussed earlier, FWM in SOA is the best candidate to perform wavelength conversion of signals with advanced modulation formats such as DQPSK [1-5]. In this chapter, the required optical signal to noise ratio (OSNR) and laser phase noise (linewidth) limits that would allow for wavelength conversion of DQPSK signals using FWM with acceptable bit error rates (BER) of 10^{-3} and 10^{-4} are calculated via Monte Carlo simulations using Matlab, so that a forward error correction (FEC) [6] scheme can be employed to provide for error free operation. Operation at a BER of 10^{-4} would be of significant interest to designers of such systems to allow for inevitable degradations so that the BER would remain below the FEC threshold of 10^{-3} . Therefore, the required OSNR versus pump linewidth for those two targeted values of BER for DQPSK signals at 10 and 25 Gbaud are mapped. For increasing pump linewidth, for a given OSNR, there is an increase in the BER due to the accumulation

of extra errors from the increased phase noise transfer. The BER increase due to an increase in pump linewidth can be compensated by increasing the OSNR of the received signal. The effectiveness of increasing the OSNR is limited by the error floor set by the accumulated phase noise of the converted signal. Linewidths limitations that produce BER floors of 10^{-3} and 10^{-4} for DQPSK signals operating at 10 and 25 Gbaud are also determined. Selecting lasers with linewidths below these linewidth limits will ensure reliable wavelength conversion. It should be noted however, that here the case of Weiner phase noise generated from white frequency modulation (FM) noise is only considered and thus the increasing low frequency FM-noise (also termed $1/f$ noise) is neglected [7]. The impact in neglecting $1/f$ noise is not severe due to the differential detection of the carrier phase for DQPSK signals; because random phase changes due to $1/f$ noise occur on timescales (tens of μ s) that are much longer than the symbol periods of interest in this paper (100 ps and 40 ps for 10 and 25 Gbaud respectively).

This chapter is organized as follows: in section 3.2 the details of Monte Carlo simulator are provided. In sections 3.3 and 3.4, the results of single and dual pump FWM conversion are discussed, respectively and finally in section 3.4 the effect of having a cascade of wavelength converters on the choice of pump laser linewidth is investigated.

3.2 Background and simulator

In this thesis, the system simulation is implemented using a time domain SOA model. The simulation schematic of this chapter is shown in Fig.3-1, where two pumps and a DQPSK signal are coupled together and passed through an SOA, also the input and received constellations are shown. The received constellations are taken from 100 received symbols for a converted DQPSK stream at 10 Gbaud with a pump linewidth of 3 MHz. These received constellations are more spread out due to the phase noise transfer from the pump to the

converted signal. In the SOA, the signal is converted to new frequencies via FWM. At the output the required wavelength converted signal is filtered from the output spectrum and then detected using an ideal coherent receiver. The SOA gain dynamics due to the carrier density pulsation (interband parameter) can be modelled according to Eq.(2-1) [8]. The output slowly varying envelope approximation (SVEA) to the optical field is given simply as:

$$E_{out}(t) = \exp\left\{\frac{1}{2}\left[-\alpha_{loss}L + (1 + j\alpha_H)h(t)\right]\right\} E_{in}(t) \quad (3-1)$$

where $-\alpha_{loss}L$ is the integrated scattering loss and α_H is linewidth enhancement factor (Henry's gain-phase coupling parameter). For the detunings of interest in this chapter, gain and phase gratings created by the carriers are considered and thus weaker gain gratings created by carrier heating and spectral hole burning are omitted. All the simulations in this chapter were conducted using $h_0 = 6$, $\tau_s = 100$ ps, $P_{sat} = 10$ mW, $\alpha_{loss}L = 2$ and $\alpha_H = 4$. The net small signal SOA gain is $\exp(4)$ or roughly 17.3 dB. The generalized slowly varying envelope approximation (SVEA) input optical field for the dual pump scheme is given by:

$$E_{in}(t) = \sqrt{P_{P1}} \exp(\phi_{P1}(t)) + \sqrt{P_{P2}} \exp(\Omega_{P2}t + \phi_{P2}(t)) + \sqrt{P_S} E_s(t) \exp(\Omega_S t) \quad (3-2)$$

where $\sqrt{P_{P1}}$ is the power of the pump and $\sqrt{P_S}$ is the average signal power. The detunings are defined as $\Omega_{P2} = 2\pi(f_{P2} - f_{P1})$ and $\Omega_S = 2\pi(f_S - f_{P1})$ where f is the optical frequency. In this chapter, phase noise is only considered for the pumps and the pump phase noise is modelled as a Wiener process with phase noise variance over an observed time difference of $\Delta\tau$ [9]:

$$\sigma_{p,\Delta\tau}^2 = 2\pi B_L \Delta\tau \quad (3-3)$$

where B_L is the linewidth of the laser source [9]. The phase noise can be computed as follows: starting with the initial value of phase noise $= \phi [0] = 0$ the phase noise at subsequent sampling times, $m\Delta t$ is given by:

$$\phi[m\Delta t] = \phi[(m-1)\Delta t] + N(0, \sigma_{p,\Delta t}^2) \Big|_{t=m\Delta t} \quad \text{for } 0 < m \leq M \quad (3-4)$$

where M is the total number of samples and $N(0, \sigma_{p,\Delta t}^2)$ is a random zero mean Gaussian distributed distribution with variance of $\sigma_{p,\Delta t}^2$, with Δt being the signal sampling period. The input DQPSK signal is created by initially generating a PRBS stream with every two consecutive bits being mapped to the DQPSK symbols $[1, j, -1, -j]$, the signal is then low pass filtered to reduce spectral broadening, and then spectrally placed relative to one of the pumps to create a gain grating. In order to get good estimate for BER to 10^{-4} , we need to employ $2^{17}-1$ symbols in all simulations of this chapter.

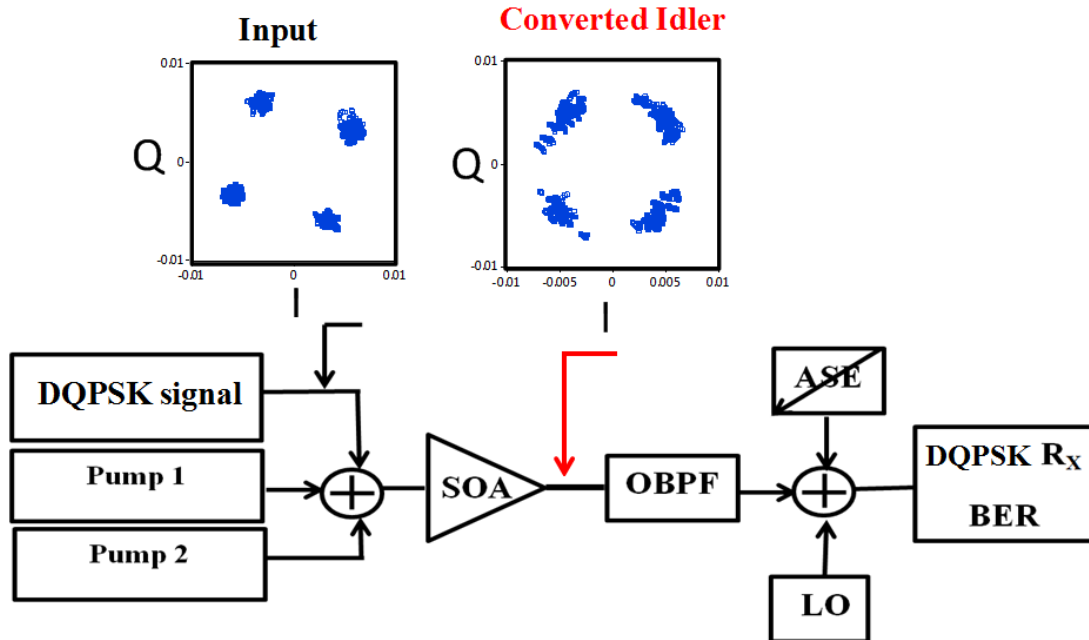


Fig.3-1 Schematic of simulation platform to calculate the BER due to OSNR and linewidth for the dual pump scheme. The input and detected constellations for 100 symbols of 10 Gbaud DQPSK when the pump P1 has a linewidth of 3 MHz are shown to highlight the impact of the phase noise transfer from pump to converted idler.

The input and output spectra of the dual pump scheme are shown in Fig.3-2. The input pump power and linewidth are 0.5 mW and 3 MHz, the average power of the DQPSK signal was 100 μ W at 10 Gbaud. From Fig.3-2, the FWM conversion efficiency is roughly -20 dB, which is reasonable for such a moderate gain SOA with 150 GHz pump-signal detuning. The expected Lorentzian-shaped broadening of the pumps is clearly visible in the input spectrum. The converted idlers that are of interest are indicated in the output spectrum. The following naming strategy is adopted for the various idlers, $E_i E_j E_k^*$ where i , j and k denote the seeding pump or signal i.e. P_1 , P_2 or S and $[*]$ denotes the complex conjugation operator. For the case of the single pump scheme (i.e. degenerate FWM) the converted idler of interest is $E_{P_1}^2 E_S^*$. For the case of the dual pump scheme the converted idlers of $E_{P_2} E_S E_{P_1}^*$ and $E_{P_2} E_{P_1} E_S^*$ are denoted at their respective spectral locations in the output spectrum in Fig.3-2(b). Owing to the limited simulation bandwidth (1 THz) which is equal to inverse of simulation time step (1ps), it was difficult to achieve good spectral separation between $E_{P_1}^2 E_S^*$ and $E_{P_2} E_S E_{P_1}^*$ in the dual pump case, so the solely concentration is on $E_{P_2} E_{P_1} E_S^*$, while noting that the results obtained would equally apply to $E_{P_2} E_S E_{P_1}^*$. For the single pump the power of P_2 is set to be zero and thus there is no issue in filtering $E_{P_1}^2 E_S^*$. After propagation through the SOA; the converted DQPSK signal is filtered out using a Gaussian shaped optical band pass filter (OBPF), then a controlled amount of optical noise (ASE) is added prior to the coherent receiver. This allows us to calibrate the optical signal to noise ratio (OSNR) at the receiver when BER estimates are being taken. The analytical expression for the BER of DQPSK signals with zero linewidth is given by [1]:

$$P_e = \frac{1}{2} \operatorname{erfc} \left[\sqrt{\frac{BW_{ref} (OSNR)}{R_b}} \right] \quad (3-5)$$

where erfc is the complimentary error function, R_b is the baud rate and $BW_{ref} = 12$ GHz is the reference bandwidth [10]. By building up a DQPSK signal and pumps with defined linewidths, the required OSNR for BERs at 10^{-3} and 10^{-4} operating at 10 and 25 Gbaud are calculated. BER calculations in this chapter are limited by the number of employed DQPSK symbols, which is $2^{17}-1$ symbols throughout; therefore calculated BER results $< 10^{-4}$ do not contain a statistically significant number of errors and are thus are not considered in the analysis.

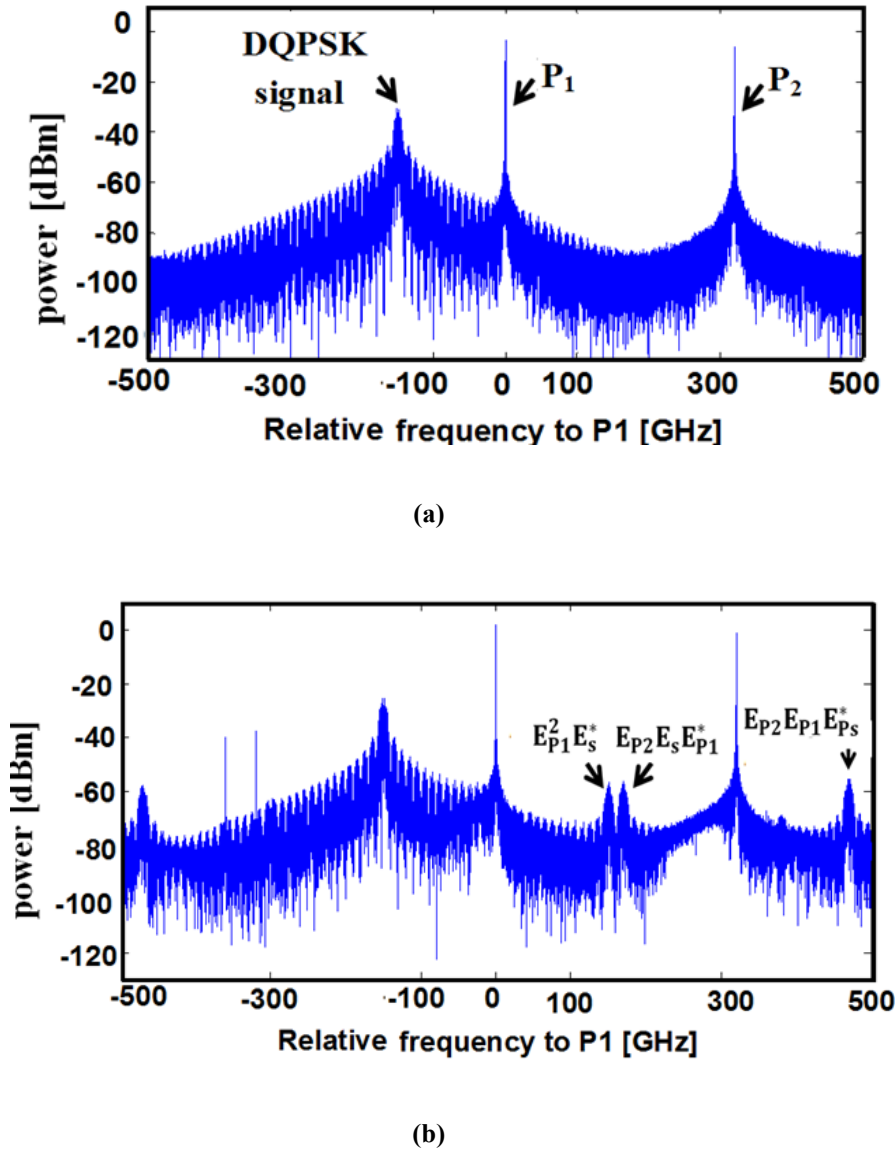
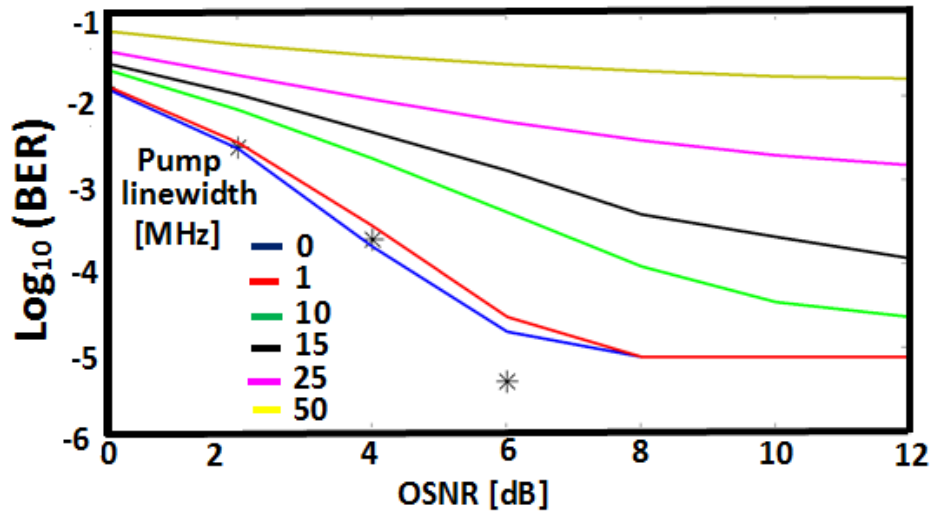


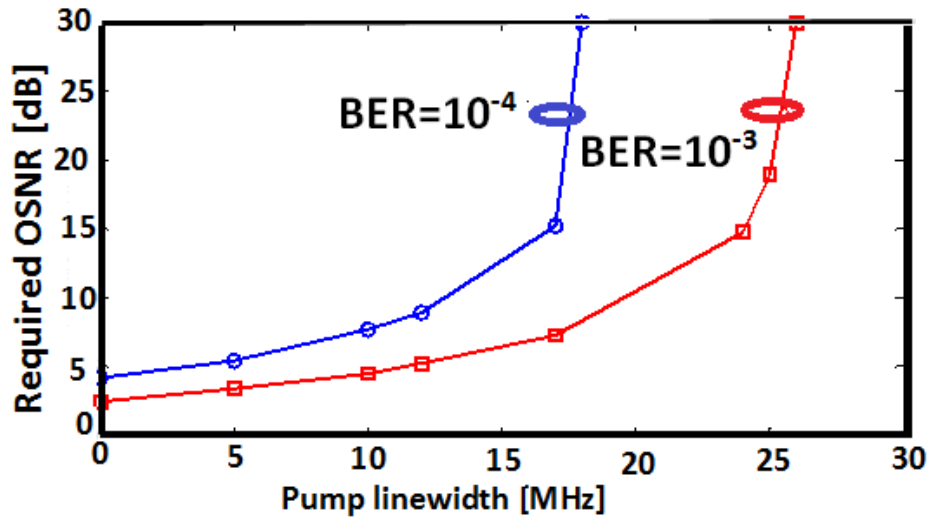
Fig.3-2 Calculated (a) input spectrum and (b) output spectrum of the dual pump scheme showing the spectral location of the DQPSK signal, pumps P_1 and P_2 along with the converted idlers

3.3 Single pump scheme

In this section, FWM-based wavelength conversion using a single pump is studied. A DQPSK signal is created with an average power of 100 μ W without any phase noise. The reason for creation of the signal without phase noise is to show, without ambiguity, the role of the phase noise transfer from pump to the converted idler waves. The power of pump, P_1 , is set to 1mW and the power of pump P_2 is set to zero for all the simulations in this section, thus $E_{P_1}^2 E_S^*$ is the only interested idler to evaluate the BER-OSNR performance as the linewidth of P_1 is increased. The modulated signal from the transmitter (DQPSK Tx) is coupled with a CW pump and then passed through the SOA. The wavelength converted signal (idler) is then filtered out by using a Gaussian optical band pass filter with bandwidths of 7 GHz and 17 GHz for 10 and 25 Gbaud signals, respectively. The pump-signal detuning is set to 150 GHz to achieve good spectral separation between the converted idler at 25 Gbaud and the phase noise broadened CW pump, so that the converted idler can be extracted without interference from the pump. A calibrated amount of ASE noise is then added to the converted idler in order to estimate the BER as a function of OSNR and then the DQPSK signal is detected using an ideal coherent receiver. The ideal homodyne coherent receiver simply consists of an ideal sine wave at the carrier frequency of the idler of interest; the mixing removes the oscillatory part of the signal allowing for the phase information to be extracted. Here, we assume that the ideal coherent receiver does not exhibit any phase noise. For a DQPSK signal at 10 Gbaud, the calculated BER as a function of OSNR is shown in Fig.3-3 (a) for various values of pump linewidth. As expected, the number of errors matches the theoretical BER when the pump linewidth is zero; though as the linewidth is increased, the calculated number of errors increases due to the phase noise transfer from the pump to the converted signal.



(a)

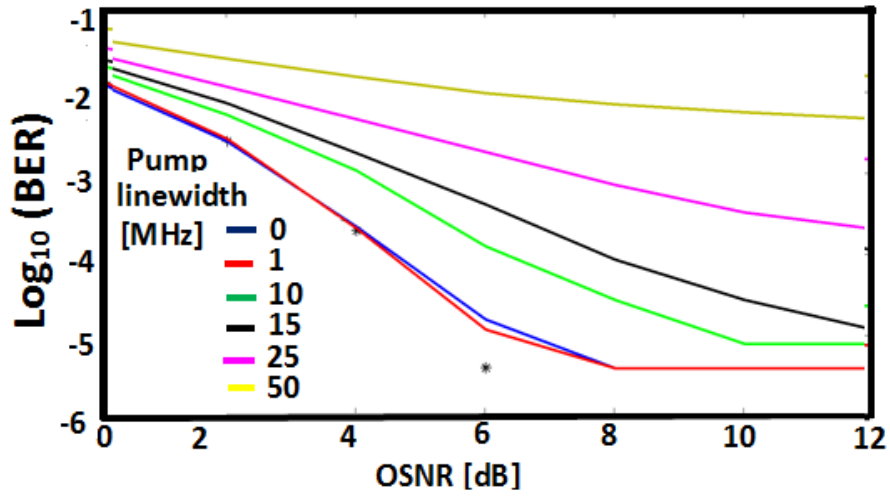


(b)

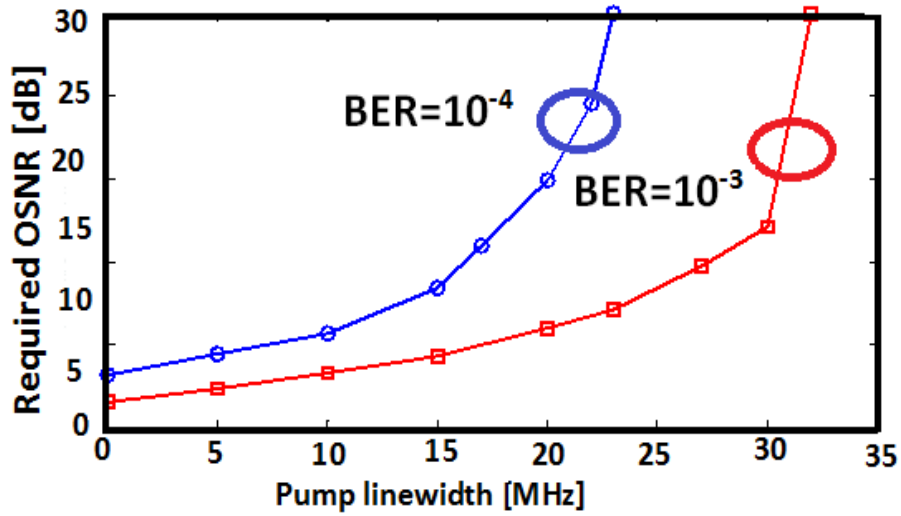
Fig.3-3 (a) Calculated BER versus OSNR of converted 10 Gbaud DQPSK signal using the single pump scheme with pump linewidth as parameter. [*] denotes theoretical BER calculation for zero pump linewidth using Eq. (3-5). (b) The required OSNR to achieve a BER of 10^{-4} and 10^{-3} for any given pump linewidth. BER values below 10^{-5} are not trustworthy due to the limited number of bits simulated.

For each curve in Fig.3-3 (a), the OSNR that yields a BER of 10^{-3} is noted and this allows us to build up a curve plotting the required OSNR to achieve a BER of 10^{-3} with increasing pump linewidth.

The result is shown in Fig.3-3(b). This process is repeated for the BER of 10^{-4} and also plotted in Fig.3-3(b). Clearly, there is a trade-off between OSNR and laser linewidth to achieve a specific level of performance. However, when the phase noise dominates the BER performance, no amount of increase in OSNR can improve the performance. From Fig.3-3(b) the pump linewidth limits that produce error floors at BERs of 10^{-3} and 10^{-4} for 10 Gbaud DQPSK are 26 and 18 MHz respectively. Therefore in order to target these levels of performance, pump lasers with linewidths lower than these limits should be selected. For a DQPSK signal at 25 Gbaud, the calculated BER as a function of OSNR is shown in Fig.3-4(a) for various values of pump linewidth. As for the 10 Gbaud case, the required OSNR to achieve a BER of 10^{-3} and 10^{-4} versus pump linewidth is shown in Fig.3-4(b). These results show that the maximum linewidths of the pump for degenerate FWM-based wavelength conversion of the DQPSK signal are 32 MHz and 23 MHz to achieve BER performances of 10^{-3} and 10^{-4} respectively. For the 10 Gbaud case, the pump linewidth limit is calculated to be about 26 MHz to achieve a BER of 10^{-3} ; in this case the equivalent linewidth of the idler is four times that of the pump i.e. 104 MHz [11]. This corresponds well to an expected result in [12] which shows that for 10 Gbaud DPSK the linewidth limit to achieve a BER of 10^{-9} is 100 MHz (the phase decision threshold being: $\pm \frac{\pi}{2}$, though for DQPSK the threshold decreases to $\pm \frac{\pi}{4}$. For a signal with a given variance, and taking a simple calculation of the complementary error function [1] halving the decision threshold produces a BER going from 10^{-9} to 2×10^{-3} . Based on this argument, the linewidth induced limits correspond quite well for the case of DQPSK at 10 Gbaud.



(a)



(b)

Fig.3-4 (a) Calculated BER versus OSNR of converted 25 Gbaud DQPSK signal using the single pump scheme with pump linewidth as parameter. [*] denotes theoretical BER calculation for zero pump linewidth using Eq. (3-5). (b) The required OSNR to achieve a BER of 10^{-4} and 10^{-3} for any given pump linewidth. BER values below 10^{-5} are not trustworthy due to the limited number of bits employed in the simulation.

Increasing the symbol rate to 25 Gbaud, one would expect that the linewidths that produce BER performance of 10^{-3} and 10^{-4} should be 2.5 times greater than those for 10 Gbaud.

The reason is as follows: the symbol period for 25 Gbaud is 2.5 times smaller than that of 10 Gbaud; therefore using Equation (3-4) to calculate the phase error variance for 25 Gbaud, the laser linewidth can be increased by a factor of 2.5 relative to 10 Gbaud to produce the same phase error variance. Our results in Fig.3-4(b) show the calculated increase in the laser linewidth limits relative to the case for 10 Gbaud, in Fig.3-3 (b), fall short of expectations.

This attributed to the fact that there is spectral leakage from the pump to the converted idler; this is not surprising given the increase in spectral width due to the pump line broadening and the greater magnitude of the pump than the idler at SOA output. The leakage at 10 Gbaud is less severe due to the narrower OBPF used as well the fact that the longer symbol duration results in a larger phase error variance at lower linewidths than 25 Gbaud. Further evidence of this effect is provided in the following section when the results of the dual pump conversion scheme are presented.

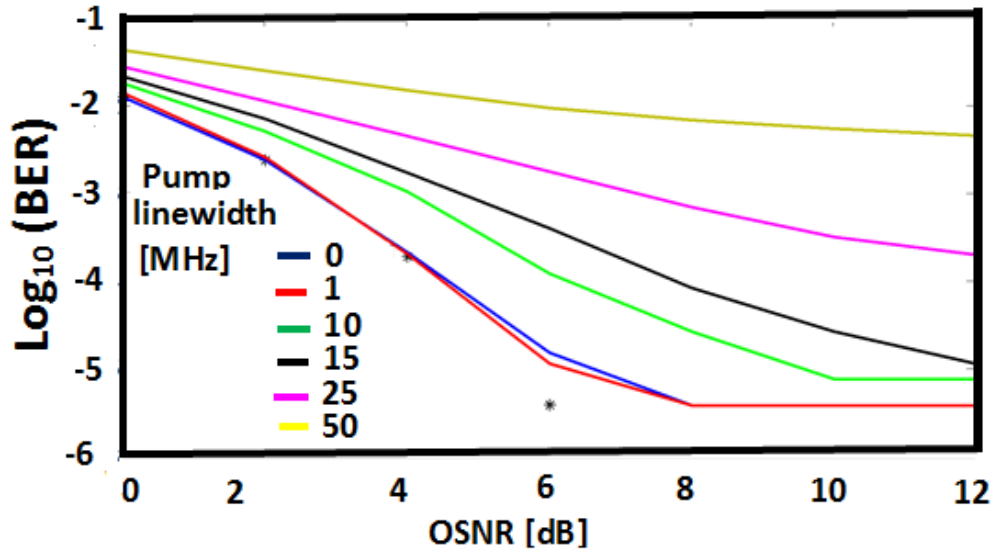
3.4 Dual pump scheme

The case of wavelength conversion using dual pumps is studied in this section. DQPSK signal is used with zero linewidth, two CW pumps with powers of 1mW each, and a SOA for achieving wavelength conversion through nondegenerate FWM. The DQPSK signal from the transmitter (TX) is coupled with two CW pumps (input spectrum of SOA is shown in Fig.3-2(a)) and then amplified in the SOA. The output spectrum from the SOA is shown in Fig.3-3(b). There are eight wavelength converted signals (idlers) as there are two pumps and one modulated signal, so choosing the best idler is very important in the dual pump scheme as some idlers are very close together or even close to one of the pumps and the interference

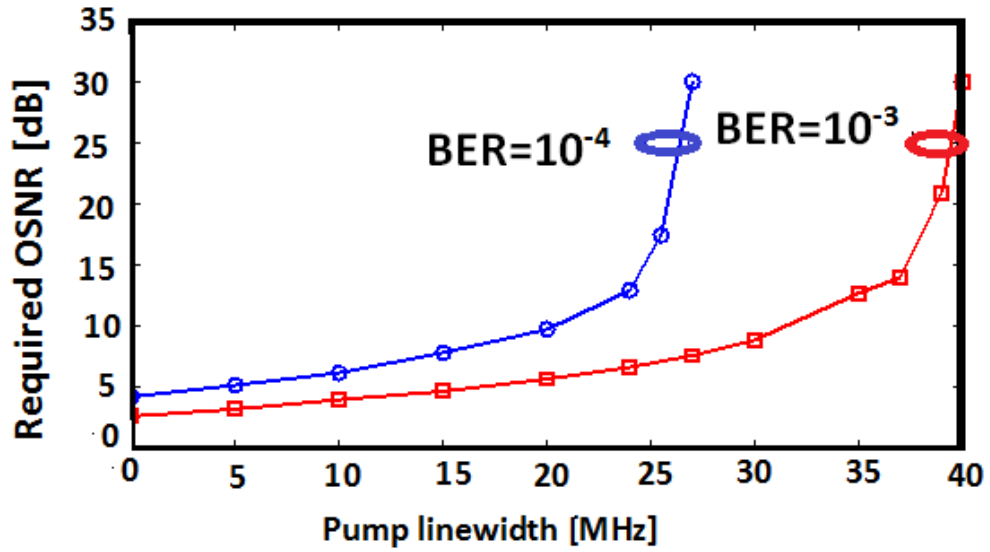
of two idlers, or pump with idler, can degrade the performance of the system. In this work, the converted idler, $E_{P1}E_{P2}E_S^*$ is chosen because this idler is not very close to the idlers or the pumps. In the simulated output spectrum in Fig.3-2(b), this idler appears at a frequency of 470 GHz relative to P_1 . This idler is then filtered out by using a Gaussian optical band pass filter whose bandwidth is 7 and 17 GHz for 10 and 25 Gbaud signals respectively. The converted idler is detected using an ideal coherent receiver after the ASE noise is added. As for the previous section, the BER versus OSNR performance is calculated for wavelength conversion with increasing pump linewidth at baud rates of 10 and 25 Gbaud. The results for 10 Gbaud are shown in Fig.3-5 (a) and the corresponding required OSNR versus pump linewidth to achieve BERs of 10^{-3} and 10^{-4} are shown in Fig.3-5(b). The maximum pump linewidths for wavelength conversion of the DQPSK signal applying dual pump wavelength conversion at 10 Gbaud is 40 MHz at 10^{-3} and 27 MHz at 10^{-4} . Comparing with the result from the previous section (section 3-3) for single pump wavelength conversion at 10 Gbaud, the result shown here agrees quite well with the expected theory that the phase noise transfer for the dual pump scheme is less than that of the single pump scheme [11].

Two scenarios are then considered at the baud rate of 25 Gbaud. The first scenario is changing the linewidth of two pumps, so that the two pump linewidths are equal ($B_{P1}=B_{P2}$), and in the second case, one pump linewidth is kept constant at 8 MHz ($B_{P2}=8\text{MHz}$), while varying the linewidth of the other pump, P_1 , so that we can limit the effect of pump leakage from P_2 to the converted idler. As in previous section, the maximum pump linewidths are calculated at BERs of 10^{-3} and 10^{-4} . The required OSNR versus average pump linewidth are plotted in Fig.3-6 (b). At the baud rate of 25 Gbaud the maximum average pump linewidths are 35 MHz at 10^{-3} and 25 MHz at 10^{-4} for the equal pump linewidth scenario ($B_{P1}=B_{P2}$), and 61 MHz at 10^{-3} and 40 MHz at 10^{-4} for the second scenario ($B_{P2}=8\text{ MHz}$). The lower maximum linewidth result for the equal linewidth scenario clearly shows that our results are

heavily influenced by the presence of inevitable pump leakage into the converted idler when the pump closest to the idler has such large values of pump line broadening. The phase noise transfer to the idler is the same for both scenarios, with the linewidth of the idler being the summation of the linewidths of the pumps [11]. When the linewidth of the pump nearest the converted idler, P_2 , is held constant at 8 MHz; it could be shown that the expected performance increases for the dual pump scheme. The reduced phase noise transfer for dual pump FWM compared with the single pump scheme is one of the advantages of using nondegenerate FWM wavelength conversion for advanced modulation formats.

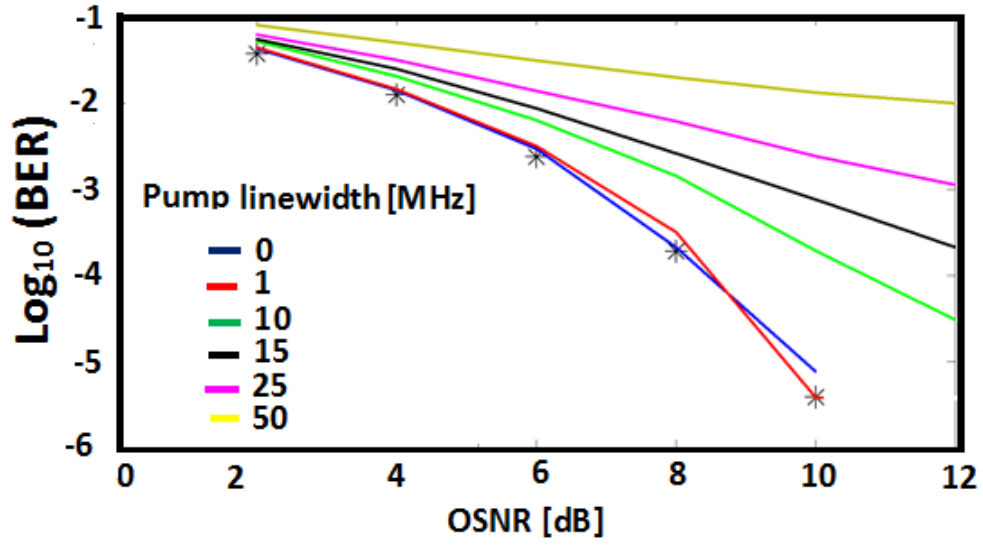


(a)

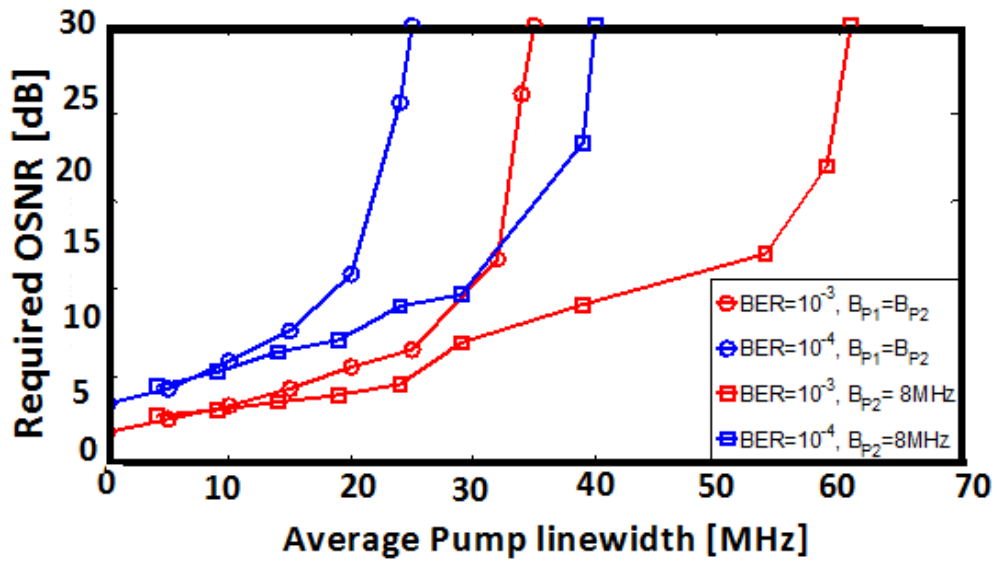


(b)

Fig.3-5 (a) Calculated BER versus OSNR of the converted 10 Gbaud DQPSK signal using the dual pump scheme with pump linewidth as parameter. [*] denotes theoretical BER calculation for zero pump linewidth using Eq. (3-5). (b) The required OSNR to achieve a BER of 10^{-4} and 10^{-3} for any given pump linewidth. BER values below 10^{-5} are not trustworthy due to the limited number of bits employed in the simulation.



(a)



(b)

Fig.3-6 Calculated BER versus OSNR of converted 25 Gbaud DQPSK signal using the dual pump scheme with pump linewidth as parameter. The linewidths of both pumps are equal. [*] denotes theoretical BER calculation for zero pump linewidth using Eq. (3-5). (b) The required OSNR to achieve a BER of 10^{-4} and 10^{-3} for average pump linewidth for the two cases when the pumps have equal linewidths and when the linewidth of P_2 is kept constant at 8 MHz. BER values below 10^{-5} are not trustworthy due to the limited number of bits employed in the simulation.

3.5 Summary and conclusion

In this chapter, the required OSNR and laser linewidth limits were calculated to achieve FWM-based wavelength conversion of DQPSK signals at baud rates of 10 and 25 Gbaud. The requirements for single pump FWM conversion are much more stringent on laser linewidth because the effective idler linewidth is quadruple that of the pump. As is shown in all calculations, increasing the baud rate (decreasing the symbol period) relaxes the linewidth limits due to the linear time increase of the phase noise variance; though the increased spectral leakage from the pump to idler makes it difficult to obtain a purely phase-noise limited error floor at higher baud rates because of the higher linewidth tolerance combined with the requirement for a wider optical filter to detect the converted idler. For an optical network in which data bursts are routed through multiple nodes, then we need to consider the case of cascading the wavelength conversion process so that a data packet or burst experiences multiple conversions. In this scenario, if it is assumed that each pump laser used for FWM in the network exhibits the same linewidth (including that used to generate the original DQPSK signal), the total linewidth of the idler after the K^{th} wavelength conversion stage is given by.

$$B_{tot} = 4B_p + B_s + 4(K-1)B_p \quad (3-6)$$

If the BER of 10^{-4} is targeted, from the result in Section 3-3 for single pump FWM at 10 Gbaud, the total linewidth of the idler is $4 \times 17 \text{ MHz} = 68 \text{ MHz}$. For equal linewidth pumps performing 1, 2, 3 and 4 cascaded wavelength conversions; the maximum pump linewidth for each of those numbers of cascades are: 13.6, 7.5, 5.2 and 4 MHz, respectively. Therefore, the selection of the laser sources in optical burst/packet switched networks that employ wavelength conversion for advanced modulation format transmission is of great importance,

and this importance is of even greater significance when we consider that fast tuning lasers, whose tuning times are < 100 ns, tend to have linewidths of the order of a few MHz [7].

Bibliography

- [1] J.G. Proakis, M. Salehi, Digital Communications (5th edition), ISBN-10: 0072957166, McGraw-Hill, New York, 2008.
- [2] S. T Naimi, S. O Duill, and L.P. Barry, ‘Detailed Investigation of the Pump Phase Noise Tolerance for the Wavelength Conversion of 16-QAM Signals Using FWM,’ *IEEE/OSA JOCN*, vol. 6, no. 9, pp. 793-800, 2014.
- [3] S .T. Naimi, S.Ó Dúill and L. P. Barry, “Simulations of the OSNR and Laser Linewidth Limits for Reliable Wavelength Conversion of DQPSK Signals Using Four-Wave Mixing,” *J. Optics Communications* ,vol. 310, no. 1, pp. 150-155, 2014.
- [4] S. P. Ó Dúill, S. T. Naimi, A. P. Anthur, T. N. Huynh, D. Venkitesh and L. P. Barry, “Simulations of an OSNR limited wavelength conversion scheme, *IEEE Photon. Tech. Lett.* 25, No. 23, pp 2311 – 2314, 2013.
- [5] B. Filion, W. C. Ng, A. T. Nguyen, L. A. Rusch, and S. LaRochelle, “Wideband wavelength conversion of 16 Gbaud 16-QAM and 5 Gbaud 64-QAM signals in a semiconductor optical amplifier,” *Opt. Express*, vol. 21, no. 17, pp. 19825– 19833, 2013.
- [6] T. Mizuochi, “Recent Progress in Forward Error Correction and Its Interplay With Transmission Impairments.” *IEEE J. Sel. Topics in Quant. Electron.* vol.12, no. 4, pp.544 -554, 2006.
- [7] T. N. Huynh, F. Smyth, L. Nguyen and L. P. Barry, "Effects of Phase Noise of Monolithic Tunable Laser on Coherent Communication Systems," *Opt. Expr.* vol20, no.6, pp.B244, 2012.
- [8] G. P. Agrawal and N. A. Olsson, “Self phase modulation and spectral broadening of optical pulses in semiconductor laser amplifiers,” *IEEE J. Quantum Electron.*, vol. 25, no. 11, pp. 2297–2306, 1989.
- [9] D. Marcuse, “Computer Simulation of FSK Laser Spectra and of FSK-to-ASK Conversion,” *IEEE J. of Lightw. Techn.* vo.8, no.7, pp.1110-1122, 1990.
- [10] M. Nakazawa, K. Kikuchi, T. Miyazaki, “High Spectral Density Optical Communication Technologies,” ISBN 978-3-642-10418-3, Springer Berlin Heidelberg, 2010.
- [11] R. Hui and A. Mecozzi, “Phase noise of four-wave mixing in semiconductor lasers,” *Appl. Phys. Lett.*, vol.60, 2454– 2456 , 1992.

[12] C. Henry, "Dynamic Single-Mode Semiconductor Lasers with a Distributed Reflector," in *Semiconductor and Semimetals*, W.T. Tsang, ed. (*Academic, Orlando, Fla.*, 1985), Vol. 22, Part B.

Chapter 4- Pump Phase Noise Tolerance of All Optical Wavelength Conversion of M-QAM Signals Using Four-Wave Mixing

4.1 Introduction

In this chapter, the limitations on the optical pump linewidth to successfully wavelength convert QAM signal using degenerate and non-degenerate FWM in an SOA are determined. These limitations are calculated using Monte Carlo simulations in SOAs at 10 Gbaud using single pump (degenerate) and dual pump (nondegenerate) FWM. The performance limitations are set to bit error rates (BER) of 10^{-3} and 10^{-4} , and forward error correction (FEC) can subsequently be employed to achieve error free operation [2]. With these calculations, the performance of wavelength conversion of 16-QAM and 64-QAM will be guaranteed by selecting lasers with linewidths below these linewidth limits. This chapter is an extension of previous work done in chapter 3 for the conversion of differential quadrature phase shift keying (DQPSK) signals. Due to the sensitivity of M-QAM signals (include 16-QAM) with respect to phase noise, the conversion performance using two different decision-directed phase-locked loop carrier phase recovery algorithms are investigated in this chapter. In comparison with chapter 3, the process of FWM is based on inter- and intra-band contributions to the nonlinear gain dynamics in SOAs; thus the SOA model is modified to include carrier heating (CH) and spectral hole burning (SHB) effects in addition to the inter-

band carrier density pulsations (CDP). It must be added that even though this work is effectively dealing with a single polarization signal, the estimated linewidth limits would be equally valid for converting dual-polarization signals because FWM-based wavelength conversion of dual-polarization would require that each polarization be separated and converted separately via FWM. In such WC schemes, each polarization component could be demultiplexed and converted individually in separate SOAs or in a counter propagating scheme as in [3].

The chapter is organized as follows. In Section 4.2, the details of our Monte Carlo simulator are discussed: the SOA model including the intraband effects; and the carrier phase recovery algorithms. Linewidth limits for wavelength converting 16-QAM and 64-QAM signals using FWM in SOA are discussed in section 4.3 and 4.4, respectively. Finally, in section 4.5, the results are discussed.

4.2 Background and simulator

The simulations of the wavelength conversion of 16-QAM signals are implemented using FWM in SOAs. The fundamentals of FWM in SOAs have been studied in section 2.3 [4-11]. In this chapter, constructing a simulator that can process $2^{17}-1$ symbols is interested in order to measure BER's successfully down to 10^{-4} ; therefore for rapid computer runtime, an existing SOA model is adopted to suit our needs. A lumped SOA model considering the various inter- and intraband contributions to the SOA gain was developed in [6] and was later implemented in a system simulator in [10]. The lumped SOA model allows the SOA gain to be calculated without accounting for neither spatially-resolved gain nor spatially-resolved propagating fields and thus simplifying the complexity of the simulator. As was discussed in subsection 2.4.2, the rate equations describing the spatially-integrated gain contributions from CDP, CH and SHB are given by Eqs (2-2),(2-3), and (2-4) [10],[11]. The total overall optical

gain of the SOA is $G_{tot} = \exp[h_{cdp}(t) + h_{ch}(t) + h_{shb}(t)]$. All the SOA parameters are listed in Table 4-1 and are in line with typical values in [7]. In the wavelength conversion system, strong CW pumps are injected into the SOA. Therefore, under strong CW gain saturation conditions the average device gain is smaller than h_0 , thus allowing the last term on the right hand side (RHS) of Eq (2-4) to be neglected. Numerically solving Equations (2-3) and (2-4) would require signal sampling times to be $\ll \tau_1$ (~ 1 fs), and this would result in an excessive over sampling of our optical field and unrealistic computational requirements. Eqs (2-3) and (2-4) can be solved quite efficiently in the quasi-equilibrium limit that variations in $|E_{in}|^2$ occur over time scales $\gg \tau_{ch}$ and τ_1 , i.e. $dh_{ch}/dt = dh_{shb}/dt = 0$ allowing us to write the CH and SHB contributions directly as Eqs (2-6) and (2-7).

The quasi-equilibrium assumption allows $h_{ch}(t)$ and $h_{shb}(t)$ to be calculated without having to solve the differential equations directly; the assumption is valid as long as the signal-pump detuning is $< \min(\frac{1}{2\pi\tau_{CH}}, \frac{1}{2\pi\tau_1})$ (300 GHz in this case). As mentioned previously, the signal-pump detuning is set to 100 GHz for all simulations, therefore Eqs(2-2), (2-6) and (2-7) are sufficient to capture the gain grating generated between the QAM signals and pump P_1 for both degenerate and nondegenerate FWM scenarios.

Table 4-1 SOA parameters [7]

Symbol	Definition	Value
h_0	Unsaturated gain parameter	10
P_{sat}	Saturation power	10 mW
τ_S	Carrier lifetime	60 ps
α_{cdp}	Gain-phase coupling parameter	4
$\alpha_{loss}L$	Internal losses	2
α_{ch}	Carrier heating gain-phase coupling	3
\mathcal{E}_{ch}	Carrier heating nonlinear gain suppression factor	1.2 W^{-1}
\mathcal{E}_{shb}	Spectral hole burning nonlinear gain suppression factor	1.5 W^{-1}
NF	Noise Figure	$\sim 7.8 \text{ dB}$

The slowly varying envelope of the input optical field is:

$$E_{in}(t) = \sqrt{P_{P1}} \exp(j\phi_{P1}) + \sqrt{P_{P2}} \exp(j\Omega_{P2}t + \phi_{P2}(t)) \quad (4-1)$$

$$+ \sqrt{P_{P2}} E_s(t) \exp(\Omega_{P1-s}t + j\phi_s)$$

where P_{P1} , P_{P2} and P_s are the powers of pump P_1 , pump P_2 and the average power of the signal respectively. The QAM signal is contained within $E_s(t)$. The uncorrelated phase noise terms on the pumps and signal are ϕ_{P1} , ϕ_{P2} and ϕ_s .

Fig.4-1 shows a schematic of the nondegenerate FWM-based wavelength converter; the QAM signal is created by initially generating a PRBS stream with every four consecutive bits being mapped to the relevant 16-QAM symbol. The QAM signal is then combined with two separate pumps and input into the SOA. The input optical field E_{in} is created using (4-1) and then the SOA gain can be calculated using Eqs(2-2), (2-6) and (2-7) the output field E_{out} is thus given by:

$$E_{out}(t) = \exp \left\{ \frac{1}{2} \left[-\alpha_{loss} L + (1 + j\alpha_{cdp}) h_{cdp}(t) + (1 + j\alpha_{ch}) h_{ch}(t) + h_{shb} \right] \right\} E_{in}(t) \quad (4-2)$$

where $\alpha_{loss}L$ being the internal SOA losses, the gain-phase coupling (linewidth-enhancement) factors for CDP and CH are given by α_{cdp} , α_{ch} respectively. The issue of the phase noise transfer is emphasized by showing 100 symbols of the input and detected wavelength converted 16-QAM signal when the linewidth of the pumps equals 1MHz in Fig.4-1. The spreading of the detected 16-QAM constellation points is due to the phase noise transfer and requires carrier phase recovery methods to unwind the phase noise induced spreading of the constellations. Calculated input and output spectra of the dual pump scheme are shown in Fig.4-2(a) and Fig.4-2(b) and the spectral locations of the signal, pumps and

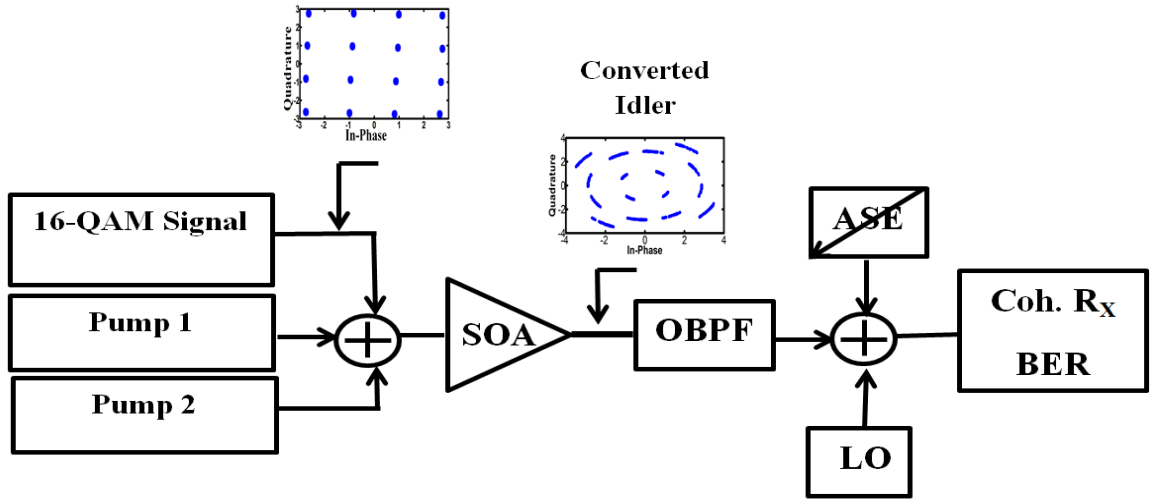


Fig.4-1 Schematic of simulation platform to calculate the BER due to OSNR and linewidth for the dual pump scheme. The input and detected constellations for 100 symbols of 10 Gbaud 16-QAM when the pump P_1 has a linewidth of 1 MHz are shown to highlight the impact of the phase noise transfer from pump to converted idler.

idlers are indicated. The following naming convention for the various idlers are adopted (shown in Fig.4-2(b)), $E_i E_j E_k^*$, where i , j and k denote the seeding pumps or signal i.e. P_1 , P_2 or S ; $[\ast]$ denotes the complex conjugation operator. The conversion efficiency of the FWM wavelength conversion process is estimated to be about -9dB. In all the simulations, the average power of the 16-QAM signal and pumps are set to 100 μ W and 5mW, respectively. Strong CW pump powers, of the order of the SOA gain saturation power, are required to avoid the multi-level 16-QAM signal from saturating the SOA gain that would then distort the converted 16-QAM signal [13]. After propagation through the SOA; the converted 16-QAM signal is filtered out using a narrow bandwidth Gaussian-shaped OBPF with full width at half maximum (FWHM) equal to 16.4 GHz. Assuming that the operation is on a 25 GHz WDM grid for the system, then the OBPF bandwidth would be around 80% of WDM channel grid spacing. In addition, the narrow filter bandwidth is necessary to avoid pump leakage. The filtered 16-QAM signal is then detected using a homodyne receiver. A controlled amount of noise loading calibrates the optical signal to noise ratio (OSNR) at the

receiver. The structure of the homodyne coherent receiver is shown in Fig.4-3(a) which the central frequencies of received 16-QAM signal and local oscillator being equal.

The digital signal processing (DSP) required to detect the 16-QAM signal consists of a symbol normalizer and decision-directed phase-locked loops to detect the signal in the presence of phase noise [14]. The symbol normalizer is required to scale the amplitude of the received symbols so that they would match the expected complex numbers of the 16-QAM symbols. In the simulations, the back-to-back wavelength conversions is performed without fiber transmission, therefore the assumption would be fine for perfectly chromatic dispersion compensated optical links, or else the DSP in the receiver would include chromatic dispersion compensation [15] before implementing the carrier phase recovery algorithms. In order to detect the 16-QAM symbols in the presence of phase noise, two different carrier phase recovery algorithms are considered. Firstly, a first order decision-directed phase-locked loop (DD-PLL) is used [16], [17] as a standard PLL which is shown by the block diagram in Fig.4-3(b). The estimated phase error between the n^{th} symbol detected by the homodyne phase-diversity receiver, $x_c(n)$ and the closest ideal 16-QAM symbol, $x_d(n)$, is given by:

$$e_1(n) = \text{Im}[x_c(n)x_d^*(n)] \quad (4-3)$$

where $\text{Im}[\cdot]$ denotes the imaginary part, and $[\cdot]^*$ denotes the complex conjugation operator. The phase estimation from this standard PLL is amplitude dependent, and thus appropriate for modulation formats whose constellation points possess a single amplitude level such as M-ary phase shift keying. For multi-level amplitude formats like 16-QAM; the amplitude dependency can be removed by normalizing the phase estimate in Eq. (4-3) with respect to $|x_d(n)|^2$ [18].

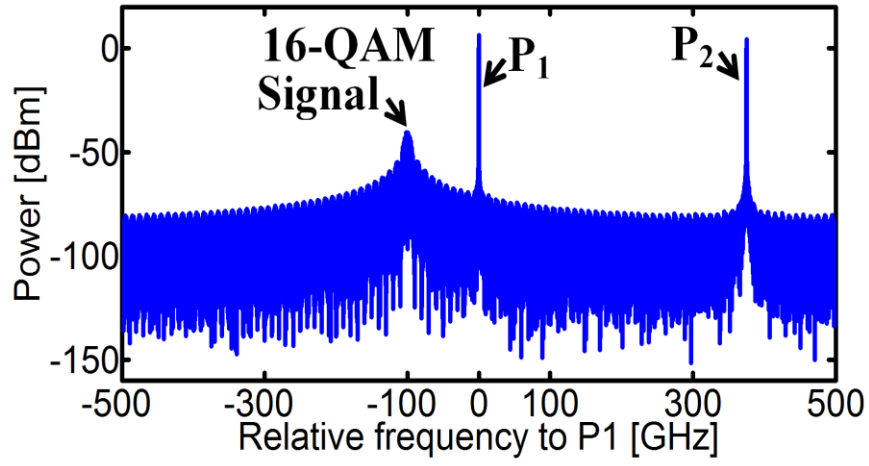
The schematic for the PLL which we term the ‘amplitude normalized DD-PLL (ANDD-PLL)’ is shown in Fig.4-3 (c). The phase error estimation for the ANDD-PLL is proportional to:

$$e_2(n) = \frac{\text{Im}[x_c(n)x_d^*(n)]}{|x_d(n)|^2} \quad (4-4)$$

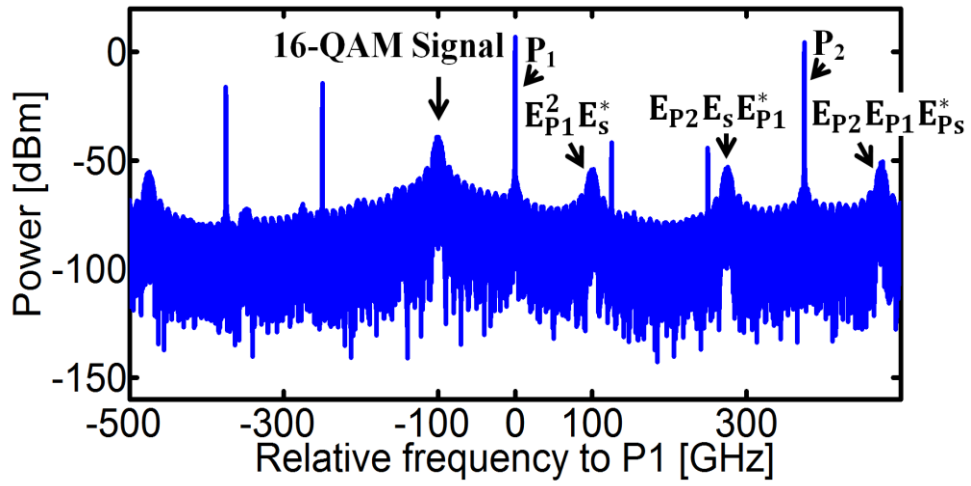
The accumulated recovered carrier phase estimate for both PLLs is given by:

$$\phi_i(n+1) = \phi_i(n) + \mu e_i(n) \quad i = 1, 2 \quad (4-5)$$

where μ is called the step size parameter and determines the loop dynamics. In order for the carrier-phase recovery to obtain acceptable BER performances for the WC of 16-QAM signals, the value of the step size parameter of both PLLs are optimised for each value of pump linewidth in the single pump WC scheme. For each value of pump linewidth the value of μ is varied and the BER vs. OSNR curves are calculated for each value of μ ; the optimised value of μ is determined based on the smallest value that the converted signal achieves a BER of 10^{-4} . The optimised values of μ for both PLLs are shown in Fig.4-4. As it will be shown in the next section, the performance of ANDD-PLL is much better than DD-PLL when the pump linewidths are relatively large; however the real-time implementation of the ANDD-PLL may be more complex than DD-PLL due to the requirement of performing the division in Eq. (4-4). In the next step, the degenerate and non-degenerate wavelength conversion of 16-QAM using FWM in SOAs are implemented.

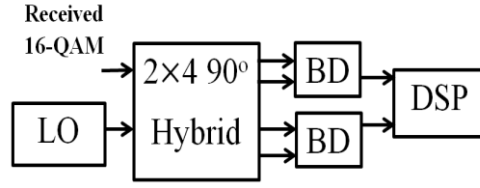


(a)

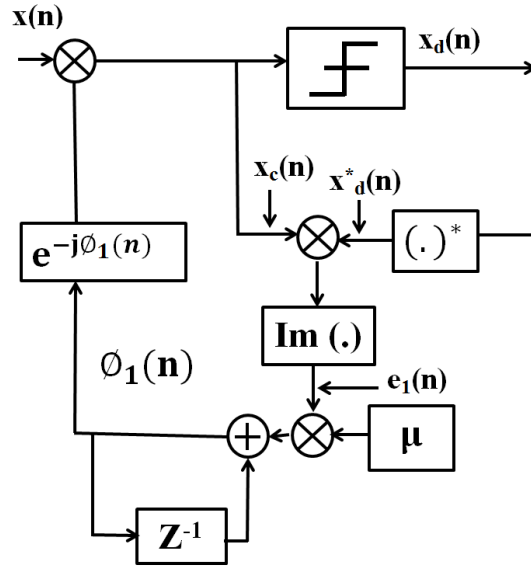


(b)

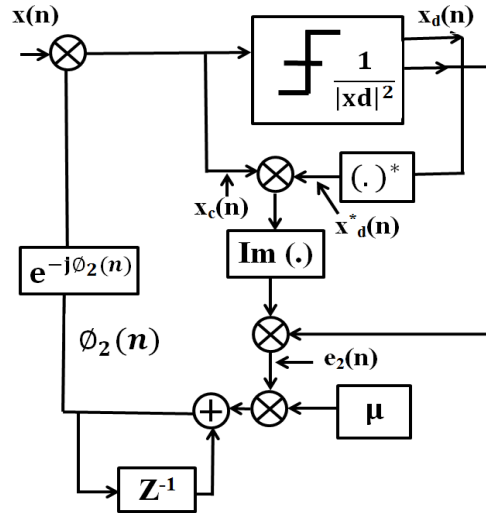
Fig.4-2 Calculated (a) input spectra and (b) output spectra of the dual pump scheme showing the spectral location of the 16-QAM signal, pumps P_1 and P_2 , and the converted idlers.



(a)



(b)



(c)

Fig.4-3 (a) Structure of homodyne coherent detection, BD: Balanced Detector, (b) Decision-directed phase-locked loop carrier phase recovery (DD-PLL), (c) Amplitude normalized decision-directed phase-locked loop carrier phase recovery.

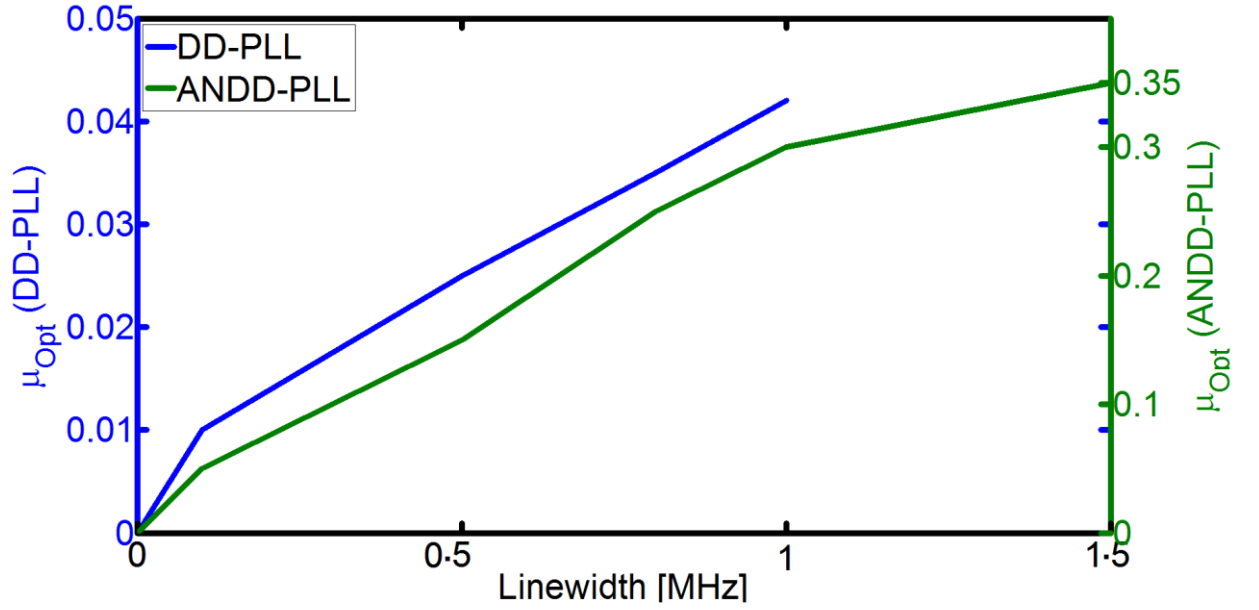


Fig.4-4 Calculated optimum value of μ for each pump linewidth using the single pump scheme for both DD and ANDD-PLLs. The receiver using the DD-PLL was unable to detect the 16-QAM signal for pump linewidths greater than 1 MHz.

4.3 Linewidth Limits for Wavelength Converting 16-QAM Signals Using FWM

4.3.1 Single Pump All- optical Wavelength Conversion of 16-QAM

In this section, the results on wavelength conversion of 16-QAM signals at 10 Gbaud using degenerate (single pump) FWM in an SOA are presented. Determining the pump linewidth limits for the wavelength conversion of 16-QAM signals are the main focus of the work, therefore, 16-QAM signals are created without phase noise to show the role of the phase noise transfer from pump to the converted idler. The performance is calculated by measuring

the BER vs. OSNR of the converted signal for each value of pump linewidth. For the case of degenerate wavelength conversion, there is no power considered for pump P_2 , and the only generated idler is $E_{P_1}^2 E_S^*$, as shown in Fig.4-2. The pump-signal detuning is set to 100 GHz and $E_{P_1}^2 E_S^*$ appears at a spectral location of +100 GHz relative to the pump P_1 . 100 GHz detuning is sufficient to extract the converted idler without any interference from the signal and the pump. The converted 16-QAM signal is demodulated using both carrier phase recovery algorithms, DD-PLL and ANDD-PLL, and their performances are compared. The calculated BER vs. OSNR using both PLLs are shown for various values of pump linewidths in Fig.4-5. There is no phase noise transfer between the pump and idler when the pump linewidth is zero and is in excellent agreement with the back-to-back reception of 16-QAM signals without undergoing wavelength conversion (black curve), highlighting that the WC process does not distort the converted 16-QAM signal.

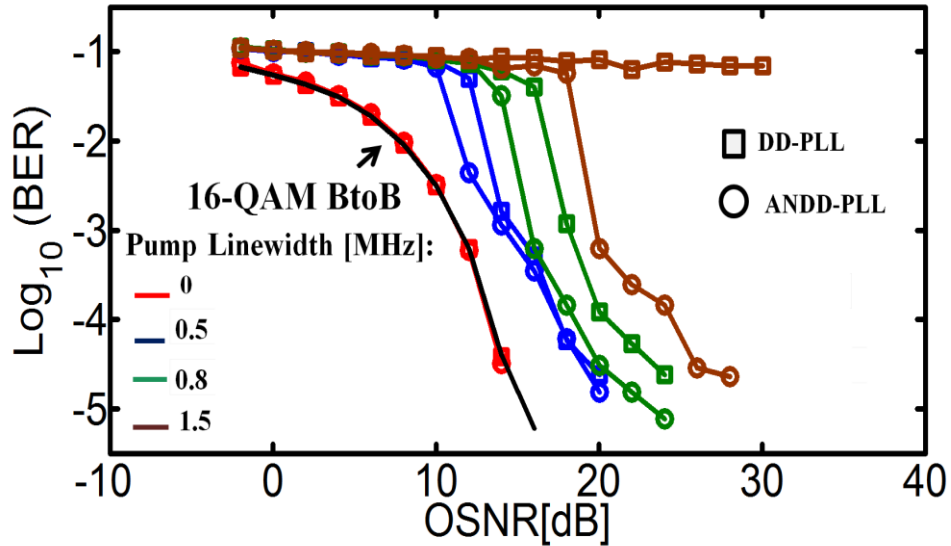


Fig.4-5 Calculated BER versus OSNR of degenerate wavelength conversion of 16-QAM signals at 10 Gbaud using DD-PLL and ANDD-PLL.

When the pump linewidth is increased, the calculated number of errors increases due to the phase noise transfer and hence a higher OSNR is required to achieve the same level of BER performance. In order to interpret the data in Fig.4-5, the required OSNR to achieve BERs of 10^{-3} and 10^{-4} are noted for each value of pump linewidth. This is done for both PLLs and the results are shown in Fig.4-6. The results show that at lower pump linewidths (0 and 500 kHz), there is similar performance for both PLLs because the phase error between the received signal and ideal 16-QAM symbol is low and there is no need for much accuracy for tracking of carrier phase. Thus, the DD-PLL is sufficient to track the phase error. However at higher pump linewidths of 0.8, 1 and 1.5 MHz, the performance of the ANDD-PLL is better due to the more accurate phase error estimation by removing the dependency on the amplitude level of the received 16-QAM symbol; and this would be considered advantageous in a WC scenario where the pump phase noise could be relatively large. The maximum pump linewidths for the wavelength conversion of 16-QAM signals using degenerate FWM at 10 Gbaud using the DD-PLL is 1.4 MHz at BER of 10^{-3} , and 1.2 MHz at BER of 10^{-4} . By using the ANDD-PLL, the pump linewidth limitations can be increased to 2 and 1.6 MHz at BERs of 10^{-3} and 10^{-4} , respectively. The results highlight the importance of selecting pump lasers for use in WC employing FWM in SOA's. Lasers with linewidths lower than the limits outlined in Fig.4-6 are needed to obtain satisfactory performance of wavelength converters based on degenerate FWM.

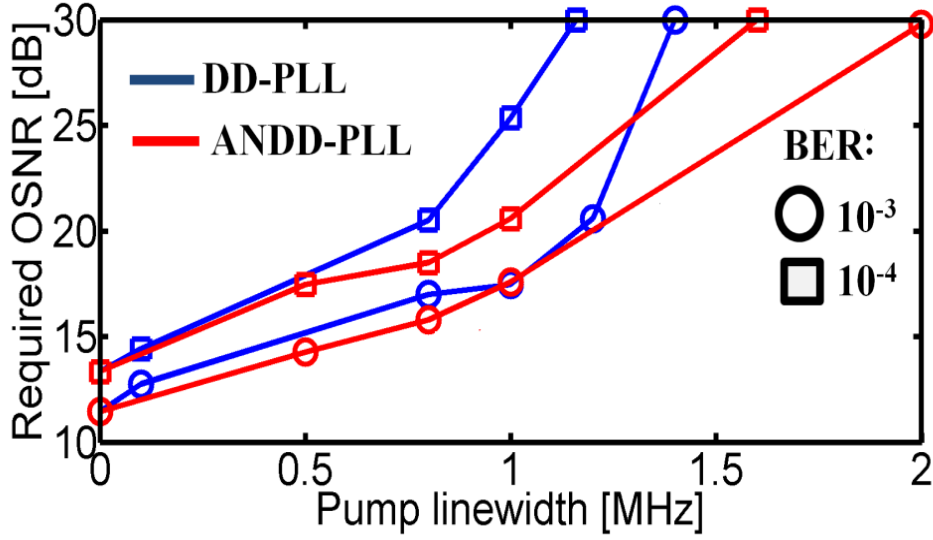


Fig.4-6 the required OSNR of degenerate FWM to achieve a BER of 10^{-3} and 10^{-4} using DD-PLL and AND-PLL.

4.3.1.1 Inclusion of ASE noise

In this subsection, the effect of ASE noise from the SOA is included in the simulations of wavelength conversion based on degenerate FWM. The results are obtained by varying the pump linewidth and noting the BER as the OSNR is increased while considering ASE generation in the SOA, i.e. by including an equivalent optical noise at the input to the SOA in the simulator. The noise figure of the SOA is chosen to be 7.8 dB. Simulations are performed for two different OBPFs with FWHM equal to 16.4 and 47.1 GHz. The results are obtained for both PLLs and the BER vs. OSNR results are shown in Fig.4-7 and Fig.4-8. All the results are compared to the case without ASE noise. The input optical power level of the pump is held constant; therefore the total amount of ASE noise emanating from the SOA remains constant. The SOA is operating under strong gain saturation conditions due to the high input power of the pump therefore the total ASE contribution is small.

When the Full width at half maximum (FWHM) of the OBPF is 16.4 GHz: the results in Fig.4-7 and Fig.4-8 show that the ASE does not affect the performance because the

narrowband OBPF limits the amount ASE noise that reaches the receiver. However, in a real system it may not be feasible to have a filter with such a narrow bandwidth; hence the performance with ASE is investigated when a larger bandwidth filter is employed. When the FWHM of the OBPF is increased to 47.1 GHz then there is degradation in performance when large pump linewidths, > 800 kHz, are used. The degradation is most pronounced when using the standard DD-PLL. From Fig.4-7, it can be read off the required OSNR to achieve a level of performance for each pump linewidth.

For the cases when the pump linewidths are 0 and 500 kHz, the PLLs can operate at a BER of 10^{-4} when the OSNR levels are set to < 20 dB. The OSNR set by the ASE contribution must be much larger than 20 dB resulting in a negligible OSNR penalty for the lower linewidths. However, for larger pump linewidths, > 800 kHz, the required OSNR increases dramatically with a minimum OSNR level of ~ 20 dB required to achieve a BER at 10^{-3} for 800 kHz pump linewidth. Fig.4-8 shows that the ANDD-PLL requires a lower OSNR than the DD-PLL to achieve a similar level of BER performance, and hence the ANDD-PLL outperforms the DD-PLL when the ASE from the SOA becomes significant.

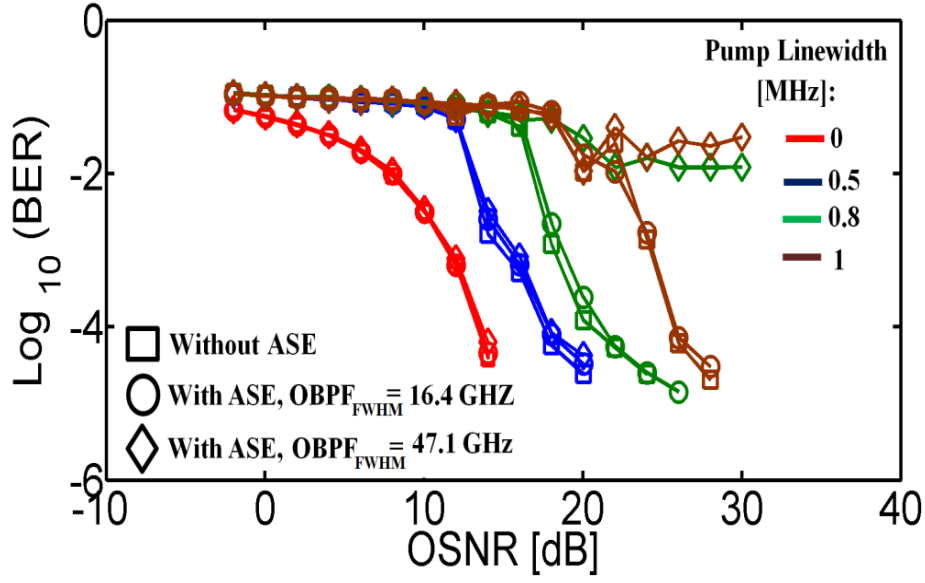


Fig.4-7 Investigation of ASE noise effect on the single pump wavelength conversion of 16-QAM signal at 10 Gbaud using FWM in SOA and DD-PLL.

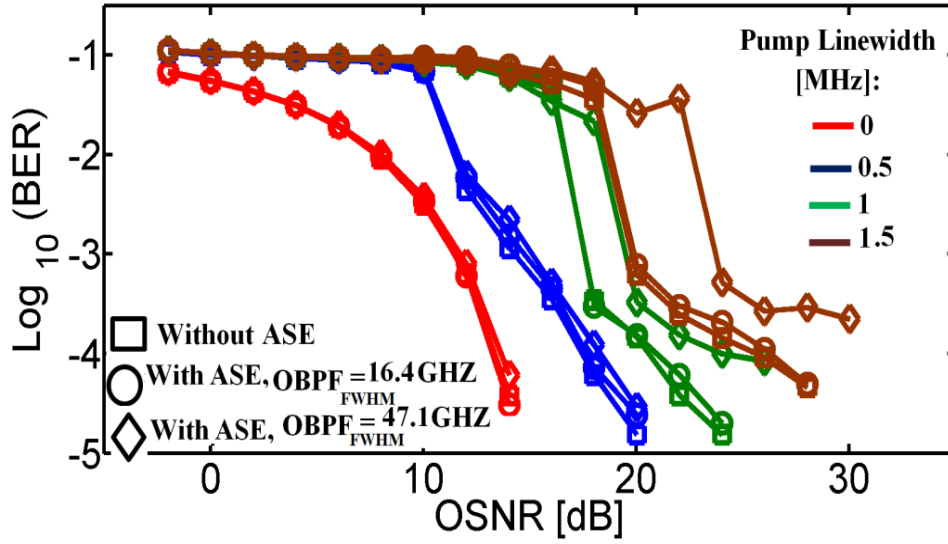
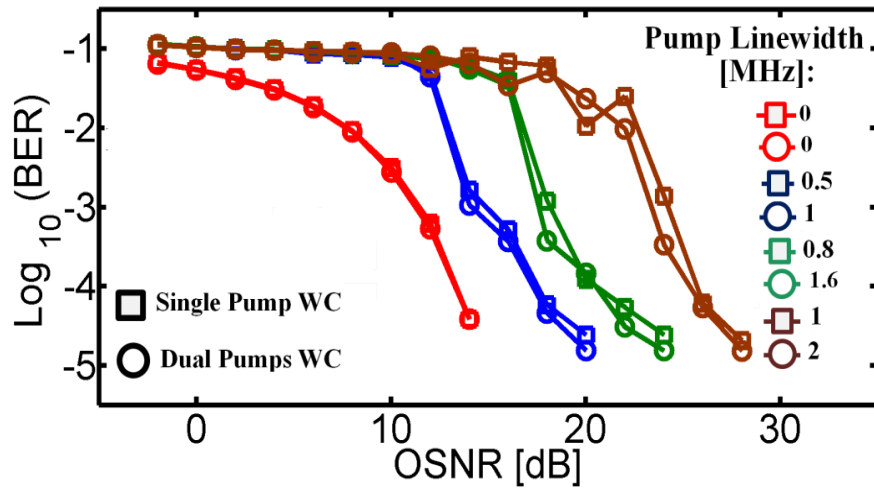


Fig.4-8 Investigation of ASE noise effect on the single pump wavelength conversion of 16-QAM signal at 10 Gbaud using FWM in SOA and ANDD-PLL.

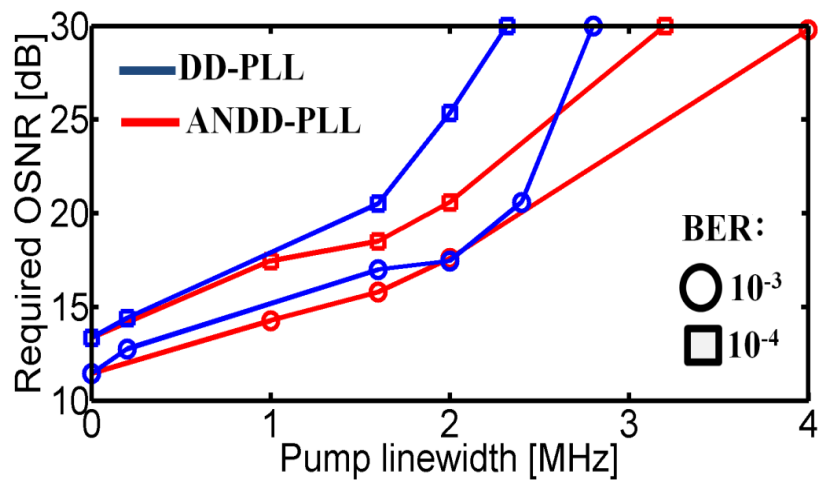
4.3.2 Dual Pump all- Optical Wavelength Conversion of 16-QAM

In this section, non-degenerate wavelength conversion of 16-QAM using FWM in SOA is studied. The 16-QAM signal and two CW pumps are combined, and the SOA is used to achieve wavelength conversion through nondegenerate FWM. Nondegenerate FWM components appear in the SOA output spectrum, as outlined in Fig.4-2. The signal S is placed spectrally close to the pump P_1 . The beating between P_1 and S modulates the pump P_2 and copies of the signal appear at new frequency locations either side of P_2 . The strength of the beating between P_1 and S is determined by the detuning Ω_{P1-S} . The nondegenerate FWM components, $E_{P1}E_{P2}E_S^*$ and $E_{P2}E_SE_{P1}^*$, appear at spectral locations $\pm\Omega_{P1-S}/2\pi$ about P_2 . $E_{P1}E_{P2}E_S^*$ is selected to calculate the BER vs. OSNR performance, and all the results shown here for $E_{P1}E_{P2}E_S^*$ apply equally to $E_{P2}E_SE_{P1}^*$. As it is shown in the simulated output spectra in Fig.4-2(b), $E_{P1}E_{P2}E_S^*$ appears at a frequency of +475 GHz relative to P_1 . The BER versus OSNR performance for $E_{P1}E_{P2}E_S^*$ is calculated with increasing pump linewidth with the linewidths of both pumps being equal ($B_{P1} = B_{P2}$). The results are shown in Fig.4-9(a) using the DD-PLL and compared with the results for degenerate FWM to show the equivalent phase noise transfer to the idler. As expected in order to produce idlers with identical linewidths, the pump linewidth for nondegenerate FWM is double that for degenerate FWM. The corresponding required OSNR versus average pump linewidth to achieve BERs of 10^{-3} and 10^{-4} are shown in Fig.4-9(b). The maximum possible useful pump linewidths for nondegenerate FWM wavelength conversion of the 16-QAM signal at 10 Gbaud using DD-PLL is 2.8 MHz at 10^{-3} , and 2.4 MHz at 10^{-4} . The maximum pump linewidths are increased to 4 and 3.2 MHz at the BERs of 10^{-3} and 10^{-4} when using the ANDD-PLL. The phase noise transfer is decreased for dual pump FWM compared with the single pump

scheme, and is one of the advantages when using non-degenerate FWM to implement wavelength conversion of signals with advanced modulation formats.



(a)



(b)

Fig.4-9 (a) Comparison of relevant linewidth of degenerate and non-degenerate FWM based wavelength conversion of 16-QAM signal at 10 Gbaud using two separate pumps and DD-PLL. (b) The required OSNR of non-degenerate FWM to achieve a BER of 10^{-3} and 10^{-4} using DD-PLL and AND-PLL.

4.4 Wavelength Converting 64-QAM Signals

In this section, the wavelength conversion of 64-QAM signals using degenerate and non-degenerate FWM in a SOA is demonstrated with particular attention paid to the phase noise transfer from pump(s) to the converted idlers. By employing 64-QAM format, the data carrying capacity of lightwave communication systems can be increased by a factor of 6 over traditional on-off keyed transmission. The simulation platform employed is shown in Fig.4-10, where the 10 Gbaud 64-QAM signal is created in the transmitter (T_X) and is combined with two continuous wave pumps (P_1 and P_2) and amplified in an SOA to perform AOWC of the 64-QAM signal.

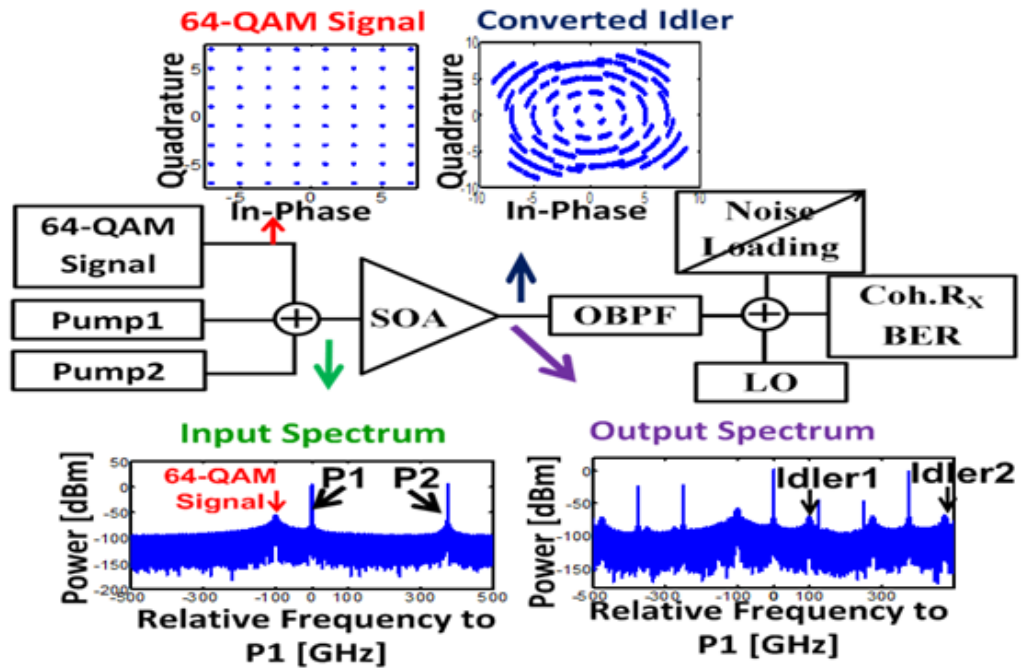


Fig.4-10 AOWC of 64-QAM schematic using FWM in SOA with the optical spectra at the SOA input and output. Constellation diagram of the 64-QAM signal and detected idler with pump linewidth is set to 50 kHz.

The wavelength converted 64-QAM signals; Idler1 and Idler 2 as indicated in Fig.4-10, are then filtered out using an optical band pass filter (OBPF) and then detected using an ideal coherent receiver. The converted 64-QAM signal is demodulated using the amplitude normalized decision directed-PLL (ANDD-PLL) in order to detect the 64-QAM symbols, as outlined in section 4.2. Degenerate FWM and nondegenerate FWM products (labeled Idler 1 & Idler 2 respectively in Fig.4-10) appear in the SOA output spectrum. Constellation diagrams of the 64-QAM signal are also plotted in Fig.4-10 to highlight the effect of phase noise transferring from pump(s) to the idler for the scenario of single pump WC in which P_2 is turned off and the only idler generated is $E_{P1}^2 E_S^*$ (Idler 1). For the case of dual pump FWM based WC, $E_{P1} E_{P2} E_S^*$ (idler2) is selected and calculate the BER versus OSNR performance with increasing pump linewidth for both scenarios of degenerate and nondegenerate WC. The linewidth of both pumps are equal ($B_{P1} = B_{P2}$) for the case of dual pump FWM. The calculated BER results are shown in Fig.4-11. When the pump linewidth increases, the OSNR of the detected idler must be increased to achieve the same BER performance. As it is shown in section 4.3.2 for the case of 16-QAM, the pump linewidth tolerance of degenerate (single pump) FWM is half that of nondegenerate FWM, therefore similar BER curves are obtained when the pump linewidth for degenerate FWM is half that of the pump linewidth for nondegenerate FWM. For the case of degenerate FWM, the pump linewidth that achieves a 2 dB OSNR penalty at the BER of 10^{-4} is 50 kHz (relative to the case of an ideal pump); correspondingly the pump linewidth for nondegenerate FWM that achieves a similar penalty is 100 kHz. The maximum pump linewidths for nondegenerate (degenerate) FWM WC of 64-QAM signals at 10 Gbaud using ANDD-PLL are 900 kHz (450 kHz) at the BER of 10^{-3} and 800 kHz (400 kHz) at the BER of 10^{-4} .

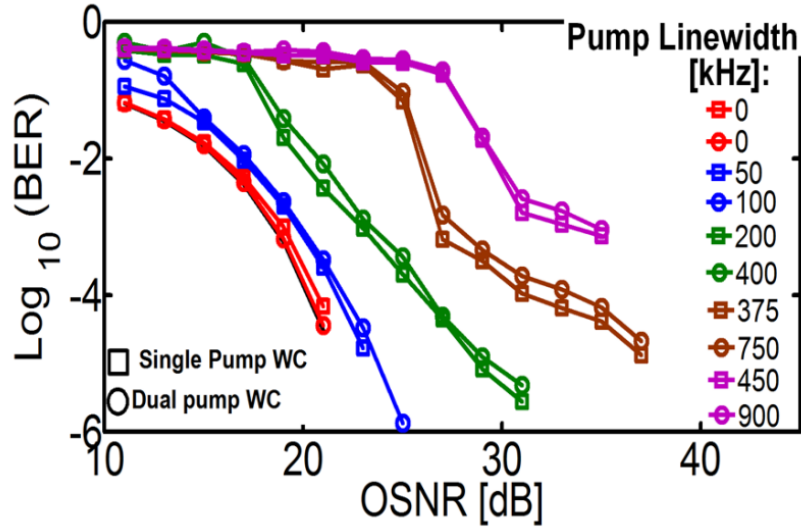


Fig.4-11 BER versus OSNR of degenerate wavelength conversion of 64-QAM signals at 10 Gbaud using ANDD-PLL.

4.5 Summary and conclusion

Combining coherent transmission techniques with optical packet/burst switching can enable optical networks that are highly efficient. A key function that will need to be implemented in these networks is the wavelength conversion of signals employing advanced modulation format. FWM using SOAs is a very suitable candidate to perform wavelength conversion of these signals; however the selection of the appropriate pump lasers used for wavelength conversion in these packets switched networks is vital, as the linewidth of the pump laser will significantly affect system performance. This is especially the case for obtaining fast tuning lasers for use in packet/burst switched networks, where tuning times < 100 ns are necessary, but the laser linewidths can be of the order of a few MHz [19]. In this chapter, the required OSNR and laser linewidth limits to achieve wavelength conversion of 16-QAM and 64-QAM signals using FWM in SOA at 10 Gbaud are presented. The results shown here can be appropriately scaled for different signal baudrates and FWM as a wavelength conversion technique is transparent to baudrate. By increasing the symbol rate to 30 Gbaud, for example, which is the baud rate of commercial WDM systems, the linewidth that produces BER

performance of 10^{-3} and 10^{-4} should be 3 times greater than those for 10 Gbaud because the symbol period for 30 Gbaud is 3 times smaller than that of 10 Gbaud. However, at higher baudrate the signals have larger bandwidth and signal-pump leakage may be experienced depending on the detuning between pump and signal, and this may become a limiting factor [1]. As is shown in the results based on 16-QAM, the system performance could be improved by using ANDD-PLL in the coherent receiver for the carrier phase recovery. These results show that by increasing the spectral efficiency (using 16-QAM and 64-QAM as an advanced modulation formats) much tighter pump linewidth tolerances are required in comparison with wavelength conversion of DQPSK because for 16(64)-QAM the constellation points are more closely spaced in the I-Q space, and hence system performance is more sensitive to phase and/or amplitude noise.

Bibliography

- [1] S. T. Naimi, S. Ó Dúill and L. P. Barry, “Simulations of the OSNR and Laser Linewidth Limits for Reliable Wavelength Conversion of DQPSK Signals Using Four-Wave Mixing,” *J. Optics Communications*, vol. 310, no. 1, pp. 150-155, 2014.
- [2] T. Mizuoichi, “Recent Progress in Forward Error Correction and Its Interplay With Transmission Impairments,” *IEEE J. Sel. Topics in Quant. Electron.* vol.12, no. 4, pp.544 -554, 2006.
- [3] M. Morshed, L. B. Du, B. Foo, M. D. Pelusi, B. Corcoran, and A. J. Lowery, “Experimental demonstrations of dual polarization CO-OFDM using mid-span spectral inversion for nonlinearity compensation,” *Opt. Express*, vol. 22, no. 9, pp. 10455–10466, 2014.
- [4] J. Zhou, N. Park, J. W. Dawson, K. J. Vahala, M. A. Newkirk, and B. I. Miller, “Terahertz four-wave mixing spectroscopy for study of ultrafast dynamics in a semiconductor optical amplifier,” *Appl. Phys. Lett.*, vol. 63, no.9, pp. 1179–1181, 1993.
- [5] G. P. Agrawal, “Population pulsations and nondegenerate four-wave mixing in semiconductor lasers and amplifiers,” *J. Opt. Soc. Am. B*, vol. 5, no. 1, pp. 147–159, 1988.
- [6] A. Uskov, J. Mørk, and J. Mark, “Wave mixing in semiconductor laser amplifiers due to carrier heating and spectral-hole burning,” *IEEE J. Quantum Electron.*, vol. 30, no.8, pp. 1769–1781, 1994.
- [7] A. Mecozzi, S. Scotti, A. D’Ottavi, E. Iannone, and P. Spano, “Four wave mixing in traveling-wave semiconductor amplifiers,” *IEEE J. Quantum Electron.*, vol. 31, no.4, pp. 689–699, 1995.
- [8] I. Koltchanov, S. Kindt, K. Petermann, S. Diez, R. Ludwig, R. Schnabel, and H. G. Weber, “Gain dispersion and saturation effects in four-wave mixing in semiconductor laser amplifiers,” *IEEE J. Quantum Electron.*, vol. 32, pp. 712–720, 1996.
- [9] K. Kikuchi, M. Amano, C. E. Zah, and T. P. Lee, “Analysis of origin of nonlinear gain in 1.5 μ m semiconductor active layers by highly nondegenerate four-wave mixing,” *Appl. Phys. Lett.*, vol. 64, no.5, pp. 548–550, 1994.
- [10] A. Mecozzi and J. Mørk, “Saturation effects in nondegenerate four-wave mixing between short optical pulses in semiconductor laser amplifiers,” *IEEE J. Sel. Top. Quantum Electron.*, vol. 3, no. 5, pp. 1190–1207, 1997.

- [11] D. Cassioli, S. Scotti, and A. Mecozzi, "A time-domain computer simulator of the nonlinear response of semiconductor optical amplifiers," *IEEE J. Quantum Electron.*, vol. 36, no. 9, pp. 1072–1080, 2000.
- [12] D. Marcuse, "Computer Simulation of FSK Laser Spectra and of FSK-to-ASK Conversion," *IEEE J. of Lightw. Techn.* vol.8, no.1110, 1990.
- [13] B. Filion, W. C. Ng, A. T. Nguyen, L. A. Rusch, and S. LaRochelle, "Wideband wavelength conversion of 16 Gbaud 16-QAM and 5 Gbaud 64-QAM signals in a semiconductor optical amplifier," *Opt. Express*, vol. 21, no. 17, pp. 19825–19833, 2013.
- [14] S. J. Savory, "Digital coherent optical receivers: algorithms and subsystems," *IEEE J. of Sel. Top. in Quant. Electron.*, vol.16, No. 5, 1164, 2010.
- [15] S. J. Savory, G. Gavioli, R. I. Killey, and P. Bayvel, "Electronic compensation of chromatic dispersion using a digital coherent receiver," *Opt. Express*, vol. 15, no. 5, pp. 2120–2126, 2007.
- [16] U. Mengali and A. N. D'Andrea, "Synchronization Techniques for Digital Receivers", ISBN 978-1-4899-1809-3, Springer, 1997.
- [17] S. Haykin, 'Adaptive Filter Theory', ISBN 13:978-0132671453, Prentice Hall, 2001.
- [18] Y. Mori, C. Zhang, K. Igarashi, K. Katoh, and K. Kikuchi, "Phase-noise tolerance of optical 16-QAM signals demodulated with decision-directed carrier-phase estimation," presented at the Optical Fiber Communication Conf, *OFC*, CA, USA, 2009, paper OWG7.
- [19] T. N. Huynh, F. Smyth, L. Nguyen, and L. P. Barry, "Effects of phase noise of monolithic tunable laser on coherent communication systems," *Opt. Express*, vol. 20, no. 26, pp. B244–B249, 2012.

Chapter 5- All Optical Wavelength of Conversion of Nyquist-WDM Superchannels Based on Advanced Modulation Format Using FWM in SOAs

5.1 Introduction

The capacity of optical networks needs to grow by 29% per annum in order to meet the ever-increasing network end-user demands [1]. Conventional wavelength division multiplexing (WDM) would not suffice to meet these demands and new approaches are being developed, with the use of multilevel modulation formats and polarization multiplexing capable of increasing the spectral efficiency to several $\text{bits}^{-1}\text{Hz}^{-1}$ [2]. Building on the use of multilevel modulation formats and polarization multiplexing, another solution to satisfy the growing demand for bandwidth in future networks will be to minimize the spectral occupation of a given channel. This can be achieved through Nyquist-WDM (N-WDM) superchannel technology, which involves the combination of several lower data rate optical wavelength carriers (sub-channels) with each subcarrier occupying the minimum possible bandwidth [3-7]. These superchannels can be routed through the optical network as a single entity [8]. Nyquist pulse shaping is employed in the sub-channels to ensure that the channels are spectrally shaped so that they occupy the minimum bandwidth, close to or equal to the

Nyquist limit (symbol rate) to avoid inter-channel interference (ICI)) [9]. The subcarriers can thus be multiplexed at the transmitter (T_x) with spacing close or equal to the baud-rate of each sub-channel. Despite all the ongoing efforts to generate and transmit these superchannels, these superchannels will still need to be routed through the network. Routing these N-WDM superchannels in the optical domain as a single channel would be a great advantage because the superchannel would not need to be detected and processed using electronic and digital signal processing (DSP) technology at intermediary network nodes. A schematic of optical–electronic–optical (O–E–O) conversion is shown in Fig.5-1 (a). By using this technique, if the superchannel comprises of N subcarriers then: N coherent receivers, N local oscillators, N DSP blocks are required to detect the superchannel and N optical sources (potentially derived from an optical frequency comb source) and N I-Q modulators are required to re-transmit the superchannel at the new wavelength. However, an all-optical wavelength converter (AOWC), as depicted in Fig.5-1 (b), would be able to convert the superchannel to a different wavelength using a *single* wavelength conversion device, thus avoiding costly O-E-O conversions at each node. As was discussed in previous chapters, four-wave mixing (FWM) in semiconductor optical amplifiers (SOA) is attracting a lot of interest recently for wavelength converting signals with advanced modulation formats [10-14]; with experimental demonstrations of converting 16-state quadrature amplitude modulation (QAM) [11],[14] and 64-state QAM [14] in SOAs.

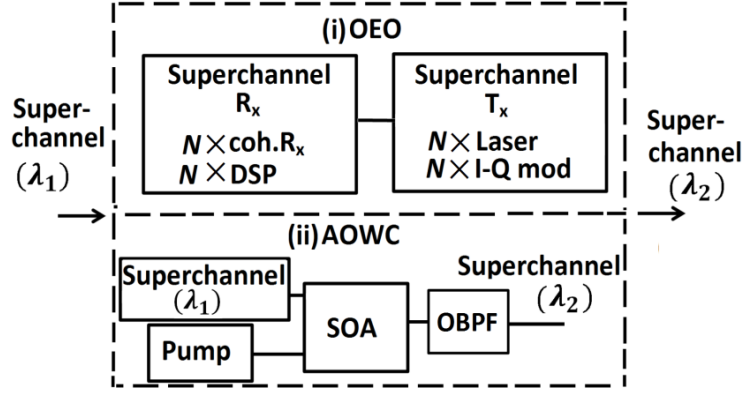


Fig.5-1 Comparison of wavelength conversion of N-WDM superchannel based on Optical-Electrical-Optical (O-E-O) conversion and all-optical wavelength conversion of N-WDM superchannel based on FWM in SOA. Rx: receiver, Coh. Rx: coherent receiver, DSP: Digital signal processing. I-Q mod: I-Q modulator, SOA Semiconductor Optical Amplifier. OBPF: optical band pass filter. Tx: Transmitter.

The transparency of FWM in semiconductor SOAs to modulation format and baudrate, in addition to the FWM process having acceptable wavelength conversion efficiency (> -10 dB) with pump – signal detunings over several hundred GHz, makes SOAs suitable candidates to perform AOWC of superchannels with bandwidths of a few hundred GHz. Even though FWM based wavelength conversion of single channel signals with DQPSK and 16-QAM formats have already been demonstrated in chapter 3 and chapter 4 [10-14] and considered for superchannels comprised of orthogonal frequency division multiplexed signals in [15], the issue of wavelength converting N-WDM superchannels in an SOA has not yet been investigated. For single carrier systems, the conversion of 16-QAM was possible with just a 1 dB power penalty [14], which means that there is scope for multi carrier systems to be wavelength converted in SOAs. In this chapter, the performance of wavelength conversion of an N-WDM superchannel using FWM in SOAs is demonstrated through numerical simulations. The effects of raised cosine (RC) and root raised cosine (RRC) signal pulse shaping are considered within the wavelength conversion process, as well considering modulation formats of DQPSK and 16-QAM for the sub-channel modulation. The system

performance is investigated for back to back (B2B) scenario to serve as the baseline comparison for all the results from the wavelength conversion using degenerate and nondegenerate FWM. It is found that the biggest issue when converting such a superchannel in SOAs is that the SOA gain saturation due to the superchannel itself plays an important role in determining the bit error rate (BER) performance of the whole scheme. Not only can the superchannel distort itself through gain saturation, which for the case of a superchannel is FWM amongst the subcarriers or simply termed ‘intra-channel FWM’, but the resulting gain modulation causes cross-gain modulation (XGM) on the pump that can interfere with the converted superchannel because the signal-pump detuning is comparable to the spectral width of the superchannel and hence degrades the performance of the wavelength converter. The issue of XGM is overcome by optimizing the pump power so that the pump power is much greater (> 23 dB) than the power of the superchannel to limit SOA gain saturation due to the superchannel, and that the input pump power should be around twice the SOA gain saturation power. In addition, the detuning between the pump and superchannel needs to be optimized to achieve the best performance balance between interference from XGM for small pump-superchannel detunings, and the roll-off in conversion efficiency due to larger pump-superchannel detuning. It must be added that intra-channel FWM will be present though is not very significant in this situation because the XGM gain fluctuations acting on the pump cause a much stronger interfering effect with larger spectral extent. The simulations are based on a SOA model that can mimic the effects of nonlinear-style SOAs [17] which are the type used for optical signal processing. The results show that an 8×28 Gbaud superchannel with DQPSK modulation format (aggregate of 448 Gbit/s) could be wavelength converted using FWM for both RC and RRC pulse shaping. For 16-QAM a total of 8×28 Gbaud (aggregate 896 Gbit/s) can be converted for RRC pulse shaping. However, when we consider increasing amounts of amplified spontaneous emission (ASE) noise levels from the SOA, this can be a

performance limiting factor for the subcarriers with the smallest conversion efficiency especially for the 16-QAM modulation format. For converting 16-QAM superchannels, SOAs with noise figures (NF) below 10 dB would be required. Even though in this chapter, AOWC of N-WDM superchannel based on a single-polarization are presented, the estimated performance would be equally valid for dual-polarization superchannel because FWM-based WC of dual polarization would require that each polarization be separated and converted individually via FWM. In such WC schemes, each polarization component could be demultiplexed and converted individually in separate SOAs or in a counter propagating scheme as in [18-19].

The chapter is organized as follows. In Section 5.2, the details of the simulator are explained, including the superchannel generation and a modified SOA model that accurately accounts for the internal scattering losses. In 5.3, the results for B2B, single and dual pump FWM conversion of Nyquist-WDM superchannel employing RC and RRC pulse shaping, with both DQPSK and 16-QAM formats are reported. Finally, in section 5.4, the results are discussed and conclusions are drawn.

5.2 Background and simulator

The simulator used to predict the performance of all-optical WC of N-WDM superchannels using FWM in SOA based on DQPSK and 16-QAM modulation formats for the sub-channels will now be described. Fig.5-2(a) depicts the simulation schematic of N-WDM superchannel generation using an optical comb generator (OCG). OCG is the optical source employed in the superchannel transmitter and each comb line is modulated using an I-Q modulator with an advanced modulation format such as DQPSK and 16-QAM. The pulse shaping is achieved by passing the modulating electrical signal through a pulse-shaping filter (PSF) (there will be a corresponding matched filter (MF) at the receiver to filter out each subchannel). All the

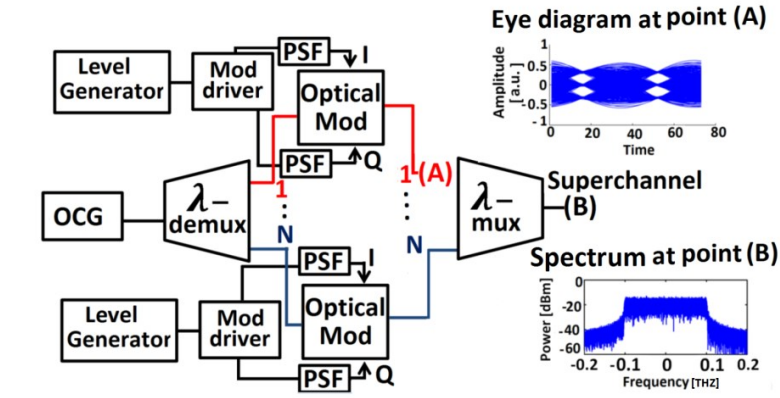
modulated optical subcarriers are multiplexed together to create the superchannel. The generated superchannel is coupled with two pumps (with uncorrelated phase noise) and is wavelength converted through degenerate and nondegenerate FWM in the SOA. In section 4.2, details of modelling wavelength conversion using SOAs based on inter-band, CDP, and intraband, CH and SHB, effects are explained. In this chapter, the SOA model is modified to accurately include for the internal scattering losses [20] which is necessary in this case given the large pump powers required. This revised, lumped SOA model in [20] was found to replicate the output powers of the pumps and idlers from FWM experiments using highly-nonlinear SOAs for optical signal processing functions [17]. SOA gain dynamics due to inclusion of SOA internal loss as well as inter-band and intraband contributions can be modeled) using Eqs.(2-8),(2-9),and(2-10)[13],[20-23].The net small signal gain $(\exp\{h_0 - \alpha_{loss}L\})$ is 34 dB. All of the SOA parameters are listed in Table 5-1. ASE noise generation in the SOA is considered by including an equivalent optical noise, with spectral density $n_{sp}h\nu$, at the input to the SOA [21]; where n_{sp} is the spontaneous emission inversion parameter. The noise figures of the SOA are chosen to be 8, 9, 10, 11 dB. The equation that describes E_{ASE} is given by:

$$E_{ASE}(t) = \sqrt{\frac{h\nu n_{sp} B_{sim}}{2}} (n_I(t) + jn_Q(t)) \quad (5-1)$$

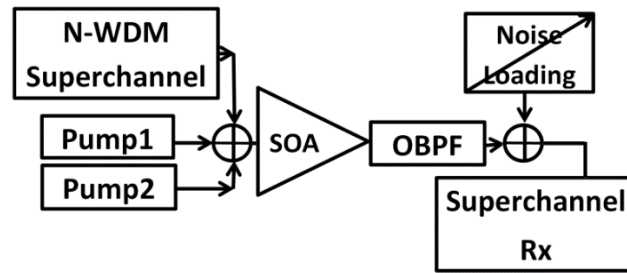
B_{sim} is the simulation bandwidth, n_I and n_Q are unity- variance zero-mean Gaussian random variables to represent the in-phase and quadrature components of the ASE noise respectively. Fig.5-2(b) shows a schematic of the nondegenerate FWM-based wavelength conversion of N-WDM superchannel.

Table 5-1 SOA parameters

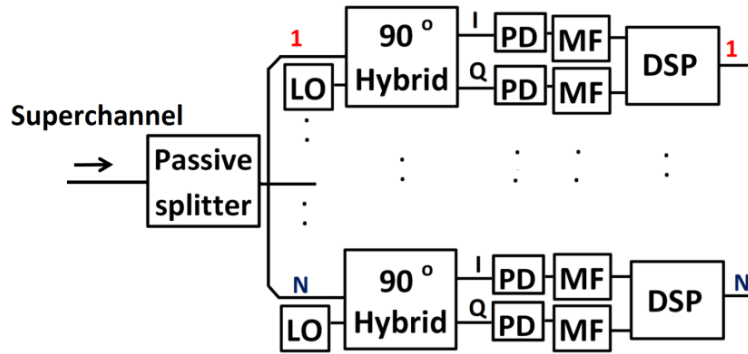
Symbol	Definition	Value
h_0	Unsaturated gain parameter	10
P_{sat}	Gain saturation power	10 mW
τ_S	Carrier lifetime	60 ps
α_{cdp}	Gain-phase coupling parameter	4
$\alpha_{loss}L$	Internal losses	2
L	Length of SOA	1 mm
α_{ch}	Carrier heating gain-phase coupling	3
ϵ_{ch}	Carrier heating nonlinear gain compression factor	1.2 W^{-1}
ϵ_{shb}	Spectral hole burning nonlinear gain compression factor	1.5 W^{-1}
NF	Noise figure	8,9,10,11 dB



(a)



(b)



(c)

Fig.5-2 (a) Generation of N-WDM superchannel with 1th Subcarrier eye diagram and superchannel spectra OCG: optical comb generator, Mod: Modulator, PSF: pulse shape filtering. (b) Simulation schematic of AOWC of Nyquist-WDM superchannel. OBPF: Optical Band Pass Filter, RX: receiver (c) Superchannel receiver. Lo: Local oscillator, PD: Photo detector, MF: Matched filter, DSP: Digital signal processing, BER: Bit error rate.

The superchannel is coupled with two CW pumps and undergoes FWM in SOA. The wavelength converted superchannel is filtered out using a wideband super-Gaussian optical band pass filter and detected using the superchannel receiver. The superchannel receiver, Fig.5-2(c), is a coherent receiver with the required local oscillators. The superchannel comprises of 8 subcarriers, therefore 8 coherent receivers, 8 local oscillators, and 8 digital signal processing blocks are required to detect the transmitted superchannel. In the receiver, the subcarriers are filtered out of the N-WDM superchannel using an electrical matched filter that is matched to the corresponding pulse shaping filter at the transmitter. Each subcarrier is filtered out and the BER performance of each subcarrier is calculated separately. Impulse responses of the RC and RRC pulse shaping is implemented numerically using matched filters in the simulator. The impulse response of the RC and RRC pulse shaping filters are given by [24-25]:

$$h_{RC} = \text{sinc}\left(\frac{t}{T_b}\right) \frac{\cos\left(\frac{\beta\pi t}{T_b}\right)}{1 - 4\left(\frac{\beta\pi t}{T_b}\right)^2} \quad (5-2)$$

$$h_{RRC}(t) = \frac{4\beta}{\pi\sqrt{T_b}} \frac{\cos\left(\frac{(1+\beta)\pi t}{T_b}\right) + \frac{T_b}{4\beta t} \sin\left(\frac{(1-\beta)\pi t}{T_b}\right)}{1 - 4\left(\frac{\beta\pi t}{T_b}\right)^2} \quad (5-3)$$

The convolution of the RRC with itself produces an RC impulse response. The RC and RRC pulse shaping is characterized by two values; β , the roll-off factor, and T_b which is the symbol period such that $1/T_b = 28$ Gbaud which is the symbol-rate used throughout this chapter. The RC pulse shape satisfies the Nyquist inter symbol interference (ISI) criteria by ensuring that there is no ISI at the symbol sampling point; however tight filtering of the subcarriers is needed to reject the other subcarriers in the superchannel. When the impulse responses of the PSF at the transmitter and corresponding matched filter at the receiver is that

of an RC, then there will be finite ISI at the receiver because the overall system response no longer supports zero ISI. On the other hand, when the impulse responses of the transmitter PSF and the receiver matched filter are of an RRC then there will be zero ISI at the symbol sampling points at the receiver because the RRC matched filter removes the ISI added by the RRC PSF at the transmitter. The envelope of input optical field to the SOA is given as:

$$E_{in}(t) = S \exp(j2\pi\Omega_{P1-S}t) + E_{P1} \exp(j\phi_{P1}) + E_{P2} \exp(j(\Omega_{P1-P2}t + \phi_{P2})) + E_{ASE}(t) \quad (5-4)$$

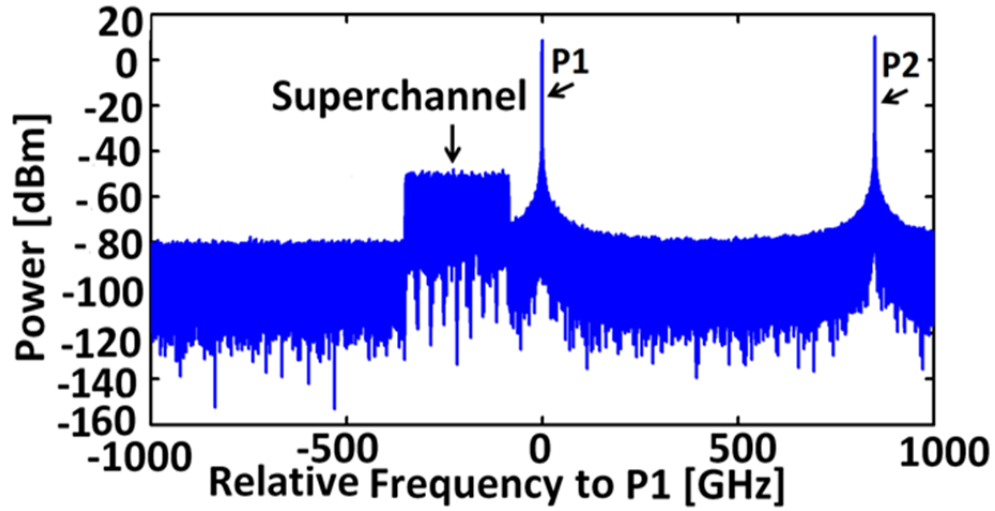
where S is the total field for the superchannel, Ω_{P1-S} is the detuning in linear frequency between the first pump and central frequency of the superchannel, E_{P1} and E_{P2} are the field magnitudes of the first and second pump(s), respectively. Ω_{P1-P2} is the detuning between the two pumps and the uncorrelated phase noise terms on the pumps are ϕ_{P1} and ϕ_{P2}

The optical field for the superchannel is explicitly given as:

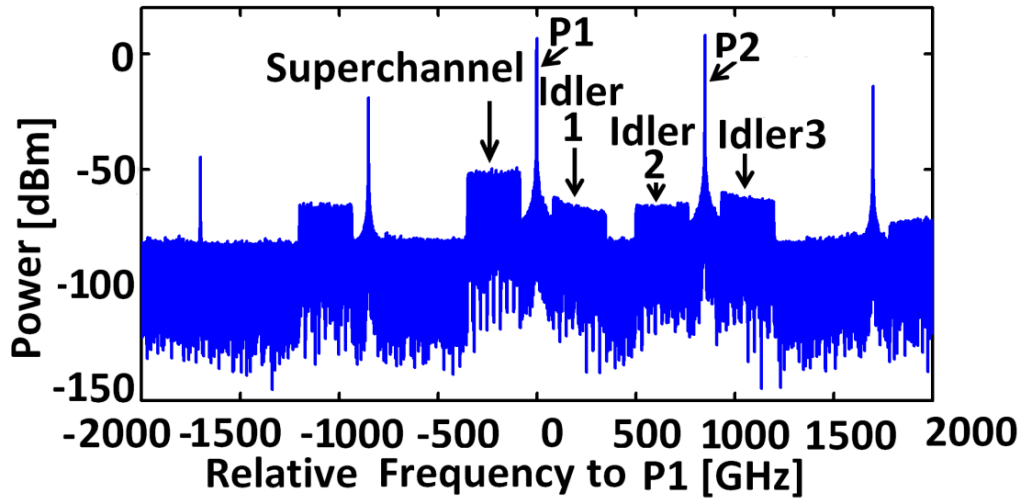
$$S(t) = \sum_{n=-N/2+1}^{N/2} \left[\sum_{m=0}^M c_{nm} h_{RC, RRC}(t - mT_b) \right] \times \exp \left[j2\pi \left(\frac{2n-1}{2T_b} + f_{GB} \right) t \right] \quad (5-5)$$

where N is the number of subcarriers; M is the number of transmitted symbols within each subcarrier; f_{GB} is the spectral guardband and set to 5% of the baudrate to minimize inter-subcarrier interference; c_{nm} is the value of the modulated symbol of the n^{th} subcarrier at the m^{th} symbol slot and $h_{RC, RRC}(t)$ is the RC or RRC pulse shape. The roll off factor of the RC and RRC pulses is set to 10%. The input optical field E_{in} is created using Eq. (5-4), and then the SOA gain can be calculated using Eqs. (2-8), (2-9), and (2-10); the output field E_{out} is thus given by Eq. (4-2). Calculated input and output spectra of the dual-pump WC of N-WDM superchannel based on DQPSK are shown in Figs.5-3 (a) and 5-3(b); the spectral locations of the signal, pumps, and idlers are indicated. It should be noted that simulation bandwidth of 10

THz is employed, in order to capture the generation of the nondegenerate idlers, 100 million sampling points are required to allow to simulate 20×10^4 symbols; the resulting spectral resolution is 100 kHz, which is four orders of magnitude smaller than typical optical spectrum analyser instrumentation. As expected, the input spectrum shows an almost rectangular shaped spectrum for the superchannel. The converted superchannel is shown in the output spectrum of the SOA; each subcarrier achieves a conversion efficiency of ~ -21.5 dB at the optimised pump power of 20 mW. The conversion efficiency is the same for the nondegenerate case as for the degenerate case as long as the detuning between P_1 and P_2 is greater than the detuning between S and P_1 , once this condition is met then the frequency detuning between pumps no longer influences the conversion efficiency, apart from the case when the pumps are placed outside the 3 dB SOA gain bandwidth (which can exceed 60 nm width about the gain peak), though this is beyond the scope of this thesis. The conversion efficiency depends on the detuning between the superchannel ' S ' and pump ' P_1 '. The beating between S and P_1 creates a gain and index grating that scatters pump ' P_2 ' to create idler2 and idler3 as shown in Fig.5-3. The strength of the gain grating depends on the detuning between S and P_1 ; the further away that S is from P_1 the weaker the gain grating and hence the reduction in FWM conversion efficiency. All the OSNR penalties are calculated with respect to the B2B performance for the superchannel by only considering noise loading by varying the OSNR at the receiver. In this work, the phase noise of the pump(s) is set to 5 MHz and 100 kHz for DQPSK and 16-QAM, respectively. In chapter 4 [13], the details of the carrier phase recovery algorithm termed the 'amplitude normalized decision-directed phase-locked loop' (ANDD-PLL) algorithm for carrier phase recovery were explained.



(a)



(b)

Fig.5-3 Calculated (a) input spectra and (b) output spectra of the dual pump scheme showing the spectral location of the N-WDM superchannel, pumps P1 and P2, and the converted idlers. Root Raised Cosine (RRC pulse shaping) is employed. N .B. the resolution bandwidth is 100 kHz.

As it is explained in section 4.2, the phase error estimation for the ANDD-PLL is

$$\text{proportional to } e(n) = \frac{\text{Im}[x_c(n)x_d^*(n)]}{|x_d(n)|^2}. \quad x_c \text{ is the received symbol value, } x_d \text{ is the closest}$$

16-QAM symbol. The accumulated carrier phase recovery estimation for ANDD-PLL is

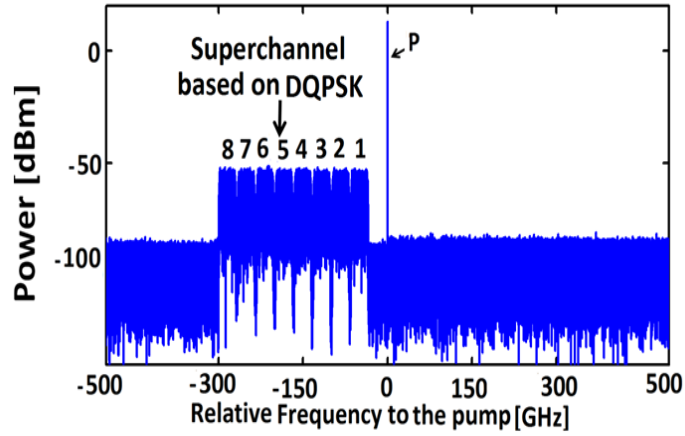
given by $\phi_{err}(n+1) = \phi_{err}(n) + \mu e(n)$. μ is the step size parameter and determines the loop dynamics. For 28 Gbaud 16-QAM, it is found that the optimized value of the loop parameter μ_{opt} should be set to 0.003 in order to achieve a BER of 10^{-4} at the lowest value of OSNR when the pump linewidth is 100 kHz for degenerate FWM.

5.3 Results

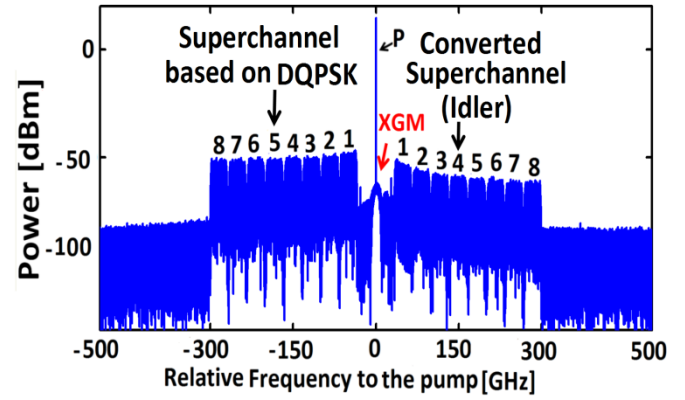
5.3.1 DQPSK

In this subsection, the results of all-optical wavelength conversion of a 448 Gb/s N-WDM superchannel comprised of 8×28 Gbaud DQPSK subcarriers are presented. The superchannel is generated and coupled with two CW pumps with linewidths of 5 MHz to undergo wavelength conversion in the SOA. The wavelength converted superchannel is filtered out using a super-Gaussian wideband OBPF and detected using the superchannel receiver. The superchannel transmitter and receiver schematics are shown in Fig.5-2(a) and Fig.5-2(c) with the number of subcarriers equal to 8 ($N=8$). The subcarriers are detected using coherent receivers with each having its local oscillator tuned to the individual subcarriers. The matched filtering is performed to reject the neighboring subcarriers and the performances of all the subcarriers are calculated. A controlled amount of ASE noise loading is applied before the LO in the receiver for the OSNR variation. The input power of the superchannel to the SOA is set to $100 \mu W$, which is at least an order of magnitude weaker than the pumps, and a typical signal launch power into FWM based wavelength conversion schemes [10-16]. It is found that an input superchannel power of $100 \mu W$ is optimal; with a stronger superchannel power we experience increased intra-channel FWM and with weaker superchannel power the influence of ASE becomes stronger because the ASE noise level is determined by the gain saturation due to the pumps and independent of the input superchannel power. For the case

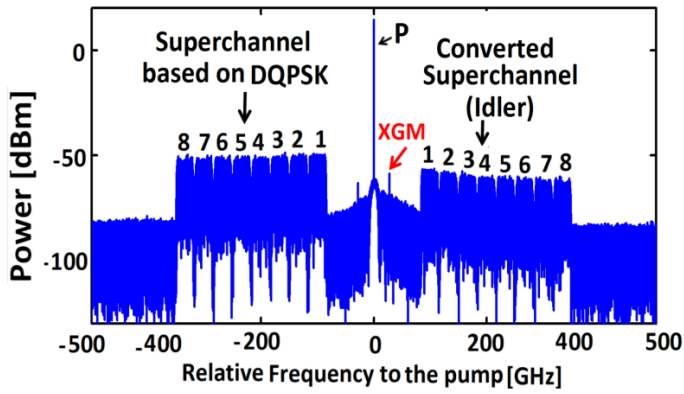
of wavelength conversion using degenerate FWM, no power is considered for pump P_2 . The only generated idler for the case of single pump WC is Idler1 in Fig.5-3(b). The superchannel-pump detuning needs to be set in order to avoid XGM interference: an N-WDM superchannel with rectangular spectrum will create a triangular shaped XGM spectrum about the pump. The triangular shape of the XGM components can easily be explained due to the spectral components being proportional to the convolution of the rectangular spectrum of the superchannel (s) with itself. The input and output spectra of the SOA are shown in Fig.5-4(a) and (b) for the case of 150 GHz detuning. The SOA output spectrum is shown in Fig.5-4(c) when the detuning is set to 200 GHz. Evidence of XGM about the pump is visible in the output spectra by noting the triangular shaped spectral component in the vicinity of the pump in both Fig.5-4(b) and (c). The crosstalk due to XGM can be minimized by setting the superchannel-pump detuning in the range of 200 to 250 GHz. By increasing the value of detuning to be much greater than this optimized range results in reduced conversion efficiencies of the subcarriers furthest from the pump and their BER performance is degraded due to ASE; note that the ASE level is independent of the FWM conversion efficiency. The BER vs. OSNR results for the case of degenerate FWM based on different pump-superchannel detunings of 150 and 200 GHz are shown in Fig.5-4(d). As a baseline comparison, theoretical BER curve for DQPSK signal is showed [26]. By setting the detuning to 150 GHz (blue curves), the performance of subcarriers 1 and 2 (the subcarriers closet to the pump) have the worst penalties because of interference from XGM on the pump (as shown in Fig.5-4 (d)). When the detuning is set to 200 GHz (red curves in Fig.5-4(d)), then all of the subcarriers achieve similar BER performance. Therefore, the detuning is set to 200 GHz which minimizes interference from XGM on the pump, and also ensures that the conversion efficiency is sufficiently high to overcome the ASE from the SOA over the entire superchannel spectrum.



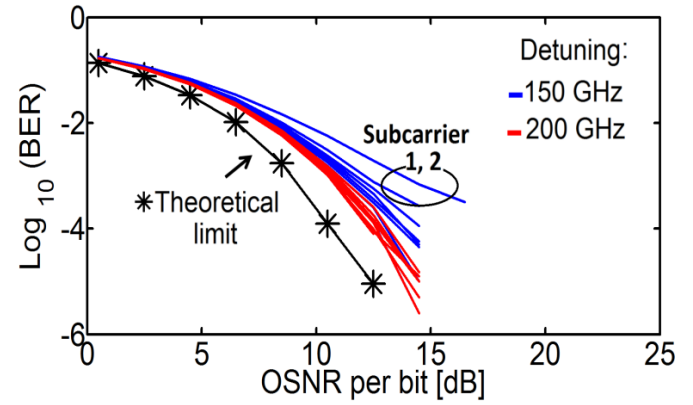
(a)



(b)



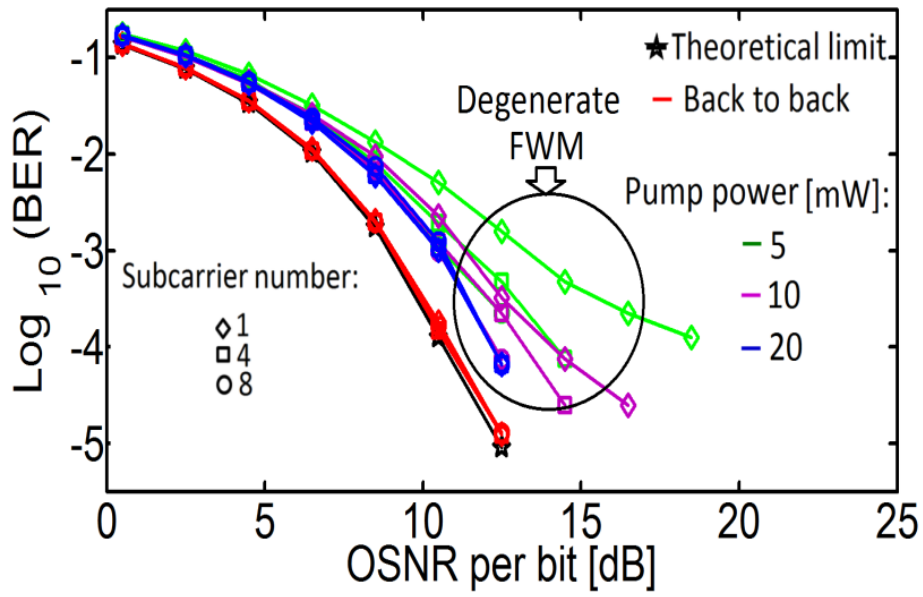
(c)



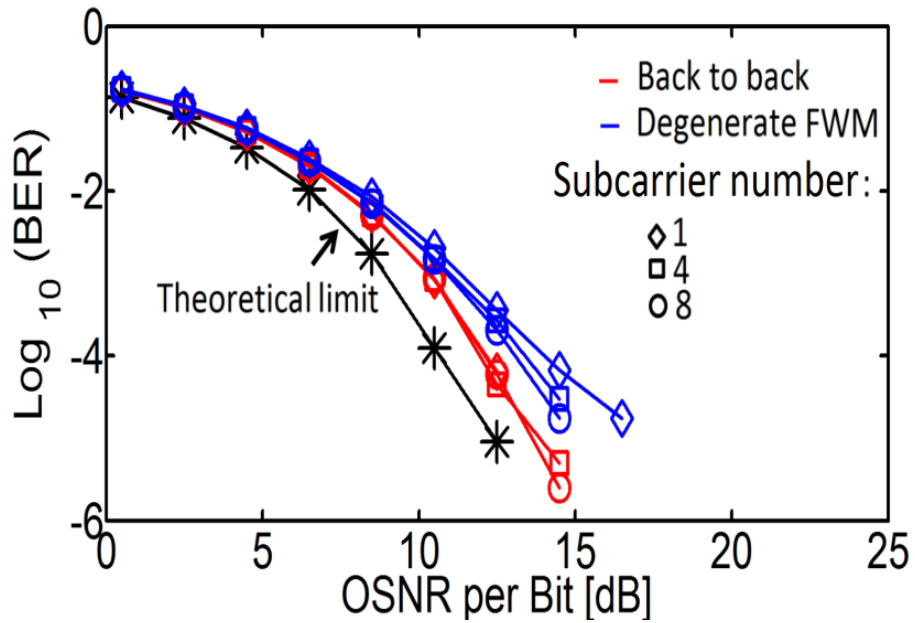
(d)

Fig.5-4 Calculated (a) input spectra of single pump WC of N- WDM superchannel based on 150 GHz detuning between central frequency of superchannel and pump (b) output spectra of the single pump WC of superchannel using 150 GHz superchannel –pump detuning. (c) Output spectra of the single pump WC of superchannel using 200 GHz superchannel –pump detuning. (d) BER vs. OSNR for degenerate WC of 448 Gb/s N-WDM superchannel using 8×28 DQPSK and different detunings. Pump linewidth=5 MHz and all the results are based on root raised cosine (RRC) pulse shaping.

It is found from Fig.5-5(a) that the optimised performance of AOWC of Nyquist superchannel based on RRC pulse shaping is achieved by setting the pump power to 20 mW (which is double the SOA gain saturation power given in Table 5-1), in this scenario the FWM conversion efficiency is -21.5 dB. By decreasing the pump power to either 5 or 10 mW, even though the FWM conversion efficiency increases to -14.5 dB and -17.5 dB, respectively because the SOA gain is less saturated, the performance of the converted superchannel is impaired by higher crosstalk due to XGM. The additional crosstalk results in an OSNR penalty of around 5 dB, at a BER of 10^{-4} for a 5 mW pump compared to a 20 mW pump. Setting the pump power to 20 mW minimizes gain fluctuations due to the intensity of the superchannel $|S|^2$, and additional increases in pump power do not enhance system performance further. When RRC and RC pulse shaping are considered, as expected the B2B performance of RRC shown by red curves in Fig.5-5 (a) is quite matched with the theoretical limit because the corresponding matched filtering at the superchannel receiver removes the ISI. However, B2B performance of RC, shown by the red curves in Fig.5-5(b), suffers a few dB OSNR penalty because of ISI due to the matched filtering operation. The wavelength conversion results for the superchannel using RC pulse shaping with optimized pump power of 20 mW are shown by the blue curves in Fig.5-5(b).



(a)



(b)

Fig.5-5 BER vs. OSNR calculations of back to back and single pump (degenerate FWM) AOWC of Nyquist-WDM superchannel based on DQPSK modulation format (a) RRC pulse shaping and different pump power (b) RC pulse shaping and optimised pump power of 20mW. For more clarity, results are based on 1st, 4th and 8th subcarriers only.

The superchannel employing RRC pulse shaping after wavelength conversion (blue curves in Fig.5-5(a)) outperforms the superchannel employing RC pulse shaping (blue curves in Fig.5-5(b)). The OSNR penalty at the BER of 10^{-4} after wavelength conversion compared to theoretical limit is 2.5 dB for all the subcarriers using RRC pulse shaping. For the case of RC pulse shaping the minimum OSNR penalty is 3 dB (subcarrier dependent). For all of the scenarios, similar performance is achieved even when there is no phase noise on the pump (pump linewidth is zero) which implies that the BER performance is related to the impairments arising within the SOA itself (XGM) and not limited by a pump linewidth of 5 MHz. Now, the BER performance is investigated considering the effects that increasing levels of SOA ASE noise has on the wavelength conversion of the DQPSK superchannel. The results in Fig.5-6 show a slight worsening of the performance when the NF is 10 and 11 dB. While this drop in performance may not be significant for DQPSK, it will be significant for modulation formats with larger symbol cardinalities like 16-QAM because the weaker subcarriers (due to their lower conversion efficiency) suffer more from the rising levels of ASE noise.

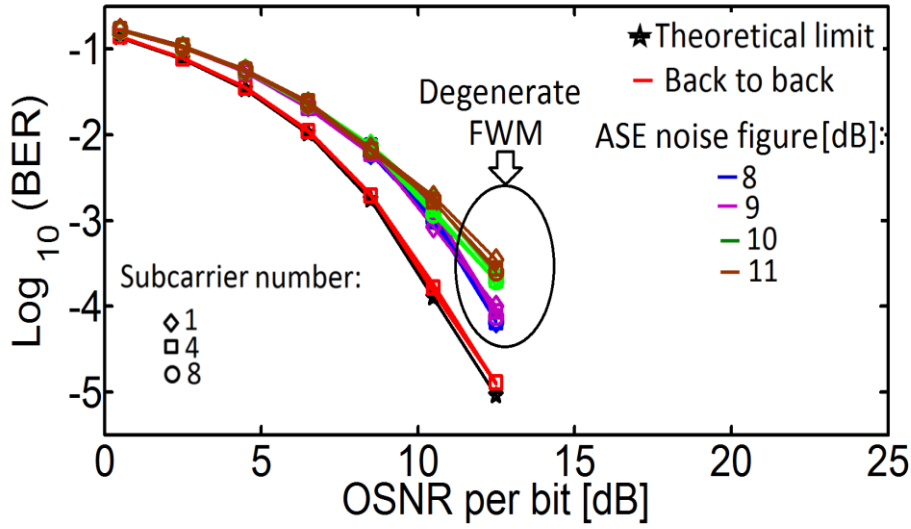


Fig.5-6 BER vs. OSNR calculations of back to back and single pump (degenerate FWM) AOWC of Nyquist-WDM superchannel based on DQPSK modulation format and different level of ASE noise figures from SOA. For more clarity, results are based on 1st, 4th and 8th subcarriers.

As a next step, the performance of nondegenerate wavelength conversion of N-WDM superchannel using the dual pumping scheme with each pump having uncorrelated phase noise is investigated. Nondegenerate FWM has a number of advantages over degenerate FWM, including converting the original signal over a wider wavelength range with constant conversion efficiency [10],[12] as well as having double the pump linewidth tolerance than degenerate FWM. Nondegenerate FWM components appear in the SOA output spectrum, denoted by Idler2 and Idler3 in Fig.5-3; the detuning between pump P_1 and pump P_2 is set to 850 GHz to avoid any spectral overlapping of Idler2 with Idler1. The BER versus OSNR performance is calculated for Idler 3. The 448 Gb/s N-WDM superchannel based on DQPSK is generated and two CW pumps with equal optimised pump powers of 20 mW, ($P_{P1}=P_{P2}=20$ mW) and linewidths of 10 MHz are combined, and the SOA is used to achieve wavelength conversion through nondegenerate FWM. The results are shown in Fig.5-7 and compared with the results for degenerate FWM. As expected, the BER performance of nondegenerate FWM is similar to that of degenerate FWM.

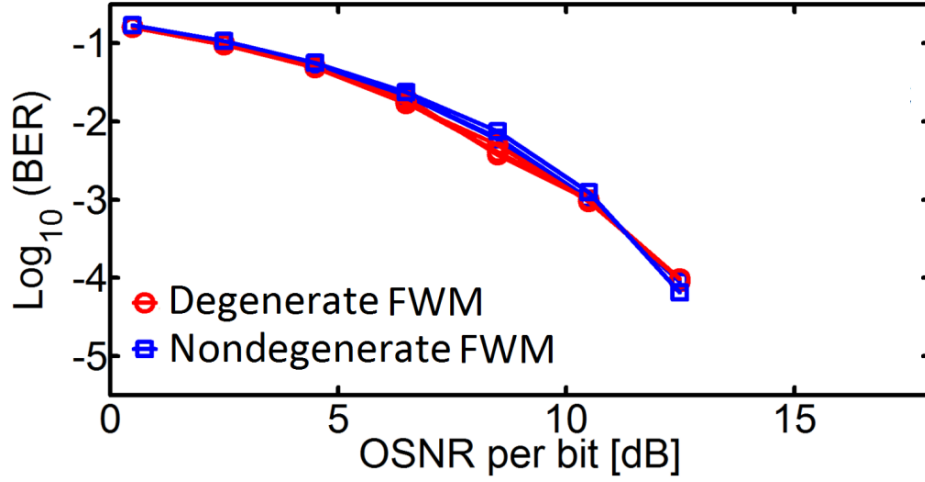
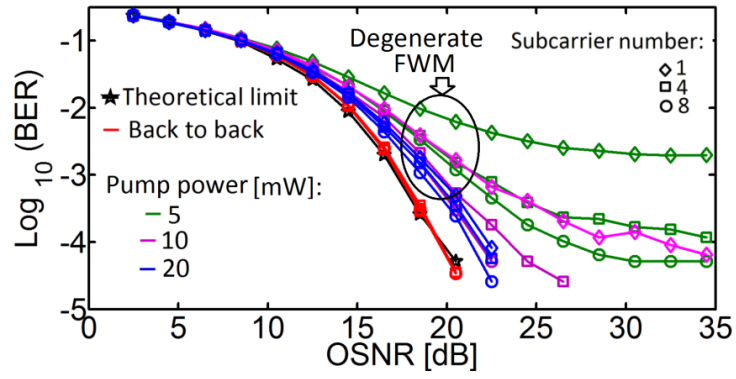


Fig.5-7 Comparison of degenerate and non-degenerate FWM based wavelength conversion of N-WDM superchannel based on DQPSK employing RRC. The pump linewidth (s) is 5/10 MHz for degenerate and nondegenerate WC. For clarity, Results are considered for 1th, 4th, 8th subcarriers.

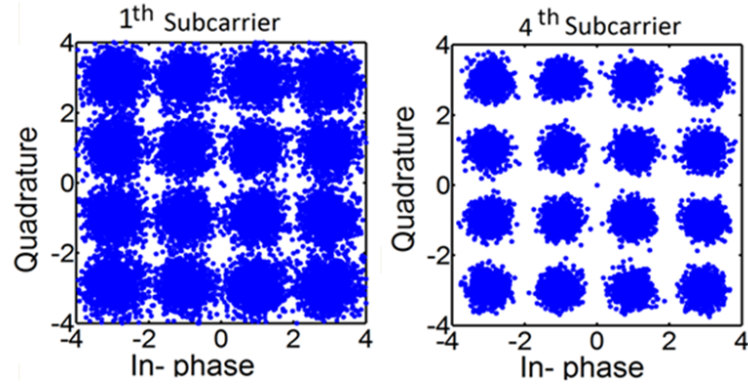
5.3.2 16-QAM

In this subsection, the results on the all- optical WC of 896 Gb/s N-WDM superchannel based on 16-QAM are reported. A superchannel with 8×28 Gbaud 16-QAM subcarriers is generated and coupled with two separate CW pumps, and then is wavelength converted using FWM in the SOA. The wavelength converted superchannel is filtered out using a super-Gaussian wideband OBPF and detected using the superchannel receiver. In order to find the optimised pump power, the BER performance of degenerate FWM with RRC pulse shaping is investigated for the subcarriers with different level of pump powers. The pump linewidth is set to 100 kHz which is the typical linewidth of commercial lasers for coherent communications. The converted N-WDM superchannel is demodulated using the ANDD-PLL with the optimized step size parameter of, 0.003, and detected using the superchannel receiver [13]. As it is shown in the previous section, XGM on the pump plays a significant role in the system degradation and given the closer spaced constellation points for 16-QAM

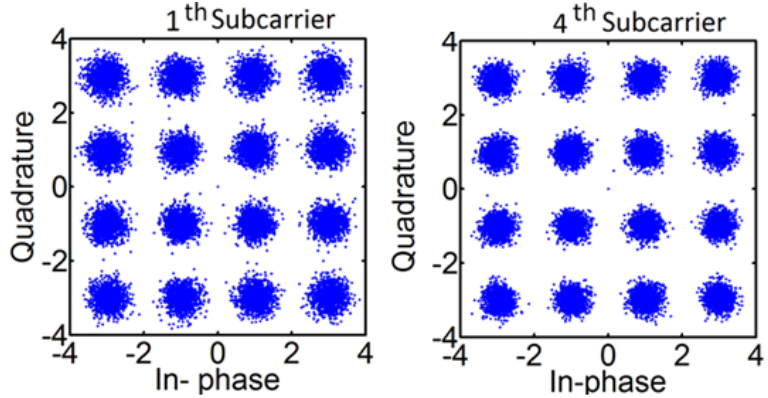
as opposed to DQPSK, it would be expected that XGM would have an even larger effect here. It is thus necessary to increase the detuning between central frequency of superchannel and pump to 220GHz (the detuning was set to 200 GHz when converting the DQPSK superchannel). The BER vs. OSNR results for the B2B performance with RRC pulse shaped subcarriers are shown by the red curves in Fig.5-8(a) which coincide with the theoretical limit for 16-QAM [26]. For the scenario of wavelength converting the 16-QAM N-WDM superchannel based on RRC pulse shaping using degenerate FWM, the BER results for 20mW pump power are shown by the blue curves in Fig.5-8(a). The performance of the 1st, 4th and 8th subcarriers are shown in Fig.5-8(a) for the cases of pump powers of: 5 mW (green), 10 mW (purple) and 20 mW (blue). As it is shown by the green curves in Fig.5-8 (a), the worst performance is achieved using 5 mW pump power and the performance of the converted superchannel is severely degraded with an error floor. The combination of very high XGM from 5 mW pumps and ASE noise from the SOA degrades the performance. By setting the pump power to 10 mW, as it is shown by purple curves in Fig.5-8(a), the performance of the converted superchannel improves due to smaller XGM from the pump. The best BER performance is achieved using a pump of 20 mW, and this is the optimised value of pump power. Additional increases in pump power do not enhance system performance further. The normalized received constellations of the 1st and 4th subcarrier of the converted signal after the matched filtering without any additional noise loading are plotted based on 5 mW and 20 mW pump power in Fig.5-8(b) and Fig.5-8(c). Clearly the constellations for 20 mW pump power show less interference than in the 5 mW pump power case, with the 1st subcarrier displaying the worst performance due to interfering XGM. Therefore, the 896 Gb/s (8×28 Gbaud) superchannel can be converted with OSNR penalty of 3 dB (for the worst performing subcarrier) at the BER of 10^{-4} when employing RRC pulse shaping and optimised pump power of 20mW.



(a)



(b)



(c)

Fig.5-8 (a) BER vs. OSNR calculations of back to back and single pump AOWC of Nyquist-WDM superchannel based on 16-QAM modulation format, different level of pump power. (b) Constellations of degenerate WC of N-WDM superchannel based on 5mW pump power for 1th and 4th subcarrier. (c) Constellations of degenerate WC of N-WDM superchannel based on 20 mW for 1th and 4th subcarriers. The results are based on RRC pulse shaping.

When employing RC pulse shaping for the subcarriers, then the B2B results suffer a 2 dB penalty at the BER of 10^{-4} compared to the theoretical limit, as is shown in Fig.5-9. The blue curves show that the performance of the wavelength converted superchannel is severely degraded and certain subcarriers have poor performance with subcarrier 1 presenting an error floor around 10^{-4} . The combination of ISI, XGM from the pump and ASE noise from the SOA degrade the performance of subcarriers numbered 1 and 4 (which are closer to the pump). In order to investigate the source of the large OSNR penalty for RC as compared to RRC, the normalized received constellations of the 1st and 4th subcarrier of the converted signal after the matched filtering without any additional noise loading are plotted in Fig.5-10(a) and Fig.5-10(b). The visible impairments on these constellations in Fig.5-10(a) are due to ASE and XGM, whereas the visible impairments on the constellations in Fig.5-10(b) are ISI, ASE and XGM. The constellations for RRC show less interference than for RC pulse shaping; as the contribution of XGM and ASE is similar for both pulse shapes and thus the ISI for the RC pulse shaping has a significant role in the overall performance of the wavelength converter.

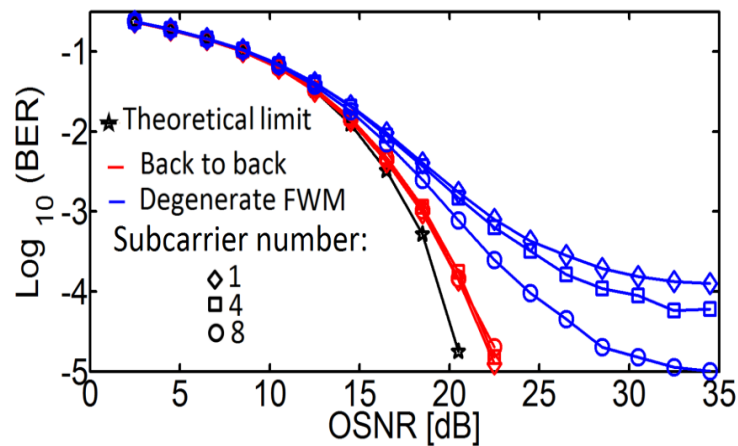


Fig.5-9 BER vs. OSNR calculations of back to back and single pump AOWC of Nyquist-WDM superchannel based on 16-QAM modulation format based on RC Pulse shaping and optimised pump power of 20mW.

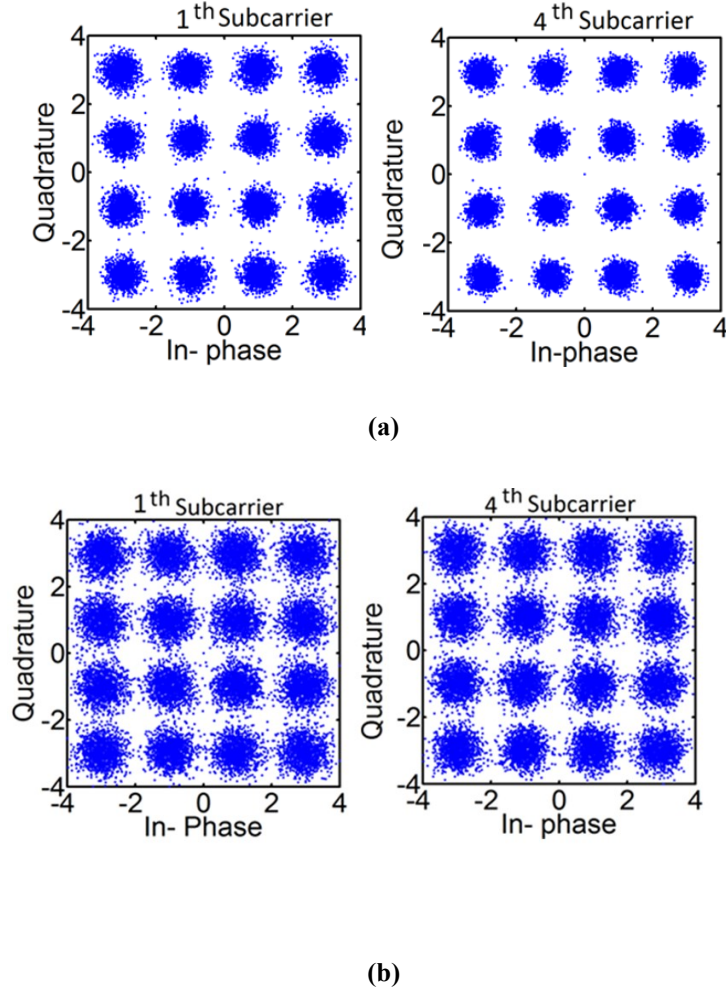


Fig.5-10 (a) Constellations of degenerate WC of N-WDM superchannel based on (a) RRC pulse shaping (b) RC pulse shaping. All the results are for 1st and 4th subcarrier and based on optimised pump power of 20 mW.

For both, RRC and RC pulse shaping, the amount of interference on the 1st subchannel is visibly larger than that on the central 4th subcarrier, which confirms the increased amount of XGM on the 1st subcarriers. Fig.5-11 presents the influence of the ASE from the SOA on the performance of AOWC of N-WDM superchannel based on RRC pulse shaping and operating at the optimised pump power level of 20 mW. Simulations of different levels of ASE noise figure from the SOA are shown. As it is clear in Fig.5-11, by increasing the noise figure to 10 dB (green curves) and 11 dB (brown curves), subcarriers that are furthest from the pump are degraded more because the rising ASE power level affects the weakest subcarriers more.

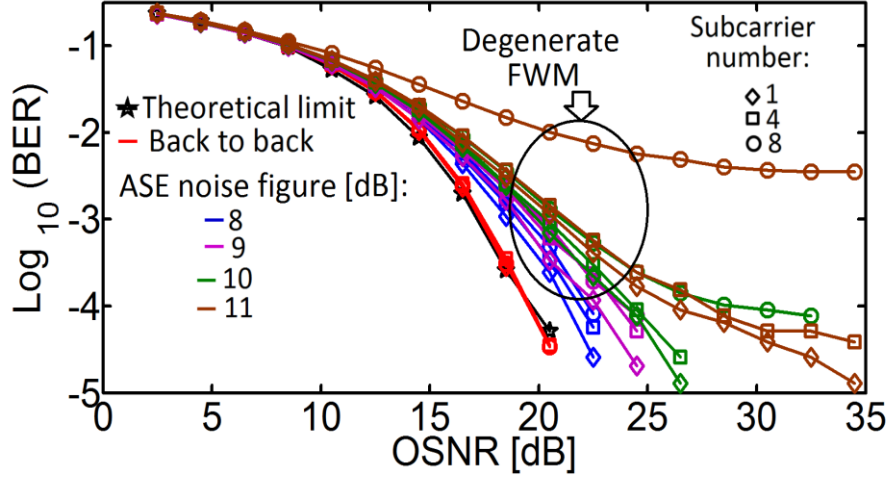


Fig.5-11 BER vs. OSNR calculations of back to back and single pump (degenerate FWM) AOWC of Nyquist-WDM superchannel based on 16-QAM modulation format and different level of ASE noise figures from SOA. Results are based on 1st, 4th and 8th subcarriers RRC pulse shaping and optimised pump power of 20 mW.

For the case here with 16-QAM superchannels, the SOA NFs of 10 dB and 11 dB could cause significant degradation in performance of the weakest converted subcarriers; and therefore care would have to be taken in choosing SOAs as the wavelength converting element.

As a final step, the performance of nondegenerate wavelength conversion of N-WDM superchannel based on RRC pulse shaping using the dual pumping scheme with each pump having uncorrelated phase noise is investigated. In order to apply WC using nondegenerate FWM of N-WDM superchannel based on 16-QAM, two separate lasers with equal pump power of 20mW ($P_{P1}=P_{P2}=20$ mW) are used. Nondegenerate FWM components appear in the SOA output spectrum are outlined in Fig.5-3, the optimized superchannel- pump detuning of $\Omega_{P1-S} = 220$ GHz is considered. BER vs. OSNR is calculated based on Idler 3 and identical pump linewidths of 200 kHz are considered for all the calculations. The detuning between the two pumps P_1 and P_2 is set to 850 GHz. The BER vs. OSNR results are shown

in Fig.5-12, with the subcarriers showing similar performance to each other. The performance of WC using nondegenerate FWM with a pump of 200 kHz linewidth is similar to that using degenerate FWM with a pump of 100 kHz linewidth.

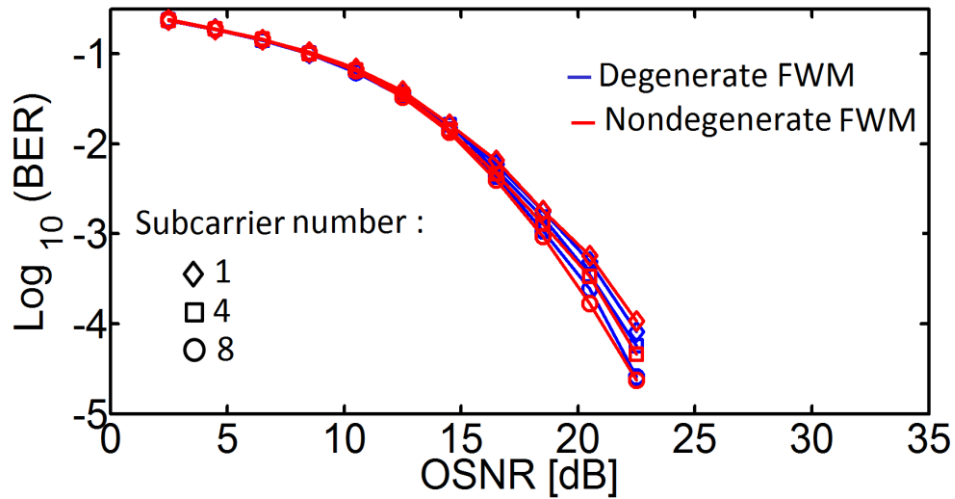


Fig.5-12 Comparison of degenerate and non-degenerate FWM based wavelength conversion of N-WDM superchannel based on 16-QAM. The pump linewidth (s) is 100/200 kHz for degenerate and nondegenerate. Results are considered for 1th, 4th, 8th subcarriers, RRC pulse shaping and optimised pump power of 20 mW.

5.4 Summary and conclusion

Future networks will demand that individual channels have data rates of 400 Gbit/s and above [27]. The most suitable way to achieve such data rates is through using multiple low baudrate carriers combined in such a fashion that the overall channel is considered to be a superchannel [8]. In this chapter, the performance of all-optical wavelength conversion of Nyquist-WDM superchannels using FWM in SOA is investigated to demonstrate that the superchannel can be routed through an optically switched network as a single entity using all-optical wavelength conversion. The Nyquist-WDM superchannel considered in this chapter is composed of DQPSK, 16-QAM subcarriers with consideration for RC and RRC pulse shaping. It is estimated that 448 Gbit/s could be wavelength converted based on DQPSK modulation format using FWM for both RC and RRC pulse shaping. For 16-QAM a total of 8×28 Gbaud (aggregate 896 Gbit/s) can be converted for RRC pulse shaping. To give guidance as to an implementation of AOWC of these superchannels, the BER performance is calculated based on different levels of pump power and SOA noise figures for the cases of DQPSK and 16-QAM. While FWM in SOA is a viable candidate to implement all-optical wavelength conversion of N-WDM superchannels, it is found that the SOA gain saturation limits the BER performance of the subcarriers closest to the pump through XGM. The results show that optimisation of the detuning between pump and central frequency of superchannel, as well as pump power optimization to be around twice the magnitude of the SOA gain saturation power with a 23 dB pump to signal power ratio, are required to minimize the deleterious effect of XGM.

The work also shows that the SOA ASE noise will have significant impact, especially if converting superchannels with 16-QAM, and suggest that SOAs with noise figures of 8 dB or 9 dB would suffice for this purpose. In the work performed here, only wavelength conversion

without considering fibre transmission was considered. The peak-to-average power ratio of dispersion-altered N-WDM superchannels will be larger owing to the further spreading out of the symbols and increased phase modulation induced by the chromatic dispersion. This increased PAPR may increase the XGM in the wavelength converter. Increasing the pump power may be unfeasible; therefore increasing the superchannel-pump detuning would be required to avoid increased XGM effects [28]. It is also important to note that AOWC of N-WDM superchannel based on a single-polarization is presented in this chapter. However, the estimated performance would equally apply for dual-polarization superchannel using a polarization-diverse wavelength conversion scheme [19]. Therefore, by considering dual polarisation, all-optical wavelength conversion of 896 Gb/s (448×2 Gb/s) with DQPSK and 1.8 Tb/s (896×2 Gb/s) based on 16-QAM and are achievable by using FWM in SOA. Concerning the implications for a real-world implementation, these results are indicative of a limitation to the ultimate signal information-rate that could be wavelength converted in SOAs. Experiments using nonlinear SOAs for converting single-carrier DQPSK and 16-QAM signals have shown that conversion with power penalties with respect to the B2B case of 0.25 dB for DQPSK [29] and 1 dB for 16-QAM are obtainable [14]. Therefore there is scope to implement wavelength conversion of multi-carrier superchannels in SOAs. The theoretical performance for 8×28 Gbaud superchannels with 16-QAM showed limitations imposed by the pump-superchannel detuning and the ASE noise subject to the signal power constraint that the signal power be 100 μ W. To be useful in a real system, the wavelength converter should impose minimal penalty with sufficient margin to allow for implementation penalties from insertion losses of filters and additive noise from extra amplifiers. The results for converting eight 16-QAM subcarriers indicate an issue regarding the ASE noise; if the number of subcarriers is halved to four then the signal power per subcarrier can be doubled and the subcarriers furthest from the pump can be converted with higher power. Also the

signal-pump detuning can be decreased to take advantage of the higher conversion efficiency because a narrow bandwidth superchannel can avoid the XGM interference from the pump [30].

Bibliography

- [1] Cisco Visual Networking Index: Forecast and Methodology, 2013–2018. Available from <http://www.cisco.com>.
- [2] R. Essiambre, G. Kramer, P.J. Winzer, G.J. Foschini, B. Goebel, ‘Capacity limits of optical fiber networks’. *J. Lightw. Technol.*, vol.28, no.4, pp.662–701, 2010.
- [3] J. Zhang, J. Yu, Y. Fang, and N. Chi, ‘High speed all optical Nyquist signal generation and full-band coherent detection.’, *Sci. Rep.* vol. 4, no.6156, 2014.
- [4] Y. Huang, D. Qian, F. Yaman, T. Wang, E. Mateo, T. Inoue, Y. Inada, Y. Toyota, T. Ogata, M. Sato, Y. Aono, and T. Tajima, “Real-time 400G superchannel transmission using 100-GbE based 37.5-GHz spaced subcarriers with optical Nyquist shaping over 3,600-km DMF link,” presented at the Optical Fiber Communication Conf., *OFC*, 2013, Paper NW4E.1
- [5] T. Hirooka, P. Ruan, P. Guan, and M. Nakazawa, “Highly dispersion-tolerant 160 Gbaud optical Nyquist pulse TDM transmission over 525 Km”, *Opt. Express*, vol. 20, pp.15001-15007, 2012.
- [6] S. Preussler, N. Wenzel, and T. Schneider, ‘Flexible Nyquist Pulse Sequence Generation With Variable Bandwidth and Repetition Rate’, *IEEE Photon. J.* vol.6, no.4, 2014.
- [7] X. Zhou and L. E. Nelson, ‘400G WDM Transmission on the 50 GHz Grid for Future Optical Networks’, *J. Lightwave Technol.* vol. 30, no.24, pp. 3779 – 3792, 2012.
- [8] G. Bosco, V. Curri, A. Carena, P. Poggiolini; F. Forghieri, ‘On the performance of Nyquist-WDM terabit superchannels based on PM-BPSK, PM-QPSK, PM-8QAM or PM-16QAM subcarriers.’ *J. Lightw. Technol.* vo. 29, no.1, pp.53–61, 2011.
- [9] R. Schmogrow, R. Bouziane, M. Meyer, P. A. Milder, P. C. Schindler, R. I. Killey, P. Bayvel, C. Koos, W. Freude, and J. Leuthold, “Real-time OFDM or Nyquist pulse generation – which performs better with limited resources?,” *Opt. Expr.*, vol. 20, no. 26, pp. B543-B551, 2012.
- [10] S. T. Naimi, S. Ó. Dúill, and L. P. Barry, “Simulations of the OSNR and laser linewidth limits for reliable wavelength conversion of DQPSK signals using four-wave mixing,” *J. Opt. Commun.*, vol. 310, no. 1, pp. 150–155, 2014.
- [11] G. Contestabile, Y. Yoshida, A. Maruta, and K-I. Kitayama, ‘Coherent wavelength conversion in a quantum dot SOA’, *IEEE Photon. Tech. Lett.* vol. 25, no. 9, pp .791 - 794, 2013

- [12] S. P. Ó Dúill, S. T. Naimi, A. P. Anthur, T. N. Huynh, D. Venkitesh, and L. P. Barry, "Simulations of an OSNR limited wavelength conversion scheme," *IEEE Photon. Technol. Lett.*, vol. 25, no. 23, pp. 2311–2314, 2013.
- [13] S. T. Naimi, S. O. Duill, and L.P. Barry, "Detailed Investigation of the Pump Phase Noise Tolerance for the Wavelength Conversion of 16-QAM Signals Using FWM," *IEEE/OSA JOCN*, vol.6, no. 9, pp. 793-800, 2014.
- [14] B. Fillion, W. C. Ng, A. T. Nguyen, L. A. Rusch, and S. LaRochelle, "Wideband wavelength conversion of 16 Gbaud 16-QAM and 5 Gbaud 64-QAM signals in a semiconductor optical amplifier," *Opt. Express*, vol. 21, no. 17, pp. 19825– 19833, 2013.
- [15] Z. Dong, J. Yu, H.-Chien, L. Chen, and G. Chang, "Wavelength conversion for 1.2Tb/s optical OFDM superchannel based on four-wave mixing in HNLF with digital coherent detection" presented at Optical Communication Conf, *ECOC*, Geneva, Switzerland. 2011, paper Th.11
- [16] H. Hu, R. M. Jopson, A. H. Gnauck, M. Dinu, S. Chandrasekhar, C. Xie, and S. Randel, "Parametric Amplification, Wavelength Conversion, and Phase Conjugation of a 2.048-Tbit/s WDM PDM 16-QAM Signal," *J. Lightw. Technol.* vol. 33, no. 7, pp.1286-, 2015.
- [17] R. P. Webb, M. Power, and R. J. Manning, "Phase-sensitive frequency conversion of quadrature modulated signals," *OSA Opt. Expr.*, vol. 21, no. 10, pp. 12713-12727, 2013
- [18] A. H. Gnauck, P. J. Winzer, S. Chandrasekhar, X. Liu, B. Zhu, and D. W. Peckham, "Spectrally efficient long-haul WDM transmission using 224-Gb/s polarization-multiplexed 16-QAM," *J. Lightwave Technol.*, vol. 29, no. 4, pp. 373–377, Feb. 2011.
- [19] M. Morshed, L. B. Du, B. Foo, M. D. Pelusi, B. Corcoran, and A. J. Lowery, "Experimental demonstrations of dual polarization CO-OFDM using mid-span spectral inversion for nonlinearity compensation," *Opt. Express*, vol. 22, no. 9, pp. 10455–10466, 2014.
- [20] S. P. Ó Dúill, L.P. Barry "Improved reduced models for single-pass and reflective semiconductor optical amplifiers," *J. Opt. Commun.*, vol. 334, no.1, pp. 170-173, 2015.
- [21] D. Cassioli, S. Scotti, and A. Mecozzi, "A time-domain computer simulator of the nonlinear response of semiconductor optical amplifiers," *IEEE J. Quantum Electron.*, vol. 36, no. 9, pp. 1072–1080, 2000.
- [22] D. Marcuse, "Computer simulation of FSK laser spectra and of FSK-to-ASK conversion," *J. Lightwave Technol.*, vol. 8, no. 7, pp. 1110–1122, 1990.

- [23] A. Mecozzi, S. Scotti, A. D'Ottavi, E. Iannone and P. Spano, "Four wave mixing in traveling-wave semiconductor amplifiers," *IEEE J. Quantum Electron.*, vol. 31, no.4. pp. 689–699, 1995.
- [24] D. Reis, A. Shahpari, R. Ferreira, D. M. Neves, M. Lima and A. L. Teixeira, "Performance Optimization of Nyquist Signaling for Spectrally Efficient Optical Access Networks]," *IEEE JOCN*, vol. 7, no. 2, pp. A200 - A208, 2015.
- [25] R. Schmogrow, S. Ben-Ezra, P.C Schindler, B. Nebendahl, C. Koos, W. Freude, J. Leuthold, "Pulse-Shaping With Digital, Electrical, and Optical Filters—A Comparison," *J. Lightw. Technol.*, vol.31, no. 15, 2570 - 2577, 2013.
- [26] J. G Proakis, D. G Manolakis. "Digital Signal Processing., Digital signal processing"(3rd ed.): principles, algorithms, and applications, ISBN:0-13-373762-4, Prentice hall, USA, 1996.
- [27] C. Cole, 'Beyond 100G client optics, *IEEE Comms Mag*, vol.50, no.2. , pp. s58-s66, 2012.
- [28] S. P. Ó Dúill, S. T. Naimi, L.P. Barry' Pump linewidth requirements for processing dispersion-altered DQPSK signals using FWM' , *J. of Optics Communications*, vol. 366, pp. 179-184, 2016.
- [29] A. Anthur, R. T. Watts, J. O'Carroll, D. Venkitesh, and L. P. Barry, "Dual correlated pumping scheme for phase noise preservation in all-optical wavelength conversion," *Opt. Expr.*, vol.21, no. 13, pp. 15568-15579 , 2013.
- [30] S. T. Naimi S. P. Ó Dúill, L.P. Barry ' All Optical Wavelength of Conversion of Nyquist-WDM Superchannels Using FWM in SOAs' , *IEEE J. of Lightw. Technol*, vol. 33, no. 19, pp. 3959 – 3967, 2015.

Chapter 6- Phase Noise Tolerant Wavelength Conversion of Nyquist-WDM Superchannels Using FWM in SOAs

6.1 Introduction

With the growth of mobile and video data, the demand for global IP communication bandwidth is continuously growing [1]. At these levels of traffic growth, future networks will demand that each individual channel provides a connection rate of 400 Gbit/s or greater. As was discussed in chapter 5, implementing such a high data rate connection can only be fulfilled using superchannel technology which is a combination of multiple lower baudrate optical wavelength carriers (also termed subcarriers) to form a high capacity superchannel. Each subcarrier of the superchannel will need to occupy the least possible bandwidth in order to maximize the overall information spectral density of the superchannel. Nyquist pulse shaping techniques are employed to minimize the excess bandwidth of the subcarriers so that the bandwidth of the subcarriers equals the subcarrier symbol rate [2]. As was discussed in chapter 5 in more detail, despite the large amount of work on implementing N-WDM superchannels in recent years [4-5], routing of these superchannels in the optical domain according to their central wavelength avoids expensive optical-to-electronic conversion at each switching node. It was discussed in chapter 3 and 4 that four wave Mixing (FWM) in semiconductor optical amplifiers (SOA) is attracting a lot of interest recently for wavelength

converting signals with advanced modulation formats [6-8] due to transparency to modulation format and baudrate. However, the major issue of nondegenerate FWM in SOA is phase noise transfer from the pumps to converted idlers. The linewidth transfer to the idler is the summation of pump linewidth for nondegenerate FWM [9]. Phase noise transfer from the pumps can be avoided using the phase noise tolerant pumping scheme when both pumps have *correlated* phase, i.e. both pumps are derived from an optical comb generator (OCG). The phase noise tolerant dual pumping scheme based on single channel signals with DQPSK and 16-QAM has already been demonstrated in [9-11]. In this chapter, the phase noise tolerant wavelength conversion of Nyquist-WDM superchannel comprising of a 8×28 Gbaud 16-QAM (total bit rate of 896Gb/s) and 6×28 Gbaud 64-QAM signals (raw bit rate of around 1.008Tbit/s) are shown through simulation using FWM in an SOA. The results are shown for both scenarios when the phase noise of the pumps is *correlated* and *uncorrelated* (separate free running lasers). Even though in this chapter, AOWC of N-WDM superchannel based on a single-polarization are demonstrated, the estimated performance would be equally valid for dual-polarization superchannel because FWM-based WC of dual polarization would require that each polarization be separated and converted individually via FWM. In such WC schemes, each polarization component could be demultiplexed and converted individually in separate SOAs or in a counter propagating scheme as in [12]. Therefore, the phase noise tolerant all-optical wavelength conversion of a superchannel with a data rate of around 1.79 Tb/s (896×2 Gb/s) based on 16-QAM and 2.016Tb/s (1.008×2 Tb/s) based on 64-QAM, are achievable by using polarisation diversity and FWM in SOA.

6.2 Results

6.2.1 16-QAM

In this section, the performance of 896 Gb/s wavelength conversion of a Nyquist superchannel is demonstrated using FWM in SOAs. Root raised cosine (RRC) signal pulse shaping is considered for the generation of the superchannel signal as well as considering the modulation format of 16-QAM for the sub-channel modulation. The system performance is investigated for the back to back (B2B) scenario which is then considered as the baseline comparison for all the wavelength conversion results using nondegenerate FWM in semiconductor optical amplifiers. A schematic of the process is shown in Fig.6-1 indicating the spectral locations of the superchannel, pumps and wavelength converted superchannel (idlers). Dual pumps with either correlated or uncorrelated phase noise are used. Pumps with correlated phase noise can be obtained by filtering two lines from an optical comb generator (OCG) [1]; if two separate free-running lasers are used then they will have uncorrelated phase noise. The two pumps are coupled with the N-WDM superchannel comprised of 8×28 Gbaud 16-QAM subcarriers and passed through a semiconductor optical amplifier (SOA) to generate new frequencies via FWM. As was discussed in section 5.3, the optimised power of the pumps is set to 20 mW to overcome cross gain modulation (XGM). The power of the superchannel is set to 100 μW . The wavelength converted superchannel is filtered out using a wideband super-Gaussian optical band pass filter (OBPF) and detected using the superchannel receiver. The subcarriers are detected using coherent receivers with each having its local oscillator tuned to the individual subcarriers. The matched filtering in the receiver is performed to reject the neighboring subcarriers and the performances of all the subcarriers are calculated. The details of modelling wavelength conversion using SOAs are explained in section 5-2 [2].

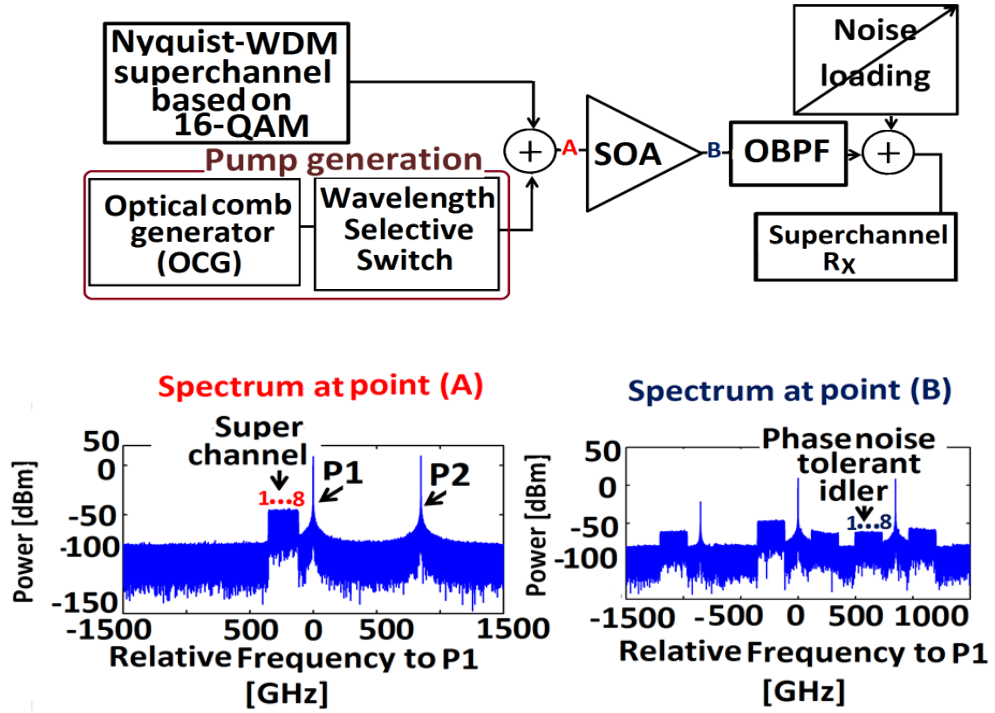


Fig.6-1 Schematic of phase noise tolerant all optical wavelength conversion of N-WDM superchannel based on OCG and using FWM in SOA. OBPF: Optical Band Pass Filter. Rx: receiver.

The noise figure of the SOA was set to 8 dB to account for amplified spontaneous emission. All of the results are compared with the superchannel in back-to-back (B2B) configuration (Fig.6-2). For the case of the pumps having zero linewidth, an implementation penalty of ~ 1.5 dB at the BER of 10^{-3} are noticed for all of the subcarriers with respect to the B2B case; this is due to XGM in the SOA. For the case of using pumps with correlated phase noise, no phase noise from the pumps is transferred to the idler and the performance is exactly the same as when zero linewidth pumps are employed. To highlight this in the simulator, the phase noise of the two pumps are set to be correlated and both have a linewidth of 10 MHz and indeed the performance is the same as the zero linewidth case. However, when the pumps have uncorrelated phase noise then the BER performance deteriorates because of the phase noise transfer from the pumps to the idlers.

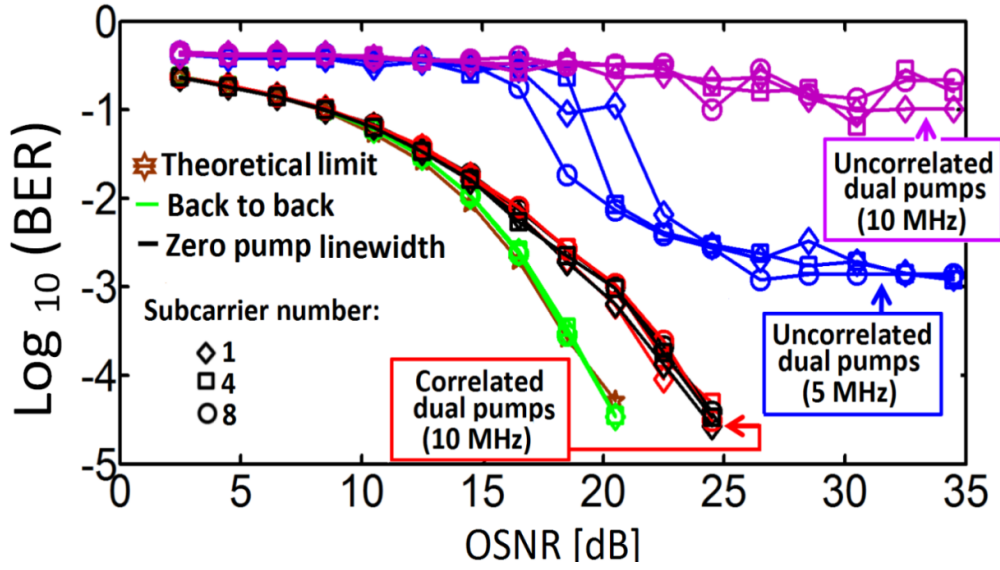


Fig.6-2 Calculated BER vs. OSNR results for the subcarriers of the superchannel for the cases of back to back, correlated and uncorrelated phase noise. For more clarity, results are only shown for 1st, 4th and 8th subcarrier.

The results for the 5 MHz uncorrelated pumps show a large OSNR penalty of 6.5 dB occurs due to the extra phase noise transfer and the scheme completely fails when the pump linewidth increases to 10 MHz. SOAs could be used to wavelength convert Nyquist-WDM superchannels provided that the scheme can overcome the effects of XGM from the pump, and preferably pumps with correlated phase noise should be employed to minimize the phase noise transfer to the idler.

6.2.2 64-QAM

The results of all-optical wavelength conversion of 1.008 Tb/s N-WDM superchannel using the phase noise tolerant nondegenerate FWM scheme are presented in this subsection. The schematic of the process and simulated input and output spectra are also shown in Fig.6-3 indicating the spectral locations of the original superchannel, the pumps and the phase noise tolerant idler. The subcarriers are detected using coherent receivers with each having its local oscillator tuned to the individual subcarriers.

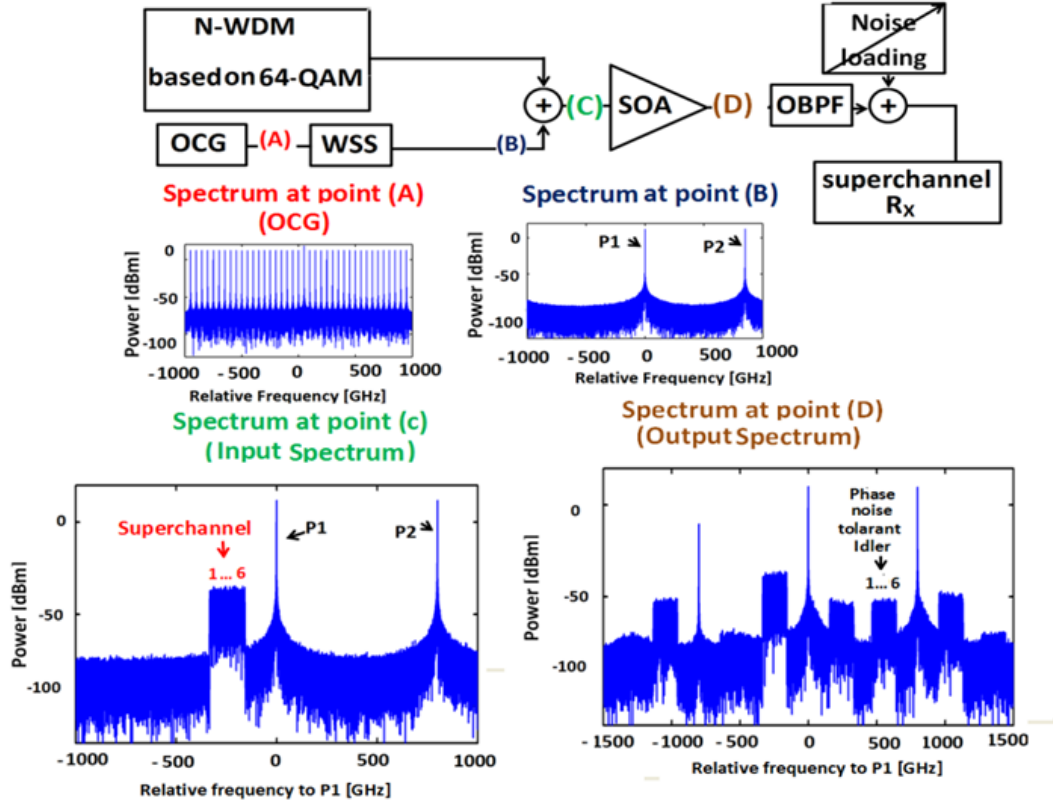


Fig.6-3 Schematic of phase noise tolerant all optical wavelength conversion of N-WDM superchannel based on optical comb generator and using FWM in SOA. OCG: Optical Comb Generator, WSS: Wavelength Selective Switch, SOA: Semiconductor Optical Amplifier, OBPF: Optical Band Pass Filter, Rx: receiver.

The matched filtering at the receiver is performed to reject the neighbouring subcarriers and the performances of all the subcarriers are calculated. A controlled amount of noise loading is applied before the LO in the receiver for the OSNR variation. The BER vs. OSNR results are shown in Fig.6-4. All of the results are compared with back to back (B2B) configuration of 6×28 Gbaud of N-WDM superchannel based on 64-QAM which is the black curve in Fig.6-4. As expected, the B2B performance of superchannel is quite matched with the theoretical limit because the corresponding matched filtering with RRC pulse shaping removes the inter symbol interference. For the case of zero pump linewidth, it is found that an implementation penalty of 2.5 dB at the BER of 10^{-3} for all of the subcarriers with respect to the B2B case; this is due to XGM in the SOA [14]. The results for 5 MHz correlated pumps

were found to be exactly the same as the case for zero pump linewidth due to phase noise cancellation from pump to the idlers and BER performances are shown by the red curves in Fig.6-4. However, when the pumps have uncorrelated phase noise then the BER experiences a worsening performance because of extra phase noise which is transferred from the pumps to converted idler. In this case, by increasing the pump linewidth to 5 MHz, the scheme completely fails as shown by the green curves in Fig.6-4.

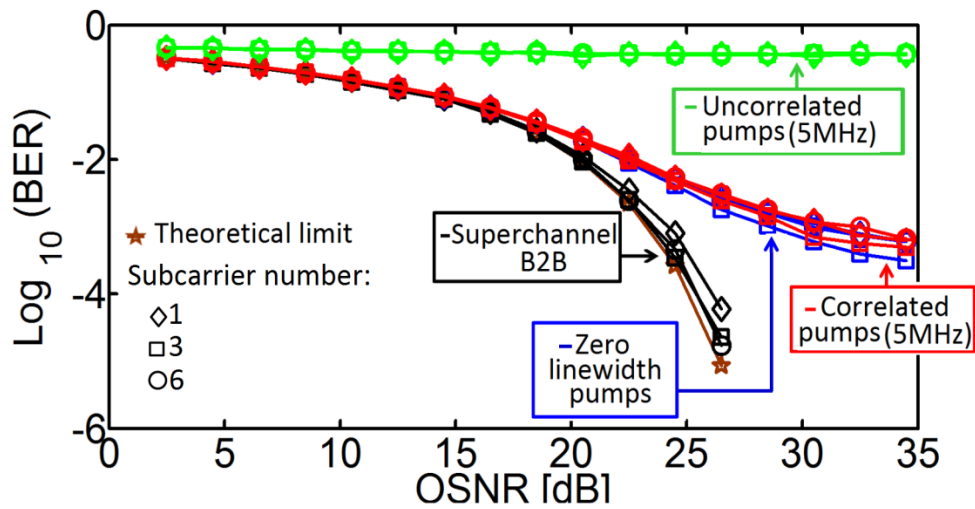


Fig.6-4 Calculated BER vs. OSNR results for the subcarriers of the superchannel after the wavelength conversion scheme. Identical BER results of the phase noise tolerant idler are obtained for the correlated pump phase noise as for the case when the pump linewidth equals zero. When the phase noise on the pumps is uncorrelated, and each pump having a 5 MHz linewidth, then the scheme completely fails. For more clarity, the results are based on 1st, 3th, and 6th subcarriers.

6.3 Summary and conclusion

In this chapter, the BER performance of wavelength converting an 896 Gbit/s N-WDM superchannel comprising of 8×28 Gbaud 16-QAM and 6×28 Gbaud 64-QAM (total bit rate 1.008 Tb/s) N-WDM superchannels are calculated using FWM in an SOA employing the dual correlated phase-noise tolerant pumping scheme. Even though in the case of 896 Gbit/s N-WDM superchannel, it is showed that the superchannel could be converted with a small implementation penalty when the linewidth of the individual comb lines are reasonably large (~ 5 MHz), in principle the comb lines could have even larger linewidths, say tens of MHz (as is often the case with mode locked laser comb sources), and the superchannel based on 16-QAM would be converted with the small implementation penalty [15-17]. The results of wavelength conversion of 1.008 Tb/s N-WDM superchannels confirm that by using dual correlated pumping scheme that no phase noise transfer from the pump to the converted superchannel occurs allowing for the superchannel based on 64-QAM to be converted even when the individual comb lines have 5 MHz linewidth.

Bibliography

- [1] Cisco Visual Networking Index: Forecast and Methodology, 2013–2018. Available from <http://www.cisco.com/>
- [2] R. Schmogrow, R. Bouziane, M. Meyer, P. A. Milder, P. C. Schindler, R. I. Killey, P. Bayvel, C. Koos, W. Freude, and J. Leuthold., “Real-time OFDM or Nyquist pulse generation which performs better with limited resources?,” *Opt. Expr.*, vol. 20, no. 26, pp. B543-B551, 2012.
- [3] R. Essiambre, G. Kramer, P. J. Winzer, G. J. Foschini, B. Goebel, “Capacity limits of optical fiber networks”, *J. Lightw. Technol.*, vol. 28, no. 4, pp. 662–701, 2010.
- [4] Bosco, G. Curri, V. Carena, A. Poggiolini, P.; Forghieri, F., ‘On the performance of Nyquist-WDM terabit superchannels based on PM-BPSK, PM-QPSK, PM-8QAM or PM-16QAM subcarriers’, *J. Lightw. Technol.*, vol. 29, no. 1, pp. 53–61, 2011.
- [5] T. Hirooka, P. Ruan, P. Guan, and M. Nakazawa, “Highly dispersion-tolerant 160 Gbaud optical Nyquist pulse TDM transmission over 525 Km”, *Opt. Express*, vol. 20, pp. 15001-15007, 2012.
- [6] S. T. Naimi, S. P. Ó Dúill, L. P. Barry, ‘Detailed investigation of the pump phase noise tolerance for wavelength conversion of 16-QAM signals using FWM’ *IEEE/OSA JOCN*, vol. 6, no. 9, pp. 793-800, 2014.
- [7] S. P. Ó Dúill, S. T. Naimi, A. P. Anthur, T. N. Huynh, D. Venkitesh, L. Barry, “Simulations of an OSNR limited wavelength conversion scheme,” *IEEE Photon. Technol. Lett.*, vol. 25, no. 23, pp. 2311–2314, 2013.
- [8] S. T. Naimi, S. P. Ó Dúill, L. P. Barry, ‘Simulations of the OSNR and laser linewidth limits for reliable wavelength conversion of DQPSK signals using four-wave mixing’, *J. Opt. Commun.*, vol. 310, no. 1, pp. 150–155, 2014.
- [9] Aravind P. Anthur, Regan T. Watts, Kai Shi, John O’ Carroll, Deepa Venkitesh, and Liam P. Barry, “Dual correlated pumping scheme for phase noise preservation in all-optical wavelength conversion,” *Opt. Expr.*, vol. 21, no. 13, pp. 15568-15579, 2013.
- [10] S. P. Ó Dúill, S. T. Naimi, T. N. Huynh, A. P. Anthur, D. Venkitesh and L. Barry, “All-optical Wavelength Conversion of Spectrally-Efficient Modulation Formats for Future Networks”, presented at Communication Systems, Networks & Digital Signal Processing Conf (CSNDSP), 2014 (Invited paper).

- [11] A. P. Anthur, R. T. Watts, R. Zhou, P. Anandarajah, D. Venkitesh, and L. Barry, "Penalty-free wavelength conversion with variable channel separation using gain-switched comb source," *J. Opt. Commun.*, vol. 324, pp 69 -72, 2015.
- [12] M. Morshed, L. B. Du, B. Foo, M. D. Pelusi, B. Corcoran, and A. J. Lowery, "Experimental demonstrations of dual polarization CO-OFDM using mid-span spectral inversion for nonlinearity compensation," *Opt. Express*, vol. 22, no. 9, pp. 10455–10466, 2014.
- [13] S. P. Ó Dúill, L.P. Barry "Improved reduced models for single-pass and reflective semiconductor optical amplifiers," *J. Opt. Commun.*, vol. 334, no.1, pp. 170-173, 2015.
- [14] S. T. Naimi S. P. Ó Dúill, L.P. Barry ' All Optical Wavelength of Conversion of Nyquist-WDM Superchannels Using FWM in SOAs' , *IEEE J. of Lightw. Technol*, vol. 33, no. 19, pp. 3959 – 3967, 2015.
- [15] S. T. Naimi, S. O Duill and L.P. Barry, 'Phase Noise Tolerant Wavelength Conversion of Tb/s Nyquist-WDM Superchannels based on 64-QAM and Using FWM in SOAs, presented at Photonic in Switching Conf (PS) ,Florence, Italy, 2015
- [16] S. O Duill, S. T. Naimi and L.P. Barry 'Phase Noise Tolerant Wavelength Conversion of Nyquist-WDM Superchannels Using FWM in SOAs', presented at *International Conf on Transparent Optical Network (ICTON)*, Budapest, Hungary, 2015 (Invited paper)
- [17] S. T. Naimi, S. O Duill and L.P. Barry, 'All-Optical Wavelength Conversion of 896 Gb/s Nyquist- WDM Superchannel Using FWM in SOAs' presented at *Photonic Ireland Conf*, Republic of Ireland, 2015.

Chapter 7: Conclusion

The goal of this thesis is to investigate and solve some of important challenges to implement all-optical wavelength conversion of higher-order modulation format data signals. In this chapter, we will summarize the achievements of the research presented in this thesis. The future research directions will also be discussed.

7.1 Conclusion

Future wavelength-labelled packet-switched wavelength division multiplexed (WDM) networks will require all optical wavelength conversion to avoid contention in a node when two signals on the same wavelength are being switched to the same output fiber; thus improving the efficiency under heavy network loads by fully utilising all the available WDM channels. In addition, the expected high capacity of the next generation networks will require advanced modulation formats with more than one bit per symbol, such as differential quadrature phase shift keying (DQPSK) and M- quadrature amplitude modulation (M-QAM) to provide for the increase in capacity. Traditional methods for wavelength conversion that rely on transferring the optical intensity to the new wavelength based on cross-phase modulation and cross gain modulation are unsuitable for modulation formats in which data is encoded on the amplitude as well as the phase of the optical carrier. To this end, a coherent nonlinear process, such as four-wave mixing is required for wavelength conversion of phase encoded data signals. Four-wave mixing in semiconductor optical amplifiers is the promising candidate to perform wavelength conversion of signals with advanced modulation formats due to: transparency to modulation format and transparency to baud rate. Apart from the FWM conversion efficiency (the ratio of the power of the converted output signal and the power of the input signal); the issue of phase noise transfer between the continuous-wave

(CW) pump and the idler is of crucial importance in employing four-wave mixing for such advanced modulation formats. The phase noise transfer degrades the performance of all-optical wavelength conversion of advanced modulation formats; thus the issue of phase noise transfer should be considered because it determines the choice of laser to be employed as the pump in such wavelength conversion schemes. In this thesis, for the first time, the required optical signal to noise ratio (OSNR) and laser phase noise (linewidth) limits that would allow for wavelength conversion of DQPSK and M-QAM (include 16-QAM and 64-QAM) signals using FWM with acceptable bit error rates (BER) of 10^{-3} and 10^{-4} are calculated via Monte-Carlo simulations using single-pump (degenerate) and dual-pump (nondegenerate) FWM. The results, which are summarized in table 7.1, show that the maximum pump linewidths for the WC of 16-QAM signals at 10 Gbaud using degenerate FWM and the DD-PLL are 1.4 MHz at a BER of 10^{-3} , and 1.2 MHz at a BER of 10^{-4} . By using the ANDD-PLL, the pump linewidth limitations are increased to 2 and 1.6 MHz at BERs of 10^{-3} and 10^{-4} , respectively. Lasers with linewidths lower than these limits are required to ensure performance of wavelength converters based on degenerate FWM. Additional results show the maximum pump linewidths for nondegenerate (degenerate) FWM WC of 64-QAM signals at 10 Gbaud using ANDD-PLL are 900 kHz (450 kHz) at the BER of 10^{-3} and 800 kHz (400 kHz) at the BER of 10^{-4} .

Table 7-1: Implementation of all- optical wavelength conversion of advanced modulation format using FWM in SOA (a) DQPSK (b) M-QAM

(a)

Modulation Format	Type of wavelength conversion	Number of pump(s)	Signal power	Pump power	Detuning	Baudrate	Maximum pump linewidth at BER=10 ⁻⁴
DQPSK	Degenerate FWM-based wavelength conversion	1	100μW	1mW	$\Omega_{S-P1}=150\text{GHz}$	10 Gbaud	18 MHz
						25 Gbaud	23 MHz
	Nondegenerate FWM-based wavelength conversion	2	100μW	1mW	$\Omega_{S-P1}=150\text{GHz}$	10 Gbaud	27 MHz
				1mW	$\Omega_{P1-P2}=320\text{GHz}$	25 Gbaud	25 MHz ($B_{P1}=B_{P2}$) 40MHz($B_{P2}=8\text{MHz}$)

(b)

Modulation Format	Type of wavelength conversion	Number of pump(s)	Signal power	Pump power	Detuning	PLL	Maximum pump linewidth at BER=10 ⁻⁴
16-QAM	Degenerate FWM-based wavelength conversion	1	100μW	5mW	$\Omega_{S-P1}=100\text{GHz}$	DD-PLL	1.2 MHz
						ANDD- PLL	1.6 MHz
	Nondegenerate FWM-based wavelength conversion	2	100μW	5mW	$\Omega_{S-P1}=100\text{GHz}$	DD-PLL	2.4 MHz
				5mW	$\Omega_{P1-P2}=475\text{GHz}$	ANDD- PLL	3.2 MHz
64-QAM	Degenerate FWM-based wavelength conversion	1	100μW	5mW	$\Omega_{S-P1}=100\text{GHz}$	ANDD- PLL	400 kHz
	Nondegenerate FWM-based wavelength	2	100μW	5mW	$\Omega_{S-P1}=100\text{GHz}$	ANDD- PLL	800 kHz
				5mW	$\Omega_{P1-P2}=475\text{GHz}$		

Subsequent work in this thesis, which is summarized in table 7.2, explored the wavelength conversion of optical superchannels that combine several lower-rate subcarriers to achieve high spectral efficiency. The effects of raised cosine (RC) and root raised cosine (RRC) signal pulse shaping were considered within the wavelength conversion process, as well considering modulation formats of DQPSK and 16-QAM for the sub-channel modulation. In this work, the SOA model is modified include internal scattering losses which is important to consider when large pump powers required. It is found that the biggest issue when converting such a superchannel in SOAs is the crosstalk due to cross-gain modulation (XGM) of the pump. The issue of XGM can be overcome by optimizing the pump power so that it is much greater (> 23 dB) than the power of the superchannel, this limiting SOA gain saturation due to the superchannel, and that the pump power should be around twice the SOA gain saturation power (the optimised value of pump power is 20 mW). Furthermore, the detuning between the pump and superchannel needs to be optimized to achieve the best performance.

Table 7-2: Implementation of degenerate FWM- based wavelength conversion of N-WDM superchannel using FWM in SOA

Modulation Format	Number of subcarriers	baud rate per channel	Pulse shaping	Pump linewidth	ASE noise (Noise figure) [dB]	Optimised Signal power	Optimised Pump power	Optimised Detuning	Raw bitrate
DQPSK	8	28 Gbaud	RC RRC	5MHz	8, 9, 10, 11	100 μ W	10mw	$\Omega_{S-P1}=200$ GHz	448 Gb/s
16-QAM	8	28 Gbaud	RRC	100 KHz	8, 9	100 μ W	10mW	$\Omega_{S-P1}=220$ GHz	996 Gb/s

The final part of the thesis investigated all-optical wavelength conversion of Nyquist-WDM superchannel based on M-QAM using dual-correlated pumping schemes. This allowed the wavelength conversion of a Tb/s Nyquist-WDM superchannel employing 64-QAM subcarrier modulation with pump linewidths as high as 5 MHz. This work employed an optical comb generator and wavelength selective switch to eliminate phase noise transfer from the pumps to the converted M-QAM superchannel thus achieving minimal implementation OSNR penalty.

7.2 Suggestions for future Work

A number of open problems must be solved to allow the development of a truly All- optical wavelength conversion of Nyquist- WDM superchannel employing advanced modulation format using FWM in SOA. These problems suggest a variety of research directions that need to be pursued to make such a system feasible.

- In the work performed here, only wavelength conversion of Nyquist-WDM superchannel without considering fibre transmission was considered. However, in real networks, a superchannel experiences accumulated chromatic dispersion when it arrives at a node where wavelength conversion is considered. The peak-to-average power ratio (PAPR) after dispersion in an uncompensated fiber link tends to be high even for single carrier modulation formats. This increased PAPR may increase the cross gain modulation in the wavelength converter. Increasing the pump power may be unfeasible; therefore increasing the superchannel-pump detuning would be required to avoid increased XGM effects. One direction for future work would be to investigate the wavelength conversion of dispersion-


altered signals. This analysis would be required to fully understand the system consequences.

- The scheme of all-optical wavelength conversion of Nyquist-WDM superchannel would work with dual-polarization signal if two SOAs are used, one for each polarizations. However, after fiber transmission, the state of polarization of the signal with respect to the input to each SOA may not be unique, but could be a mixture of the two states and this would be a time varying mixture. The issue of polarization state of the signal is very pertinent to track and rotate the incoming signal polarization to align with each SOA. Much work has been done on realizing SOAs with polarization insensitive gain with a difference of ~ 0.5 dB between the TE and TM polarization state (it is shown in Appendix I for data sheet of XN-SOA nonlinear SOA from Center for Integrated Photonics (CIP) which is used in many wavelength conversion experiments), the conversion efficiency will also depend on the saturation power being polarization independent too. Nonetheless, phase noise tolerant wavelength conversion schemes are investigated in this thesis that I believe will conclusively address the polarization issue for SOA-based wavelength converters. It would be impressive to experimentally investigate this issue.
- Finally, all-optical wavelength conversion of 1.008 Tb/s Nyquist-WDM superchannel comprising of 6×28 Gbaud 64 QAM modulation formats using FWM in an SOA is investigated in the chapter 6 of this thesis. Future work should investigate experimental results of phase noise tolerant all-optical wavelength conversion of Tb/s Nyquist-WDM superchannel based on M-QAM using FWM in SOA.

APPENDIX A- Data Sheet

This page contain data sheet of XN-SOA nonlinear SOA from CIP.

PRELIMINARY DATASHEET | SOA-NL-OEC-1550

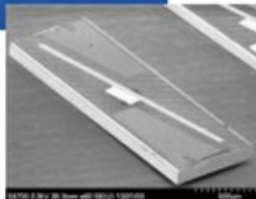


Centre for Integrated Photonics

SOA-NL-OEC-1550 - 1.55 μ m Non-Linear Semiconductor Optical Amplifier (SOA)

CIP

Centre for Integrated Photonics



Features

- 1.55 μ m operation
- High gain (30dB)
- Low saturation output power
- Fast gain recovery times
- Low saturated PDG
- InP Buried Heterostructure design
- TEC cooled
- Available as packaged device or chip-on-carrier
- APC connectors provided

Application Examples

- All optical processing
- Wavelength conversion
- Cross-phase modulation
- Cross-gain modulation
- Four-wave mixing

Description

The non-linear SOA is a high confinement factor device optimised for high gain and fast gain recovery providing fast optical switching speeds. It utilises CIPs proprietary InP buried heterostructure design and is available in either a 14-pin butterfly package with a thermistor, thermo-electric cooler and single mode fibre pigtails or as a custom chip-on-carrier product including chip arrays.

The product is appropriate in wavelength converter or four wave mixing applications and is used in CIP's hybrid integrated regenerator/wavelength converter product (40G-2R-ORP). Custom specification variants may be defined as appropriate for other non-linear applications. Arrays of non-linear SOAs are also available either packaged or as chip-on-carrier.

Optical and electrical specifications

All measurements are at 20°C & 1535-1560nm unless stated otherwise.
I = bias current P_{in} = Input optical power

Item	Test condition	Min.	Typ.	Max.	Unit
Small signal Gain	I = 200-300mA	25		34	dB
Polarisation Dependent Saturated Gain (PDG)	I = 300mA, P _{in} > 0dBm		0.5	1	dB
Saturated Output Power (SOP)	I = 200mA	6			dBm
Gain Peak	I = 200mA	1550		1570	nm
Saturated Gain Recovery Time (1/e)	I = 300mA, P _{in} > 0dBm, 1555nm			25	ps

www.ciphotonics.com

.....researching solutions

CIP, Adastral Park, Martlesham Heath, Ipswich, IP5 3RE, UK Tel: +44 (0) 1473 663210 info@ciphotonics.com

rev F

APPENDIX B- List of Publications arising from this work

Journals:

- **S. T. Naimi**, S. P. Ó Dúill, L.P. Barry, 'All Optical Wavelength Conversion of Nyquist-WDM Superchannels Using FWM in SOAs', *IEEE J. of Lightw. Technol.*, vol. 33, no. 19, pp. 3959 – 3967, 2015.
- **S. T. Naimi**, S. O Duill, and L.P. Barry, 'Detailed Investigation of the Pump Phase Noise Tolerance for the Wavelength Conversion of 16-QAM Signals Using FWM', *IEEE/OSA JOCN*, vol. 6, no. 9, pp. 793-800, 2014.
- **S. T. Naimi**, S. O Duill, and L.P. Barry, 'OSNR and Laser Linewidth Limits for Reliable Wavelength Conversion of DQPSK Signals Using Four-Wave Mixing', *J. Opt. Commun.*, vol. 310, no. 1, pp. 150–155, Jan. 2014.
- S. O Duill, **S. T. Naimi**, A P. Anthur, T N. Huynh, D Venkitesh, and L.P. Barry , 'Simulations of an OSNR-Limited All-Optical Wavelength Conversion Scheme', *IEEE Photon. Technol. Lett.*, vol. 25, no. 23, pp. 2311–2314, 2013.
- S. O Duill , **S. T. Naimi** and L.P. Barry, 'Pump Linewidth Requirements for Processing Dispersion-Altered DQPSK Signals using FWM', Submitted to *J. of Optics Letters*, available from (<http://arxiv.org/abs/1507.07379>)
- S. O. Duill, A. P. Anthur, T N. Huynh, **S. T. Naimi**, L. Nguyen, D. Venkitesh, and L.P. Barry, 'Numerical Generation of Laser Resonance Phase Noise for Optical Communication Simulators', *J. of applied optics*, vol. 54, no. 11, pp. 3398-3406, 2015.

Conferences:

- **S. T. Naimi**, S. O Duill, and L.P. Barry, ‘Impact of Four-wave Mixing Phase Noise Transfer on Wavelength Converted QPSK Signals’, Conference on Lasers and Electro-Optics Europe (**CLEO-Europe**), Munich, Germany, 2013, Paper CI-3.4.
- **S. T. Naimi**, S. O Duill and L.P. Barry, ‘Linewidth Limits for Wavelength Converting 64-QAM Signals Using FWM’ Conference on Lasers and Electro-Optics Europe (**CLEO-Europe**), Munich, Germany, 2015, CI-2.1.
- **S. T. Naimi**, S. O Duill and L.P. Barry, ‘Phase Noise Tolerant Wavelength Conversion of Tb/s Nyquist-WDM Superchannels based on 64-QAM and Using FWM in SOAs, **Photonic in Switching (PS) 2015**, Florence, Italy, 2015
- **S. T. Naimi**, S. O Duill, A P. Anthur, T.N. Huynh, D Venkitesh and L.P. Barry, ‘Wavelength Conversion of 16- QAM Signals without Excess Phase noise using four wave mixing’, **Photonic Ireland 2013**, Belfast, North of Ireland, 2013.
- **S. T. Naimi**, S. O Duill, A P. Anthur, T.N. Huynh, D Venkitesh and L.P. Barry, ‘All optical wavelength conversion of 16-QAM’, **Rince research day**, Dublin City University, Dublin, Ireland, 2014.
- **S. T. Naimi**, S. O Duill and L.P. Barry, ‘All-Optical Wavelength Conversion of 896 Gb/s Nyquist- WDM Superchannel Using FWM in SOAs’ **Photonic Ireland 2015**, Cork, Republic of Ireland, 2015.
- **S. T. Naimi**, S. O Duill and L.P. Barry, ‘All-Optical Wavelength Conversion of Tb/s Nyquist- WDM Superchannel ‘**3rd workshop on Ultrafast photonic processes and interactions**, Dublin, Republic of Ireland, 2016.

Invited papers:

- S. O Duill, **S. T. Naimi**, A P. Anthur, T.N. Huynh, D Venkitesh, and L.P. Barry ‘All-optical Wavelength Conversion of Spectrally-Efficient Modulation Formats for Future Networks’, *CSNDSP14*, Manchester, United Kingdom, 2014.
- S. O Duill, **S. T. Naimi** and L.P. Barry ‘Phase Noise Tolerant Wavelength Conversion of Nyquist-WDM Superchannels Using FWM in SOAs’, International Conference on Transparent Optical Network (*ICTON15*), Budapest, Hungary, 2015.